Conformational Plasticity and Disorder-to-Order Transition of Intrinsically Disordered α-Synuclein: Interactions with Lipid Membranes, Tau and Chaperones

KARISHMA BHASNE

Thesis submitted for the partial fulfillment of the degree of

DOCTOR OF PHILOSOPHY

Department of Biological Sciences

Indian Institute of Science Education and Research (IISER) Mohali

August 2018

CERTIFICATE

The work presented in this thesis has been carried out by me under the supervision of Dr. Samrat Mukhopadhyay at the Department of Biological Sciences, Indian Institute of Science Education and Research (IISER) Mohali.

This work has not been submitted in part or full for a degree, a diploma, or a fellowship to any other university or institute.

Whenever contributions of others are involved, every effort is made to indicate this clearly, with due acknowledgement of collaborative research and discussions. This thesis is a bona fide record of original work done by me and all sources listed within have been detailed in the bibliography.

Date **Place** **Karishma Bhasne**

In my capacity as supervisor of the candidate's thesis work, I certify that the above statements by the candidate are true to the best of my knowledge.

Dr. Samrat Mukhopadhyay

(Supervisor)

Dedicated to

Mily Bhattacharya &

My Mother, Pushpa Bhasne

Acknowledgements

This journey would not have been possible without the support and assistance of various individuals. I would like to take this opportunity to thank all of them for being there for me.

I truly want to acknowledge Dr. Samrat Mukhopadhyay for his invaluable guidance in my professional and personal development. The first thing that I enjoyed in the lab was the intellectual freedom that he gave to me, which helped me design and execute my experiments. His enthusiasm, guidance, support, patience, innovative ideas and experience have changed my scientific outlook. His knowledge is not only confined to his area of research but also in other areas of science, which makes interacting with him all the more enjoyable.

I would like to thank Dr. Mily Bhattacharya for introducing me to the world of research which has really got me to where I am today. I will always be thankful to her for her help not only in my professional pursuits but also in my personal life.

I thank the present and former members of the Mukhopadhyay's lab who guided me, during the initial stages of my research tenure. I would like to acknowledge Neha Jain for initiating the work on α-synuclein and standardizing its purification and would also like to thank her for recording tryptophan fluorescence anisotropy decays, carried out at TIFR Mumbai. I thank Prof. G. Krishnamoorthy (TIFR) for allowing Neha to record the data and Prof. N. Periasamy (TIFR) for providing us with the decay analysis software. I am also grateful to Dominic Narang for teaching me the basics of molecular biology and helping me with the anisotropy decay analysis.

I would like to thank the members of my doctoral committee, Dr. Mahak Sharma and Dr. Shravan Kumar Mishra, for their constant encouragement and valuable suggestions on my work.

α-Synuclein and Hsp interaction work was performed in collaboration with Prof. Patrick D'Silva at IISc Bangalore. I would like to thank Prof. Patrick D'Silva and Madhuja for the healthy discussions on the work. My special thanks to Madhuja, Kondalarao and Vinaya for providing us with Hsp proteins and Hema for collecting the data for the biophysical experiments.

A large number of people helped me with the α-synuclein-membrane work, Rishab for the experiments, Anubhuti and Shruti for the analysis and Anupa for manuscript writing and discussions. I would like to thank Sanjana for helping with the α-synuclein and tau work. I would like to especially acknowledge Chandrakala and Pranay for writing the python program to obtain the kinetics data from the plate reader.

My scientific development would have been impossible without Anupa, Sourav, Vijit, Shruti, Hema, Priyanka, Priyanka Madhu, Debapriya, Aishwarya and Sayanta. Their suggestions and discussions have helped me in shaping my thesis in a better form. My special thanks goes to Anupa, the most wonderful post-doctoral fellow in our lab, who has infused a lot of warmth and cheer in many a difficult times. I am also grateful to her for extensively checking my thesis chapters.

I am also thankful to Prof. Vinod Subramaniam and Prof. Elizabeth Rhodes for providing us with α-synuclein and Tau (k18) plasmids, respectively. I am grateful to the Department of Science and Technology, Govt. of India, for the DST-INSPIRE fellowship.

I am thankful to IISER Mohali and Centre for Protein Science, Design and Engineering for providing all the facilities for research. I would like to express my sincere gratitude to Professor N. Sathyamurthy, the past director of IISER Mohali for his consistent help during my stay. My special thanks to the Purchase and Stores department people (Mukhesh, Mansaram and Raman) for their help in ensuring the smooth running of the ordering facilities. I am thankful to Dr. P. Visakhi (librarian) for beautifully maintaining the library which helped me a lot while writing the different manuscripts and this thesis. I thank the security personnels of the academic blocks for becoming my coffee partners in night during the long experiments.

I truly acknowledge Prof. Lila Gierasch, Prof. Jerson L Silva and Prof. Elizabeth Komives for their encouragement and fruitful discussions during the Biophysical Society's 61st Annual Meeting (2017) in New Orleans, USA and the International Conference on Intrinsically Disordered Proteins at IISER Mohali, India. The financial support from DST, IISER and the Biophysical Society for attending the international conference is also duly acknowledged.

No journey is complete without friends, and I have a long list of people. I would like to begin with Dr. Omendra Bhooshan, Neeraj, Amol, Nitish, Shashank, Priyanka, Rohit, Chirag, Ishant, Parv and Nipurn for their love, care and support. I enjoyed my time with my personal heroes, Chandrakala and Hema, for the long discussions on both scientific and non-scientific topics. I enjoyed my time in the badminton court with my friends, especially, Rohit, Hema, Abhishek, Swagatham, Rajneesh, Ashwini, Alok, Ankit, Arnav, Bhupinder, Pradeep and many more.

Last, but not the least I want to thank the most important people of my life, my parents and my brother Himanshu for their constant love and encouragement. I would like to especially thank my cousin, Sachin who was always with me through thick and thin and was always a constant source of inspiration for me.

Karishma Bhasne

Synopsis

Conformational Plasticity and Disorder-to-Order Transition of Intrinsically Disordered α-Synuclein: Interactions with Lipid Membranes, Tau and Chaperones

Chapter 1. Introduction

The conventional sequence-structure-function paradigm states that proteins adopt a well-defined 3-dimensional structure that is encoded by the amino acid sequence. However, an emerging class of proteins, known as intrinsically disordered proteins (IDPs), confronts this traditional paradigm. IDPs being conformationaly plastic can adopt different structures depending upon their binding partners. This property of IDPs might be an evolutionary conserved strategy that makes them more useful in a wide range of physiological functions involving cell signaling, transcription, etc. Under certain stress conditions, in the cellular milieu, both folded proteins and IDPs can adopt a thermodynamically more stable state known as amyloid state. These amyloids represent exquisite protein nano-aggregates that are constituted by characteristic highly ordered cross-β structures and are known to be implicated in a large number of debilitating neurodegenerative diseases, such as Parkinson's disease (PD) and Alzheimer's diseases (AD). α-Synuclein is an IDP, mainly found in the presynaptic terminals of neurons in the brain and the central nervous system. The precise function of α-synuclein is poorly understood, though, there are few proposed functions known such as synaptic transmission, synaptic vesicle localization, maintenance of neuronal plasticity, etc.α-Synuclein adopts a helical structure in the membrane-bound form. The membrane-bound state plays a crucial role in the biological function of α-synuclein and in the etiology of Parkinson's disease. α-Synuclein being a cytosolic protein and is also known to interact with other cytosolic proteins, namely, tau, which is also an IDP that stabilizes microtubules and its amyloid formation is implicated in AD. Recent evidences suggest that tau and α-synuclein interact to form pathological co-amyloids that are localized in different regions of the brain and are associated with several neurological diseases such as PD, AD, Down syndrome, multiple

system atrophy, etc. Furthermore, protein folding and amyloid dissociation are tightly regulated at multiple levels with the help of molecular chaperones. α-Synuclein is known to associate with the mitochondria and interact with heat shock proteins (Hsps) under several stress conditions, including PD. In this thesis, efforts were directed towards understanding the structural and dynamical aspects of interaction of α-synuclein with membranes, other proteins and molecular chaperones using a variety of biophysical tools.

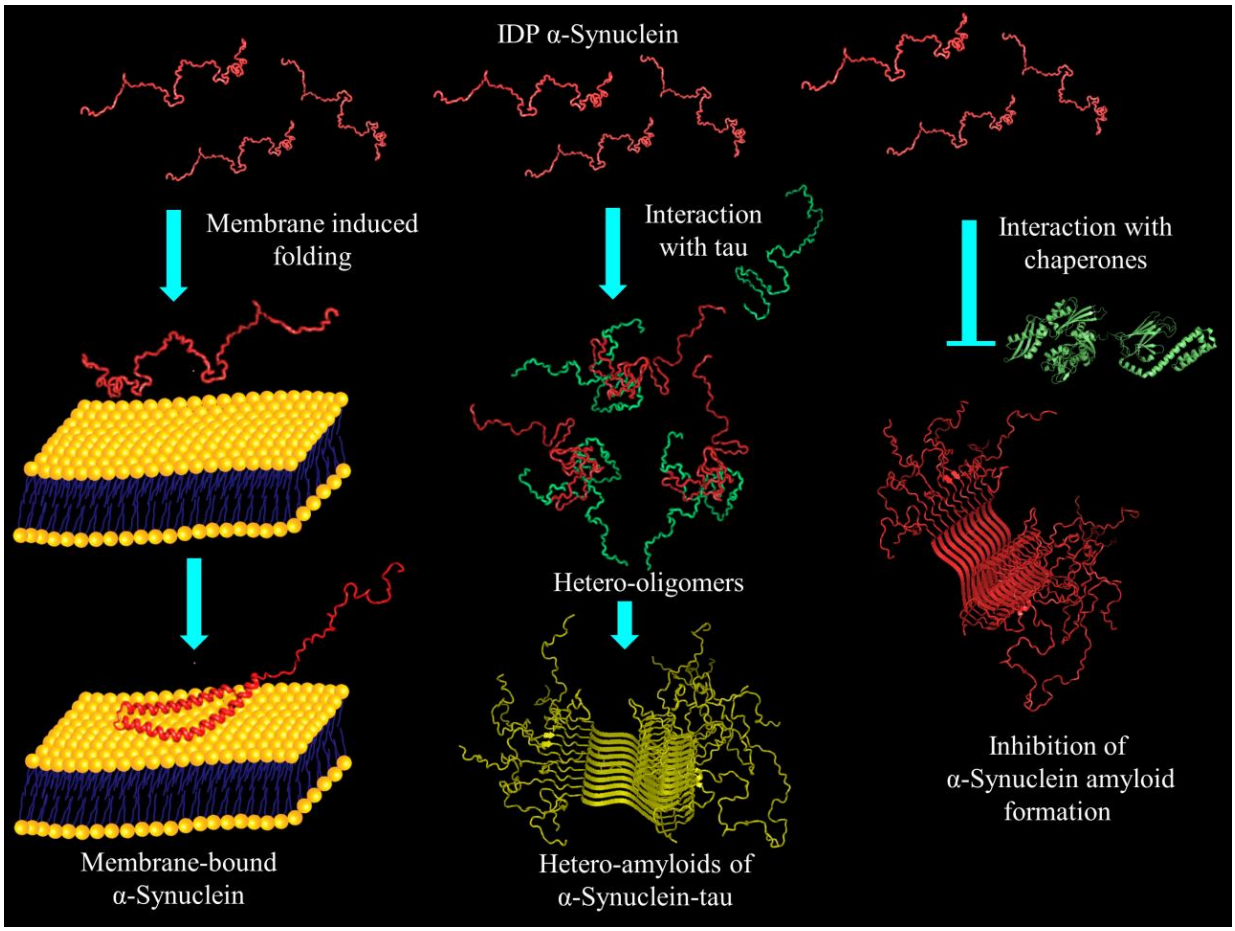

Chapter 2. Diffusion of α-Synuclein on the Lipid Membranes

Membranes are fluidic in nature and it allows the diffusion of different proteins, signalling molecules, carbohydrates, etc. for maintaining cellular milieu. α-Synuclein, present in the presynaptic terminal of neurons, is populated as an IDP in the unbound state and adopts an α-helical structure upon interacting with membranes. The membrane-bound α-synuclein plays a crucial role in the regulation of synaptic plasticity and in the etiology of PD progression. Here, we utilized time-resolved fluorescence spectroscopy, to delineate the site-specific structural and dynamical insights of the membrane-bound α-synuclein. As α-synuclein is devoid of cysteine, therefore, we have incorporated single cysteine mutations along the polypeptide chain

such that the mutations do not alter the properties of α-synuclein and behave similar to wild-type protein. We then labeled these cysteine variants using a long lifetime thiol-active fluorophore, IAEDANS ((1,5-IAEDANS, 5-((((2-Iodoacetyl) amino) ethyl) amino) Naphthalene-1-Sulfonic Acid)) and monitored the dynamics using picosecond time-resolved fluorescence. Our fluorescence depolarization results show the presence of three dynamically distinct types of motions, the local motion of the dye, the segmental motion of α-synuclein and the translational diffusion of α-synuclein on the membrane. The time-resolved fluorescence depolarization measurements allowed us to quantify the translational diffusion of α-synuclein on the synthetic lipid membranes. Our findings suggest that the strong binding of α-synuclein on the POPA (1-palmitoyl-2-oleoyl-sn-glycero-3-phosphate) SUVs (small unilamellar vesicles) results in slower diffusion, whereas on the POPG (1-palmitoyl-2-oleoyl-sn-glycero-3-phospho-(1'-rac-glycerol))

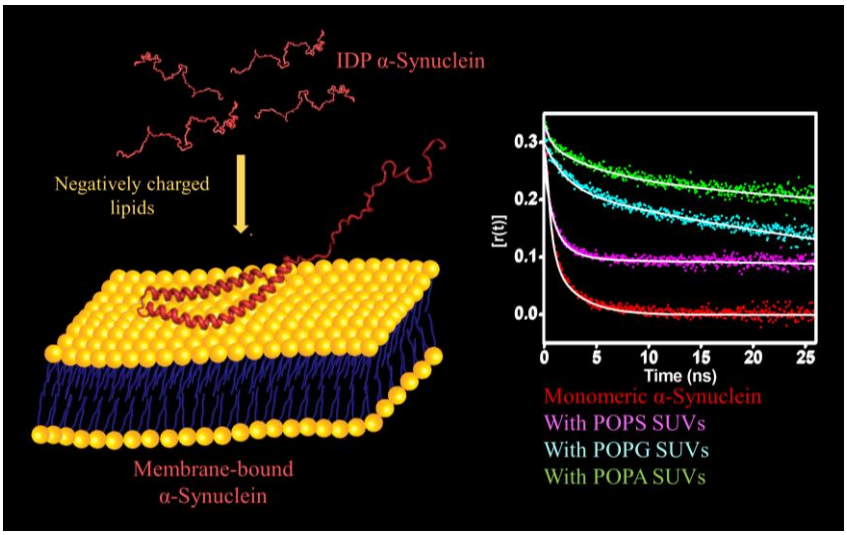

SUVs, the diffusion is faster. Our results demonstrate that the dynamics of α-synuclein is slightly altered depending on the head-group chemistry of phospholipids as well as membrane-curvature. This interplay of membrane properties and α-synuclein diffusion might be of prime importance for its regulatory role for the neurotransmitter release and in the etiology of PD progression.

Chapter 3. Synergistic Amyloid Switch Triggered by Early Heterotypic Oligomerization of Intrinsically Disordered α-Synuclein and Tau

Amyloidogenic intrinsically disordered proteins, α-synuclein and tau are linked to Parkinson's disease and Alzheimer's disease, respectively. A body of evidences suggests that α-synuclein and tau, both present in the presynaptic nerve terminals, co-aggregate in many neurological ailments. The molecular mechanism of α-synuclein-tau hetero-assembly is poorly understood. Here we show that amyloid formation is synergistically facilitated by heterotypic association mediated by binding-induced misfolding of both α-synuclein and tau K18. We demonstrate that the intermolecular association is largely driven by the electrostatic interaction between the

negatively charged C-terminal segment of α-synuclein and the positively charged tau K18 fragment. This heterotypic association results in rapid formation of oligomers that readily mature into heterofibrils with a much shorter lag phase compared to the individual proteins. These findings suggested that the critical intermolecular interaction between α-synuclein and tau can promote facile amyloid formation that can potentially lead to efficient sequestration of otherwise long-lived lethal oligomeric intermediates into innocuous fibrils. We next show that a well-known familial Parkinson's disease mutant (A30P) that is known to aggregate slowly via accumulation of highly toxic oligomeric species during the long lag phase, converts into amyloid fibrils significantly faster in the presence of tau K18. The early intermolecular interaction profoundly accelerates the fibrillation rate of A30P α-synuclein and impels the disease mutant to behave similar to wild-type α-synuclein in the presence of tau. Our findings provide the mechanistic underpinning of bypassing toxicity and suggest a general strategy by which detrimental amyloidogenic precursors are efficiently sequestered into more benign amyloid fibrils.

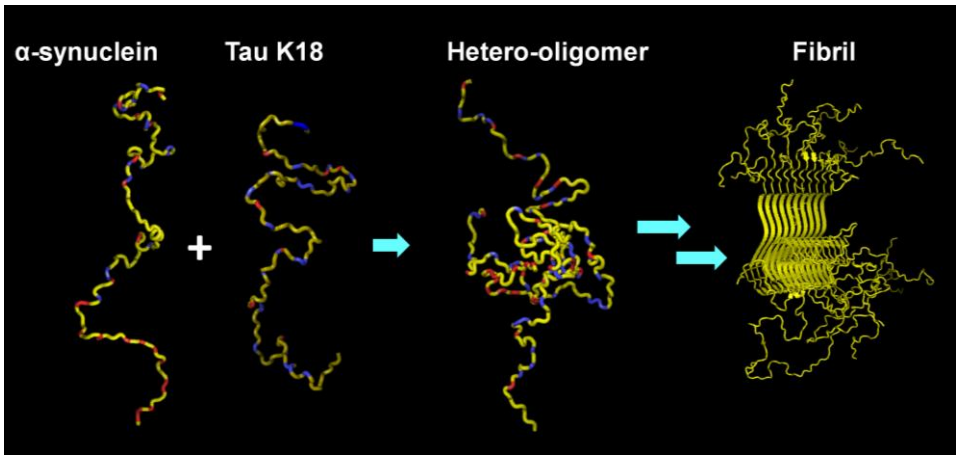

Chapter 4. Interaction of α-Synuclein with Mitochondrial Heat-shock Proteins: Implication in Parkinson's disease

The pathological feature of Parkinson's Disease (PD) involves dopaminergic neuronal death due to the deposition of proteinaceous aggregates of undefined composition known as Lewy bodies. α-Synuclein is an intrinsically disordered protein, aggregates of which are abundantly present in the Lewy bodies along with a large number of molecular chaperones including Hsp70, Hsp4 and so forth. α-Synuclein is known to associate with the mitochondria under PD conditions in spite of not having any mitochondrial-targeting sequence. To determine the specific role of α-synuclein with mtHsp70 chaperone system (mtHsp70, mtHsp40 and mtHsp78), we have developed a yeast model of heterologous expression of these proteins. In order to gain a better understanding of mitochondrial involvement in PD progression, an analogous PD-mutation P486S in yeast mtHsp70 was studied. Upon targeting A30P PD variant

of α-synuclein into yeast mitochondria leads to severe mitochondrial dysfunction phenotype in the WT Ssc1 background but not in the P486S PD-mutant background. Interestingly, our *in vitro* aggregation studies and atomic force microscopy imaging experiments corroborate the results found using a yeast model. Thus, P486S mutation could be a consequence of compensatory mutations against the A30P mutation of α-synuclein in the diseased condition. In addition to the Hsp70-Hsp40 system, Hsp78 chaperone of the yeast mitochondrial matrix represents an additional system for the resolution of protein aggregates. Our aggregation studies revealed that Hsp78 prevents wild-type and A30P α-synuclein aggregation and elongates the lag time. Taken together, our results revealed that the mitochondrial dysfunction due to α-synuclein aggregation is modulated by the effect of multiple chaperone networks of the mitochondria and the final cellular outcomes are determined by their levels within the organelle matrix.

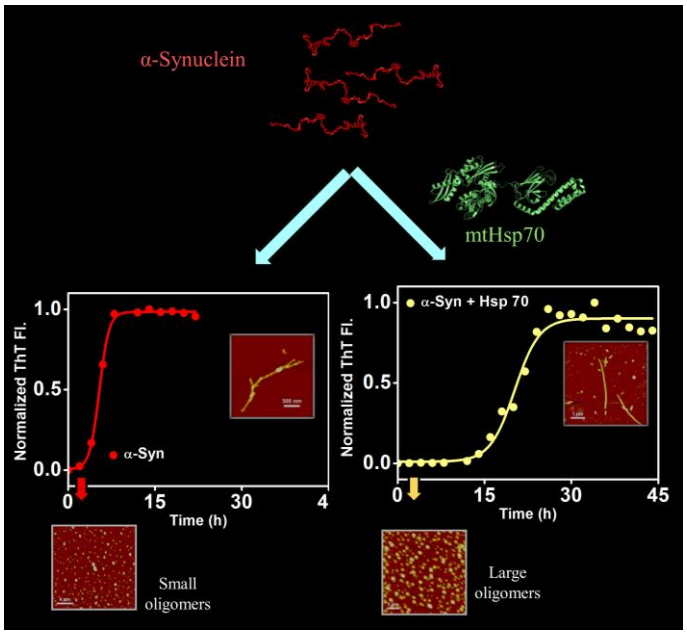

Chapter 5. Conclusions and future direction

The work described in this thesis provides structural and dynamical insights into α-synuclein interaction with membrane (chapter 2), tau (chapter 3) and chaperones (chapter 4). This chapter provides a bigger picture obtained from the results and conclusions of the individual chapters. The salient features of the thesis includes: (i) how α-synuclein dynamics differ on different head group of negatively charged lipids (POPG, POPA and POPS) and effect of curvature on α-synuclein dynamics (chapter 2) (ii) the mechanism of interaction between α-synuclein and tau results in disorder-to-amyloid transition via heterotypic oligomers formation that transformed into heterotypic amyloids (chapter 3) and (iii) how molecular chaperones work together to modulate the amyloid formation of α-synuclein and the final cellular outcomes are determined by chaperones levels within the organelle matrix (chapter 4). This thesis will improve our current understanding towards the α-synuclein interaction with multiple partners which is believed to be involved in the etiology of Parkinson's disease.

List of Publications

- ✓ **K. Bhasne,** S. Sebastian, N. Jain & S. Mukhopadhyay. "Triggering Amyloid Switch by Coupled Binding and Folding of Tau and α-Synuclein**.** ***J Mol Biol*** **2018** 25, 30273-30270. (Featured in Faculty of 1000)
- ✓ **K. Bhasne,** N. Jain, S. Arya, R. Karnawat & S. Mukhopadhyay. "Translational diffusion of α-synuclein on lipid membranes". (manuscript in preparation)
- ✓ M. Samaddar*, **K. Bhasne***, K. Bankapalli, L. P. Darbha, V. Vishwanathan, S. Mukhopadhyay & P. D'Silva. "Modulation of α-synuclein toxicity by the mitochondrial Hsp70 chaperone machinery: Implications for Parkinson's Disease progression." (*joint first author) (manuscript in preparation)
- ✓ **K. Bhasne** & S. Mukhopadhyay. "Formation of Heterotypic Amyloids: α-Synuclein in Co-aggregation." (under review)
- ❖ S. Arya, A. K. Singh, **K. Bhasne**, P. Dogra, A. Datta, P. Das & S. Mukhopadhyay. "Femtosecond Hydration Map of Intrinsically Disordered alpha-Synuclein." ***Biophys J*** **2018**, 114, 2540-2551.
- ❖ N. Jain, D. Narang, **K. Bhasne**, V. Dalal, S. Arya, M. Bhattacharya & S. Mukhopadhyay. "Direct Observation of the Intrinsic Backbone Torsional Mobility of Disordered Proteins." ***Biophys J*****.** **2016** 23;111(4):768-74.
- ❖ N. Jain*, **K. Bhasne***, M. Hemaswasthi*, S. Mukhopadhyay. "Structural and Dynamical Insights into the Membrane-Bound α-synuclein". ***PLoS ONE*** **2013**, 8(12), e8375. (*joint first author)
- ❖ M. Bhattacharya, N. Jain, **K. Bhasne**, V. Kumari & S. Mukhopadhyay. "pH-induced Conformational Isomerization of Bovine Serum Albumin Studied by Extrinsic and Intrinsic Protein Fluorescence". ***J. Fluorescence*** **2011**, *21*, 1083-1090.
- ❖ S. Arya*, **K. Bhasne*** & S. Mukhopadhyay, "Ordering of Water Molecules in the Amyloidogenic NAC Domain of α-Synuclein upon Disorder-to-Order Amyloid Transition" (*joint first author) (manuscript in preparation)

- ❖ Not part of the thesis work.

Presentations and abstracts

- **Poster Presentation:** **K. Bhasne**, M. Samaddar, K. Bankapalli, L. P. Darbha, V. Vishwanathan, P. D'Silva & Samrat Mukhopadhyay A Symphony of Molecular Chaperones and α-Synuclein, *International Conference on Intrinsically Disordered Proteins* (2017), Indian Institute of Science Education and Research (IISER), Mohali, India.
- **Platform talk:** **K. Bhasne**, S. Sebastian & S. Mukhopadhyay: A Tale of Two Amyloidogenic Intrinsically Disordered Proteins: Interplay of Tau and α-Synuclein, *Biophysical Society 61st Annual Meeting* (2017), New Orleans, Louisiana, USA.
- **Poster Presentation:** **K. Bhasne**, S. Sebastian, N. Jain & S. Mukhopadhyay: A Tale of Two Amyloidogenic Intrinsically Disordered Proteins: Tau and α-Synuclein, *The Annual Symposium of the Indian Biophysical Society* (2017), Indian Institute of Science Education and Research (IISER), Mohali, India.
- **Poster Presentation:** **K. Bhasne**, S. Sebastian, N. Jain & S. Mukhopadhyay: A Tale of Two Amyloidogenic Intrinsically Disordered Proteins: Tau and α-Synuclein, *Third International Symposium on Protein Folding and Dynamics* (2016), National Centre for Biological Sciences, Bangalore, India.
- **Poster Presentation:** **K. Bhasne**, M. Bhattacharya, N. Jain & S. Mukhopadhyay: Studies on Protein Conformational Changes and Aggregation using Fluorescence Spectroscopy, *International Symposium on Protein Folding and Dynamics* (2012), National Centre for Biological Sciences, Bangalore, India.

Table of Contents

Introduction

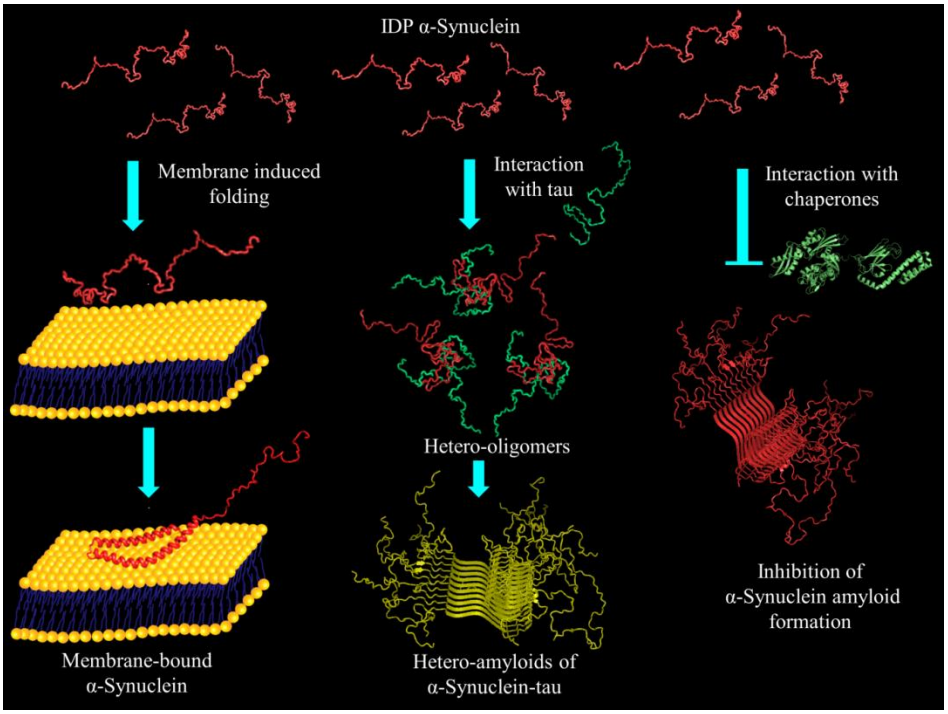

1.1 Protein Folding, Misfolding and Aggregation

Proteins are the most versatile macromolecular polymer chains of amino acids that provide structure to cell and perform specific functions. The common examples include enzymes, molecular motors, receptors, hormones, cytoskeletal network and components of extracellular matrix.[1] For most proteins, the polypeptide chain must fold into a specific structure to perform a specific function.[1-2] However, there is an emerging class of proteins known as natively unfolded or intrinsically disordered proteins (IDPs) that remain unfolded in their native state and perform multiple functions according to their binding partners, discussed later in details (section 1.5). The correct folding of proteins is a crucial step in the conversion of genetic information into biological activity in the living cell. A polypeptide chain can adopt a large number of different conformations and a systematic search for the lowest energy native state structure would take an astronomical length of time.[3] For instance, in a polypeptide chain of 100 amino acids, if each amino acid could adopt two possible conformations in the polypeptide chain, then there would be 1.26 x 10^{30} different conformations possible. And, if we assume that search for one conformation takes only 10^{-11} s then the folding of a 100 amino acid chain would take ~10^{11} years. This paradox was enounced as the Levinthal paradox.[4] A newly synthesized unfolded polypeptide chain of a

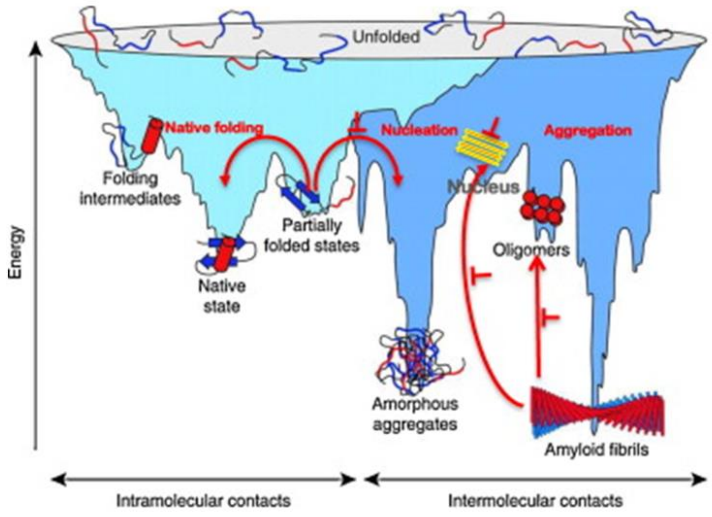

Figure 1.1 A schematic energy landscape of protein folding and aggregation. The light blue surface corresponds to the multitude of conformations 'funnelling' to the native state via intramolecular contacts and the dark blue area corresponds to the conformations that lead to the amorphous aggregates or amyloid fibrils via intermolecular contacts. Aggregate formation can occur from the metastable intermediates populated during *de novo* folding or by destabilization of the native state into partially folded states. The misfolding of proteins and aggregation is normally prevented by molecular chaperones. Reproduced with permission from [12].

protein adopts different possible states as illustrated by a free energy landscape shown in Figure 1.1. The funnel shows the dynamic ensembles of interconverting conformational states with various downhill routes emerging towards the native functional structure of the polypeptide chain.[3, 5-7] The energy surface of the funnel varies from protein to protein and is believed to be dictated by the length and the amino acid sequence of the polypeptide.[8] The folding energy landscape of small proteins (<100 amino acid residues) is relatively smooth, having less populated intermediates. For larger proteins (>100 amino acid residues), the folding funnel has a large number of partially folded intermediates where the intermediates get transiently populated during the folding process.[6, 8] The search for the native structure of the protein via metastable intermediates might be the rate limiting step for protein folding. The local and temporal concentration of the proteins might also trigger the amyloid formation

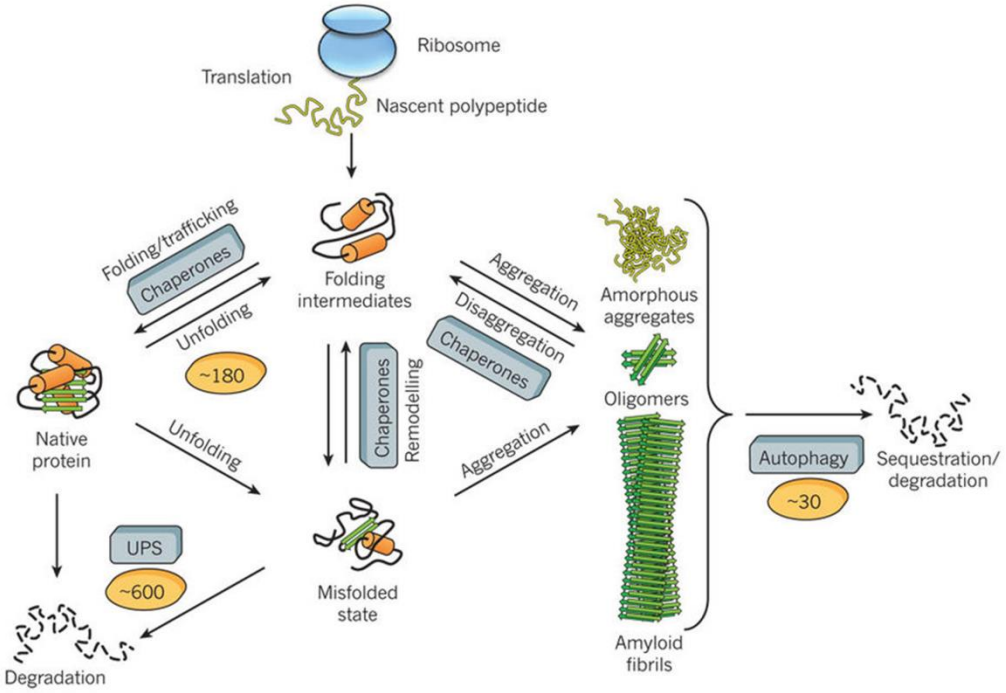

Figure 1.2 Protein fates in the proteostasis network. The proteostasis network integrates chaperone pathways for the folding of newly synthesized proteins, for the remodelling of misfolded states and for disaggregation with the protein degradation mediated by the ubiquitin–proteasome system (UPS) and the autophagy system. Approximately 180 different chaperone components, ~600 UPS and ~30 different components of autophagy system and their regulators orchestrate these processes in mammalian cells. Reproduced with permission from [11].

in a concentration-dependent manner. During protein folding in the cell, a small fraction of protein remains in their partially folded intermediate state and this result in the accumulation of proteins. Such protein aggregates were the results of the intermolecular contacts between the exposed hydrophobic patches.[9] Inside the cell, protein folding is tightly assisted by highly sophisticated chaperone machinery which restricts the intermediate state of polypeptide to form amyloids and forces the protein to stay in a biologically active state.[9] However, if these intermediate states are not protected by chaperone machinery, not degraded by the ubiquitin-proteosome system or not removed by autophagy system, then it results in the formation of protein aggregates (Figure 1.2).[10-12] Under certain metabolic stress conditions (cell aging or in the presence of exogenous or infectious agents) proteins can misfold and form highly ordered β-sheet structure which are deposited as extracellular and/or intracellular aggregates commonly known as amyloids.[10] Alois Alzheimer for the first time in 1907 described plaque and neurofibrillary tangle in the brain of middle-aged women affected by memory deficits.[13]

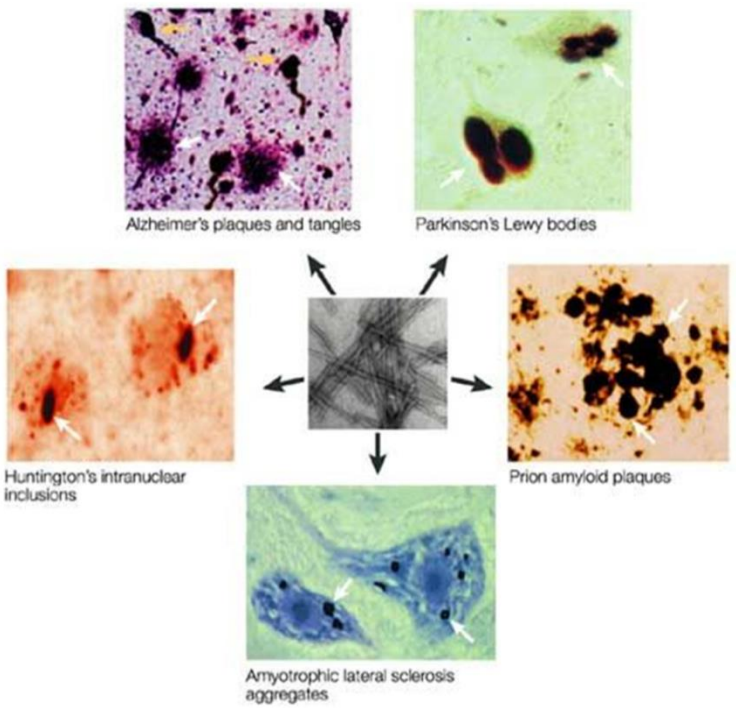

Figure 1.3 Amyloid deposits in patients. Pathological signatures of Alzheimer's disease are extracellular amyloid plaques (white arrow) and intracytoplasmic neurofibrillary tangles (yellow arrow). Intracytoplasmic aggregates in the neurons of Parkinson's disease and amyotrophic lateral sclerosis patients. Intranuclear inclusions of huntingtin proteins are observed in Huntington's disease patients and extracellular prion amyloid plaques that are located in different brain regions are present in some cases of transmissible spongiform encephalopathy. In spite of the different protein compositions, the ultrastructure of these deposits seems to be similar and composed mainly of a network of fibrillar polymers (centre). Reproduced with permission from [18]

The most devastating amyloid related neurodegenerative diseases are Alzheimer's (AD), Parkinson's (PD), Huntington's, prion diseases and a variety of other systemic amyloidosis.[14-15] These protein amyloids can be present in the different regions of the cells, such as, extracellular amyloid plaques and intracytoplasmic neurofibrillary tangles, which are the hallmark of AD, intranuclear inclusions of huntingtin are observed in Huntington's disease patients and many others. In spite of the different protein compositions, the ultrastructure shares common network of fibrillar polymers (Figure 1.3).

1.2 The impact of amyloids in human health

The term "amyloid" comes from the early mistaken identification of the substance as starch by Rudolf Virchow in 1854.[16] It was initially debated that the amyloids are the deposits of fatty acids or carbohydrate deposits. In 1859, it was demonstrated that the amyloids are the abnormal deposits of protein aggregates within the brain tissues. Afterwards many amyloid related diseases were discovered, some are sporadic and/or hereditary and some are transmissible in nature. Many diseases are linked with amyloid formation and some of those are listed in Table 1.1.[16-18] These protein amyloids are sometimes deposited in the tissues of central nervous system or peripheral nervous system resulting in organ impairment. This group of diseases infringes an enormous social and personal damage; therefore, it is crucial to understand the detailed mechanism of their genesis.

Table 1.1

Peptides or proteins forming amyloid deposits or inclusions in human diseases. [17]

*Fragments of various lengths are also reported.

Disease	Aggregated protein or peptide	Number of Residues*	Structure of the protein or peptide
Alzheimer disease Hereditary cerebral hemorrhage with amyloidosis	Amyloid-β peptide	40 or 42	Intrinsically disordered
Parkinson disease Parkinson disease with dementia Dementia with Lewy bodies Multiple system atrophy	α-Synuclein	140	Intrinsically disordered

Pick disease Frontotemporal dementia with parkinsonism linked to chr17 Progressive supranuclear palsy	Tau	352–441	Intrinsically disordered
Huntington's disease	Huntingtin fragments	103–187	Intrinsically disordered
Creutzfeldt-Jakob disease Fatal insomnia Spongiform encephalopathy with neuropsychiatric features New variant Creutzfeldt-Jakob disease Kuru Hereditary sensory and autonomic neuropathy	Prion protein or its fragments	208	Intrinsically disordered (1–102) All-α, prion-like (103–208)
Amyotrophic lateral sclerosis	Superoxide dismutase 1	154	All-β, Ig-like
Dialysis-related amyloidosis Hereditary visceral amyloidosis	β2-microglobulin	99	All-β, Ig-like
Type II diabetes Insulinoma	Amylin or islet amyloid peptide	37	Intrinsically disordered
Hereditary hyperferritinemia cataract syndrome	γ-crystalline	4,176	All-α, ferritin-like
Lysozyme amyloidosis	Lysozyme	130	α+ β, lysozyme fold
Aortic medial amyloid	Medin	50	Intrinsically disordered
Secondary systematic amyloidosis	Full or N-term fragments of serum amyloid A protein (SAA)	45-105	All-α, SAA-like four helix bundle
Senile systemic amyloidosis Familial amyloidotic polyneuropathy Familial amyloid cardiomyopathy Leptomeningeal amyloidosis	Transthyretin	127	All-β, prealbumin-like

1.3 Structure and genesis of amyloids

Amyloids represent protein nanoaggregates having a characteristic highly ordered cross-β structure despite the lack of sequence homology or the length of the polypeptide.[5] The transmission electron microscopy and atomic force microscopy images of amyloids show long and straight fibril along with some twisted filaments having a diameter of around 6-12 nm. According to the X-ray diffraction studies, the highly-ordered cross-β structure are oriented perpendicular to the fibril axis, and the inter-strand hydrogen bonds as well as the

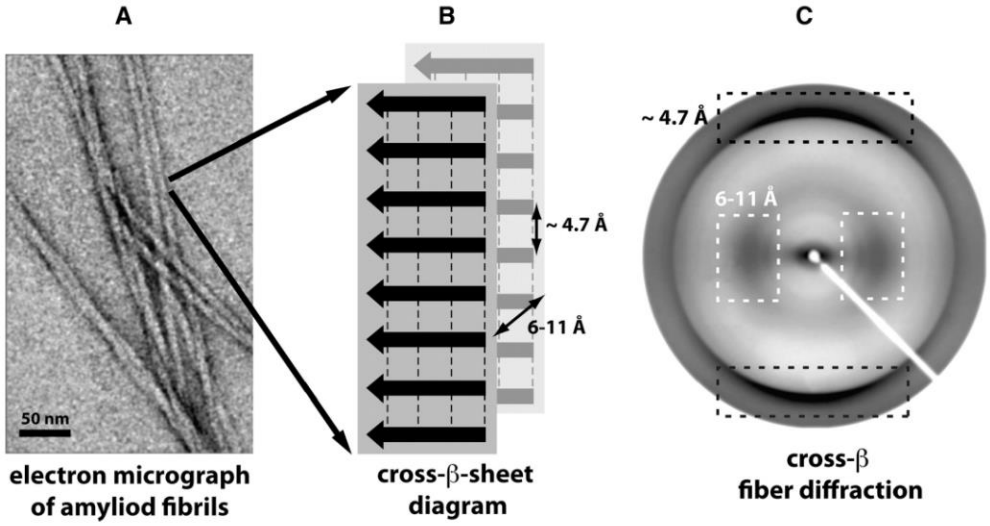

Figure 1.4 (A) Transmission electron micrograph of amyloid fibrils shows long filaments. (B) The schematic representation of the cross-β sheet arrangement within fibrils, with the backbone hydrogen bonds shown by dashed lines, and (C) the characteristic cross-β diffraction pattern with a meridional reflection at ~4.7 Å and an equatorial reflection at ~6–11 Å, that correspond to inter-strand and inter-sheet spacing, respectively. Reproduced with permission from [19].

amino acid side chains are parallel to the fibril axis(Figure 1.4).[5, 19] These amyloids interact with specific dyes, such as Conga red and thioflavin T (ThT) which intercalate between the cross-β structures. Amyloids show characteristic circular dichroism (CD) signatures, infrared spectra of β-sheet structure and they are known to be thermodynamically more stable. [10, 13-16, 20] Recent advances in magic angle spinning, solid-state nuclear magnetic resonance (NMR) spectroscopy, single-crystal X-ray diffraction and amide hydrogen-deuterium studies together with cryo-electron microscopy have provided insights into the amyloid structure.[16, 21-23]

Various structural arrangements possible for amyloids are summarized below:

(i) Parallel arrangement of β-strands: This type of packing is known as parallel in-register packing commonly observed for functional as well as pathological amyloids. In this case, amino acid residues of the polypeptide chain are positioned on top of one another in the β-sheet structure along the fiber axis.[24] The backbone hydrogen bonds are arranged parallel to the fiber axis (Figure 1.5A). Examples: α-synuclein[25] and β_2-microglobulin.[26]

(ii) Antiparallel arrangement of β-strands: In this case, the β-strands of amyloids run antiparallel to each other (Figure 1.5B).[27] Example: fragments of Aβ peptide.[28]

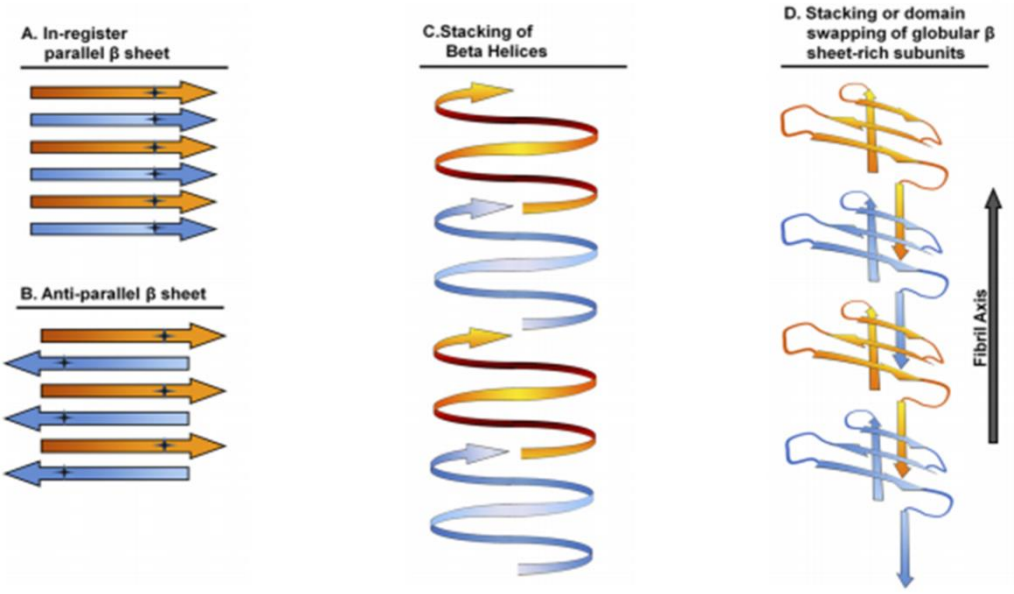

Figure 1.5 Various structural arrangements possible for amyloids (A) parallel in-register -sheet structures are composed of individual polypeptides stacking in-register every 4.7 Å along the fibril axis (B) antiparallel β-sheet structures are also composed of polypeptides stacking every ~4.7 Å, but β-strands alternately run in opposite directions. (C) β-helices are composed of a single polypeptide wrapping around an axis, forming intramolecular parallel β-sheets. (D) some β-sheet-rich proteins can linearly assemble into filamentous structures by domain swapping mechanism. Reproduced with permission from [27].

(iii) β-helical or nanotube structure: In this case, one or more β-sheets, arranged in a parallel manner, wrap around a hollow core forming a helical structure; the structure so formed is known as a β-helical or nanotube structure (Figure 1.5C).[29] Examples: polyglutamine peptide and NM-domain of Sup35 yeast prion protein.[28]

(iv) Domain swapping: In domain swapping mechanism, a β-hairpin structure of one polypeptide chain gets inserted into the β-sheet of the next one, forming aggregates. (Figure 1.5D).[30] Example: serine proteinase inhibitors.[31]

The amyloid formation process is usually modelled as a nucleation-dependent polymerization process, where the fibril formation is determined by a lag phase, log phase and stationary phase.[32-33] The lag phase is concentration-dependent, indicating the formation of a critical-oligomeric nucleus that facilitates the association and sequestration of other monomers

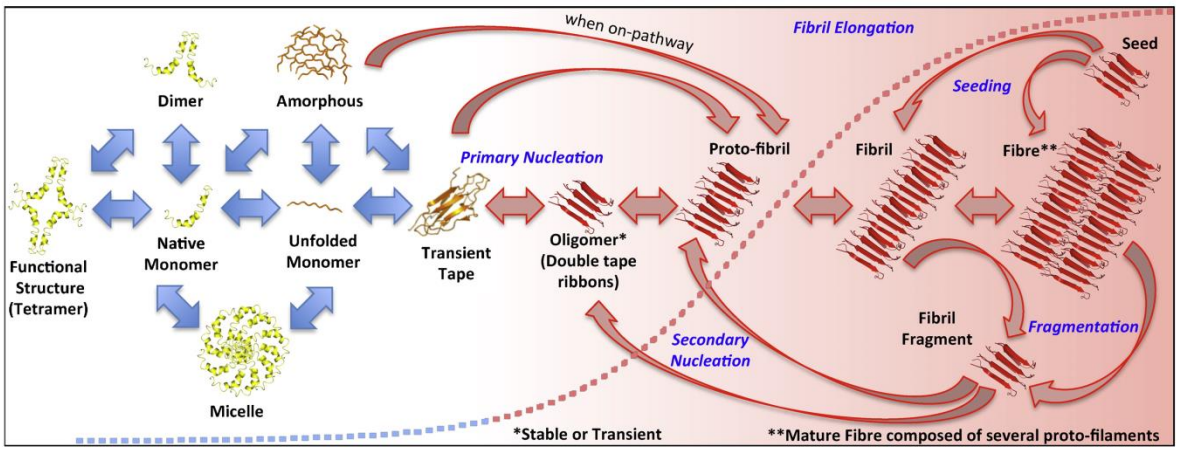

Figure 1.6 Schematic overview of amyloid assembly. Reproduced with permission from [34].

into fibrils (Figure 1.6).[32, 34] Many proteins form amyloids without the lag time, known as isodesmic polymerization.[35] The pre-formed oligomers can also serve as nucleating species in aggregation reactions. Isodesmic reactions are fastest at the beginning, have no critical concentration barrier and get slowed down as the equilibrium is reached.[36] Interestingly, studies have also established that the amyloid structures are dynamic in nature that can undergo recycling of molecules in equilibrium between bulk solution and the fibrils ends.[37] The dynamic nature of amyloid is of prime importance for the design of therapeutic strategies, especially because growing evidence suggests that the true toxic species to the cells are the dynamic soluble oligomeric intermediates.[10, 38-39]

1.4 Pre-fibrillar oligomeric precursor may be the toxic species

Recent studies suggest that the soluble pre-fibrillar oligomers are the main causative agent of cell toxicity and dysfunction. The intermediates formed during the lag phase of aggregation kinetics can be defined as the precursor in the amyloid formation.[10, 38-39] Recent studies have

established that the concentration of soluble Aβ oligomers changes the degree of synaptic alteration, neurodegeneration and cognitive decline in AD patients.[38] Furthermore, purified oligomers of Aβ when injected into rat hippocampus showed the neuronal death of animal brain.[40] Additionally, evidence suggests that Aβ dimers and oligomers play a major role in AD progression and in contrast, the amyloid fibrils show relatively low toxicity.[41]

The toxic transient oligomeric intermediates are short lived species, therefore, the structural and mechanical insights into their pathological action remains elusive. The fast sequestration of toxic oligomers might reduce the toxicity of oligomers by limiting its amount and transforming it into less toxic fibrils.[42] There is an emerging class of amyloids known as functional amyloids, which are linked with many important cellular functions. Functional amyloids of proteins such as, Curli in *E.coli*,[43-44] Sup35 in yeast,[45] and Pmel in mammals[46] are known to aggregate with no or small lag phase of polymerization.[10] However, recent reports shed light into the toxicity of oligomers and suggest that not all the oligomers are toxic to the cells. The two different oligomeric forms of α-synuclein having similar sizes and morphologies have distinct abilities to disrupt lipid bilayers, human neuroblastoma SH-SY5Y cells and rat primary cortical neurons.[47-48] Hence, the mechanistic details of amyloid formation are under intense scrutiny to understand the nature, structural and dynamical aspects of these en route oligomers and the reasons of their genesis.

1.5 Intrinsically disordered proteins (IDPs) or natively unfolded proteins

Typically, every protein upon synthesis folds spontaneously or with the help of chaperones, into a structurally and functionally active three-dimensional structure. There is an emerging class of proteins known as intrinsically disordered proteins or natively unfolded proteins which does not have any structure and can perform multiple functions according to their binding-partners.[49-62] IDPs approximately make 30 % of all mammalian proteins and some proteins have intrinsically disordered regions (IDRs) with partly structured regions.[63] IDPs are involved in cellular processes, such as cell-cell communication, growth, transcriptional regulation and apoptosis.[64] The difference between folded and intrinsically disordered proteins can be observed by their potential energy surfaces.[65] The protein folding funnel for natively folded protein shows the funnel-like energy surface during their search for the native structure via partially folded intermediates, whereas, IDPs have a relatively flat energy surface (Figure 1.7).[65] The funnel like energy surface has a global energy minimum which is the lowest energy state and corresponds to the native structure. On the contrary, IDPs have multiple local energy minima that are separated by small barriers and the interconversions

between local energy minima can take place rapidly.[65] The abundance of IDPs in the cellular cytoplasm is regulated to prevent the non-specific interactions and self-association of the IDPs.[64]

In cellular stress conditions some IDPs are known to aggregate and contribute to the etiology of many neurodegenerative diseases. AD, PD and Huntington's disease are believed to be caused by the abnormal accumulation and aggregation of IDPs, tau and/or Aβ, α-synuclein and huntingtin protein polyQ fragments, respectively.[66] Such protein aggregates are the results of the intermolecular contacts between the exposed hydrophobic patches in IDP state.[9] The dynamic behavior of IDPs results in modulating the functions of their binding partners and in promoting the assembly of supramolecular complexes. The biological functions of IDPs are often controlled by post translation modifications, such as phosphorylation, ubiquitination, acetylation and alternative splicing.[67] The high abundance of IDPs on *S. pombe* and human cells suggest that the tight regulation of IDPs is likely to be an evolutionary conserved strategy to overcome the demand of multiple functions by a single

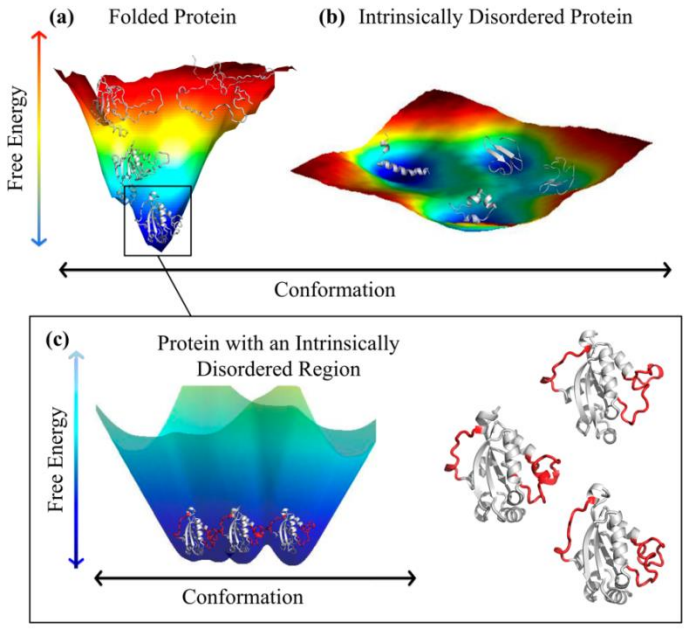

Figure 1.7 A schematic representation of energy landscapes for (a) a folded protein (human nucleoside diphosphate kinase (NDPK), PDB ID: 1nsk) and (b) an intrinsically disordered peptide (CcdA C-terminal, PDB ID: 3tcj); (c) for better visualization, close-up of the minimal free energy well shown, where IDRs are shown in red and ordered regions are shown in white. The lower free energy (dark blue) represents more probable conformations. Reproduced with permission from [65].

IDP.[68] The availability of IDPs in the different compartments of the cell requires fine-tuning by post translational modifications and via other regulatory strategies that would result in the

abundance and longer half-life of the proteins, by protection from the degradation machinery.[67] Therefore, in order to function properly in the cells, IDPs are tightly regulated at multiple levels.[69]

1.6 α-Synuclein in Parkinson's disease

α-Synuclein is an IDP, highly evolutionarily conserved and abundantly present in the central nervous system (CNS), particularly in presynaptic terminals of neurons.[70] It is a small protein of 140 amino acids and its sequence is divided into three distinct regions (Figure 1.8): positively charged N-terminal (1-60 amino acid) that is known to initiate the binding to the negatively charged membranes, a hydrophobic central region (61-95 amino acid) known as NAC region (non-amyloid β component of Alzheimer disease amyloid) which is known to form the amyloid core and negatively charged C-terminal (96-140 amino acid) which facilitates the binding of calcium and other ions.[71-75] α-Synuclein is an unstructured protein

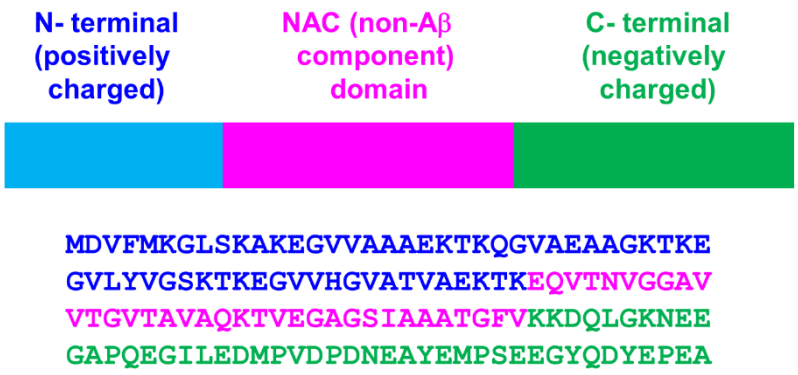

Figure 1.8 A schematic representation and amino acid sequence of α-synuclein. The amino acid sequence showing various regions of the protein: N-terminal (blue), NAC domain (pink) and C-terminal (green).

which does not have a particular structural conformation. The ensemble structures of α-synuclein were obtained by NMR and molecular simulation studies.[76-77] Figure 1.9 shows an overlay of 50 different conformations of α-synuclein. The precise function of α-synuclein is poorly understood, however, there are some putative functions, such as, it helps in synaptic transmission, synaptic vesicle localization and also maintenance of neuronal plasticity.[78-80]

A considerably large number of neurodegenerative diseases are linked with the amyloid formation of α-synuclein, such as PD, Lewy body variants of AD, multiple system atrophy and many others.[81] Single point mutations A30P, E46K and A53T in α-synuclein are linked with the familial form of PD. Recently, two other familial PD mutations were discovered that are localized in the central region of α-synuclein (G51D and H50Q).[82-84] Moreover, the E46K and H50Q PD mutations in the α-synuclein protein has been reported to accelerates its aggregation kinetics compared with the wild-type α-synuclein, but the G51D PD variant aggregate with longer lag time compared to wild-type protein.[85-87] Several mechanisms have been postulated for α-synuclein mediated cellular toxicity that result in cell death and are divided into two major classes: a toxic gain of function or a toxic loss of function.[88] Both the mechanisms include failure of the ubiquitin-proteasome system, oxidative stress, impaired axonal transport and mitochondrial damage. Although, it the involved cellular processes both these postulated mechanisms may not be mutually exclusive and could possibly act synergistically.

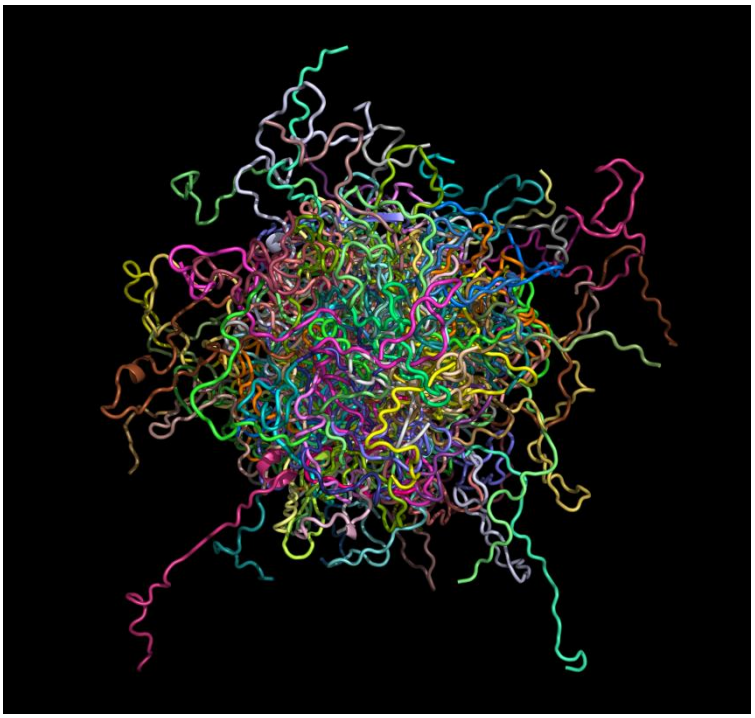

Figure 1.9 The structural ensemble of intrinsically disordered α-synuclein showing an overlay of 50 different structures taken from the protein ensemble database (PeDB: 9AAC) generated using PyMOL (Schrödinger, Inc. New York).[77]

The aggregation of α-synuclein follows a nucleation-dependent polymerization pathway, with a variable lag phase followed by an exponential phase.[32, 89] The lag phase or nucleation

phase is the rate limiting step and once the nucleus is formed, it progresses towards the elongation by the addition of monomeric α-synuclein. Many factors are known to affect the aggregation process, such as addition of α-synuclein oligomeric seeds,[90] pH variation,[91] presence of salt in the solution,[92] chemical modifications in the amino acid sequence by nitration, oxidation, phosphorylation, acetylation and many others,[89, 93-95] agitation of the solution and also the addition of anionic surfactants which can accelerate the amyloid formation of α-synuclein.[89, 96] PD linked point mutations, including A30P, E46K, and A53T have been shown to alter the fibrillization kinetics.[97] The soluble oligomeric intermediates of α-synuclein have been shown to be the most potent toxic species in both *in vivo* and *in vitro* system.[38-39, 47-48] However, some studies suggest that oligomeric and fibrillar species have a neuroprotective role in PD.[98] This protective role is also supported by the death of the dopaminergic neurons in PD conditions without the formation of Lewy bodies, raising the question about the precise role of α-synuclein in PD.

1.7 α-Synuclein interaction with membranes

α-Synuclein is present in the presynaptic terminal of the neurons and is known to interact with a SNARE (soluble N-ethyl maleimide sensitive factor attachment protein receptors) complex protein known as synaptobrevin which helps in neurotransmitters release into the presynaptic cleft of the neurons.[99-101] *In vivo* and *in vitro* studies showed that α-synuclein remains unstructured and adopts an α-helical structure in the membrane-bound state.[10, 81, 102] The precise balance between the membrane bound and unbound state plays a crucial role in the biological function of α-synuclein, including the regulation of synaptic plasticity and in the pathological aggregation of α-synuclein. The weak association of α-synuclein to lipid bilayers is important for its regulatory role at the synapse and is maintained because of the presence of imperfect 11 amino acid repeats, which resembles apolipoproteins.[103] Previous studies on α-synuclein interaction with sodium dodecyl sulphate (SDS, membrane mimetic) or negatively charged membranes, using solution-state NMR and EPR suggest that the first 100 amino acids adopt an extended helix structure.[104-107] Studies also shed light into the formation of α-synuclein -SDS complex having an alternative horseshoe conformation, which was supported by the interaction between α-synuclein and small unilamellar vesicles (SUVs) (Figure 1.10).[106-108] Presently, there is a consensus that the multiple conformations of α-synuclein on the membrane can be present and these conformations can undergo interconversions.[107, 109-110] The strong evidences suggest that the lipid-bound state of α-

synuclein is also regulated by the chemical and physical properties of the phospholipid bilayer, such as anionic charge, curvature, fluidity and many others.[111-114] It has been reported that α-synuclein binds to SUVs in preference to large unilamellar vesicles (LUVs) of a given composition.[103, 115] The membrane-bound structure of α-synuclein is believed to play a role in function as well as in the genesis of PD.

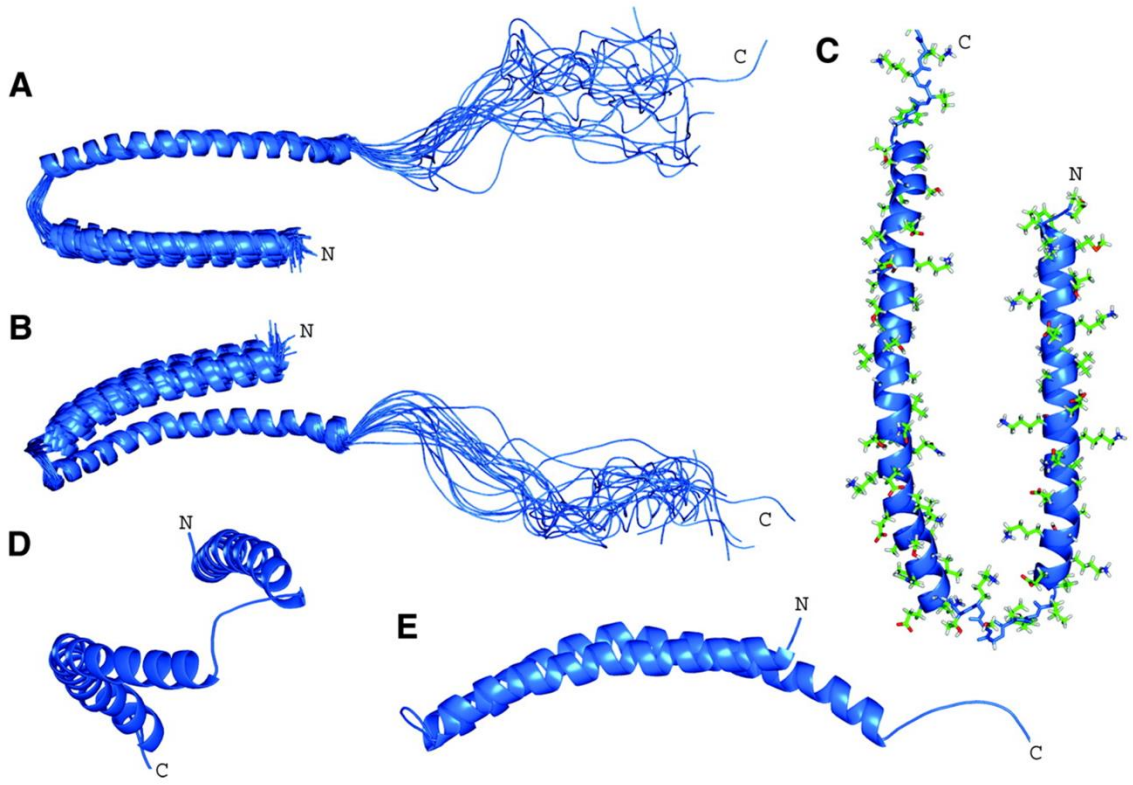

Figure 1.10 Structure of micelle-bound α-synuclein (A and B) ensemble of twenty structures superimposed on helix-C. Helix-N (Val3-Val37) and helix-C (Lys45-Thr92) are connected by a short linker, followed by another short extended region (Gly93-Lys97) and a predominantly unstructured tail (Asp98-Ala140). A (C–E) average of twenty structures is shown in different orientation. Reproduced with permission from [108].

1.8 α-Synuclein interaction with other IDPs in disease conditions

α-Synuclein is known to form amyloids in PD conditions.The molecular structure of α-synuclein amyloid fibrils is poorly understood. However, several studies using infrared spectroscopy,[116] small angle X-ray scattering,[117-118] nuclear magnetic resonance[21, 119] and electronic paramagnetic resonance[25, 120] provide insights into the structure of the fibrils and suggest that the NAC domain forms the solvent-protected core of the amyloids (Figures 1.11 A and B).[121-122] Recent high-resolution structural studies revealed the architecture of the toxic

core which is comprised of 11-residue peptide segment of the NAC domain of α-synuclein (Figures 1.11 C and 11D).[123] The amyloid formation of α-synuclein can be triggered independently or in the presence of other IDPs. The conformational plasticity of α-synuclein allows it to interact with multiple partners, including some IDPs, such as, islet amyloid polypeptide (IAPP),[124] tau[125] and Aβ peptide.[126]

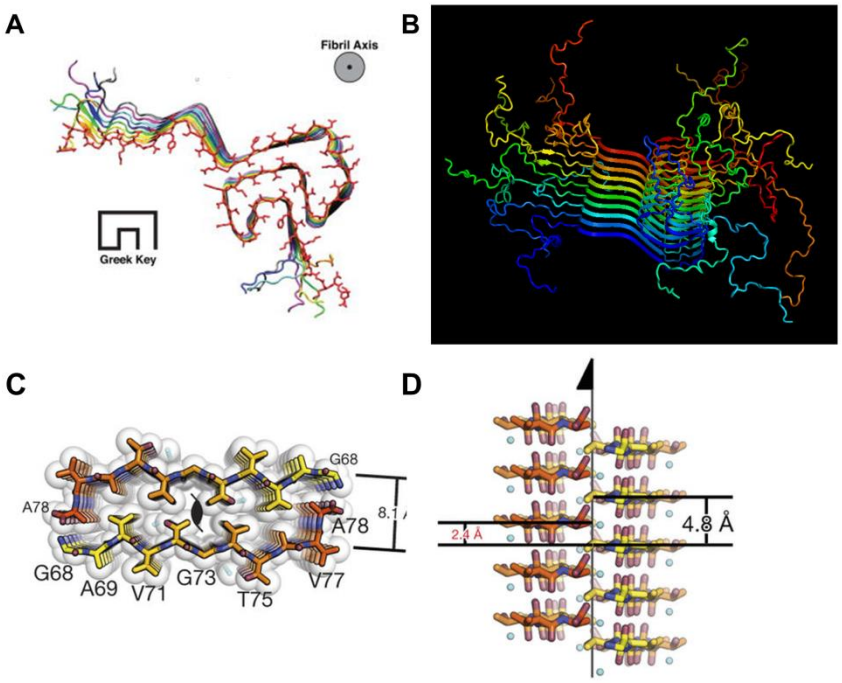

Figure 1.11 Three-dimensional structure of α-synuclein fibrils. (A) Residues 25 to 105 of eight monomers of full length α-synuclein showing the β-sheet alignment of each monomer in the ssNMR structure of the fibril and the Greek-key topology of the core, as viewed down the fibril axis. (B) Full length α-synuclein amyloid structure was taken from the protein data bank (PDB: 2n0a) and generated using PyMOL (Version 1.8, Schrödinger, LLC, New York) (C) The crystal structure of NACore (residue 68-78) region of α-synuclein reveals pairs of sheets in the spines of amyloid fibrils. (D) Orthogonal views of NACore region of the fibrillar assemblies. Reproduced with permission from [21 and 123].

A large body of evidence showed the pathological co-amyloids of these proteins are present in many neurological ailments.[80, 125, 127-128] Type II diabetes is a disease involving amyloid formation in the pancreas. Although, α-synuclein is predominantly present in the neuronal cells, it is also expressed in the pancreas, where it interacts with IAPP and results in the amyloid formation.[124] Additionally, the existences of pure synucleinopathies and tauopathies have emerged in many neurodegenerative diseases, which is supported by clinical

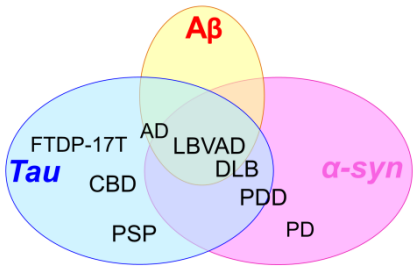

Figure 1.12 Overlap of proteinopathies. A large number of neurodegenerative disorders showed amyloid deposits composed of α-synuclein (α-syn) protein (pink circle), tau protein (blue circle) and Aβ peptide (orange circle). These neurodegenerative diseases are histopathologically classification on the basis of nature and localization of these proteins amyloid deposits in the nervous system. AD; Alzheimer's disease, CBD; corticobasal degeneration, DLB; dementia with Lewy bodies, FTDP-17T; frontotemporal dementia with parkinsonism linked to tau mutations on chromosome 17, LBVAD; Lewy body variant of AD, PD; Parkinson's disease, PDD; Parkinson's disease with dementia, PSP; progressive supranuclear palsy. Adapted from the reference [126].

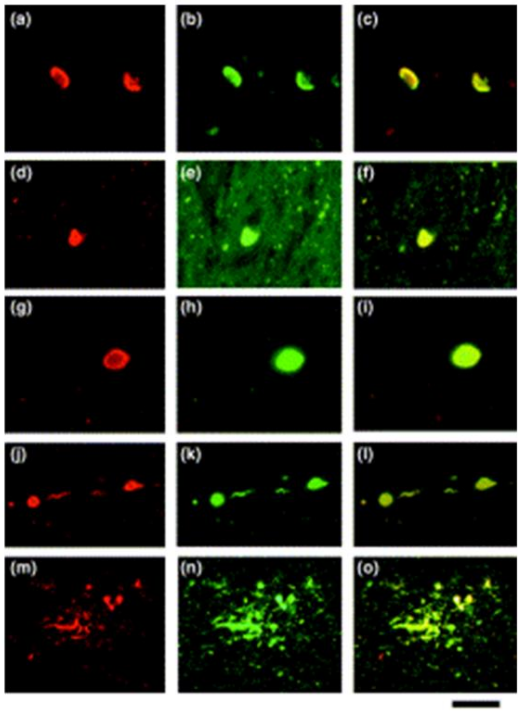

Figure 1.13 Colocalization of α-synuclein and tau in some pathological inclusions. Pathological lesions were stained by immunofluorescence with a rabbit anti-α-synuclein antibody (left panels; red) and a mouse anti-tau antibody (middle panels; green). The overlays of both stains are shown in the right panels. (a–c) In a multiple system atrophy patient, glial cytoplasmic inclusions observed in the cerebellar white matter (d–f) A Pick body in the hippocampus of a patient with Pick's disease. (g–i) A Lewy body and (j–l) spheroids in the substantia nigra pars compacta of a patient with Parkinson's disease. (m–o) Dystrophic neurites within a senile plaque of a patient with the Lewy Body variant of Alzheimer's disease. Scale bar, 20 mm for all panels. Reproduced with permission from [129].

observations and overlap between neurodegenerative disorders (Figure 1.12).[126, 129] Earlier studies have shown that in human brain, tau acts as a ligand for α-synuclein and that they co-localize in axons.[130] This intermolecular interaction is known to modulate the phosphorylation of tau and can potentially affect a variety of signaling pathways.[130] Recent evidences suggest that tau and α-synuclein interact to form pathological co-amyloids that are localized in different regions of the brain and are associated with several neurological diseases such as PD, AD, Down syndrome, multiple system atrophy, etc. (Figure 1.13).[129] *In vivo* studies also revealed that Aβ, tau and α-synuclein showed synergistic interactions, resulting in pathological amyloid formation.[129] Therefore, it is imperative to understand the molecular basis of these interactions, which might be useful for drug designing and for eliminating the harmful consequences.

1.9 Effect of molecular chaperones on α-synuclein aggregation

In order to prevent protein misfolding and aggregation, a group of proteins were evolved, known as molecular chaperones that help the misfolded or partially folded proteins to fold into their native structures.[131-132] Molecular chaperones are also known as heat shock protein (Hsp), found in almost all eukaryotic *organelles* and are highly conserved across phylogenetic boundaries.[132] Hsps are involved in critical cellular processes, such as, folding of nascent polypeptide chains, trafficking of proteins across membrane bilayers, prevention of aggregation as well as refolding of aggregated proteins, assembly of complexes, and biogenesis of Fe/S cluster prosthetic groups to ensure the overall cell homeostasis.[133-134] The Hsp70 family of molecular chaperones represent an abundant and ubiquitously expressed family of proteins which are located in different compartment of the cells, such as, cytoplasm, mitochondria and endoplasmic reticulum.[134] Hsp70 recognizes and binds to hydrophobic patches of misfolded or aggregated proteins in an ATP dependent manner.[133-134] Hsp70 family of protein are characterized by the presence of two functional domains: N-terminal domain containing the ATP binding site known as nucleotide binding domain (NBD) and C-terminal domain, which is known as substrate binding domain (SBD) connected with a highly conserved and hydrophobic linker segment (Figures 1.14).[135] These chaperones perform their function more effectively in the presence of their respective co-chaperones. Hsp40 is a co-chaperone of Hsp70 and plays a critical role in cellular protein homeostasis.[136-138] In *saccharomyces cerevisiae*, different paralogs of Hsp70 are present in

mitochondria: Ssc1, Ssq1 and Ssc3. Specifically, Ssc1 is abundantly present in the mitochondrial matrix and responsible for the vast majority of housekeeping functions.[139-140]

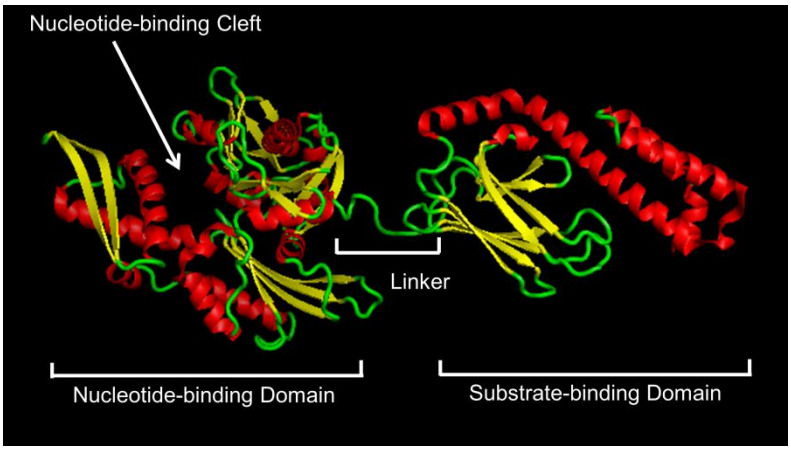

Figure 1.14 Crystal structure of the canonical Hsp70. The structure of full length Hsp70 in complex with ADP (PDB ID: 2KHO) was generated using PyMOL (Version 1.8, Schrödinger, LLC, New York) to indicate the various secondary structure elements (helices in red, sheets in yellow and random coil structure in green). The various domains and linker chain are indicated.

The pathological feature of PD involves dopaminergic neuronal death due to the deposition of protein aggregates known as Lewy bodies. These Lewy bodies are rich in heterogeneous protein aggregates of ubiquitin and α-synuclein along with a large number of molecular chaperones including Hsp70, Hsp40, Hsp60, Hsp90 and Hsp27.[141-143] Interestingly, despite the absence of mitochondria target signal sequence in α-synuclein, it translocates to the mitochondria under neuronal stress conditions and promotes mitochondrial dysfunction and oxidative stress.[144-146] Hsp70 is known to alter the aggregation kinetic of α-synuclein and solubilize the amyloids responsible for PD.[147] Further, a drosophila model of PD demonstrated that the overexpression of Hsp70 prevented the dopaminergic neuronal loss.[148] In mammalian system, such as mouse model, it has been established that overexpression of Hsp70 results in the reduction of high molecular weight insoluble α-synuclein species.[149] In drosophila, α-synuclein toxicity was found to be modified with a genetic modifier, tumor necrosis factor receptor associated protein-1 (TRAP1) which is a mitochondrial chaperone and its low expression results in the loss of dopaminergic neurons.[150] Phosphorylated TRAP1 is also implicated in PD.[151] These observations highlight the versatile nature of α-synuclein's interaction with cellular chaperones to overcome the detrimental effect of PD. The mechanism of α-synuclein interaction with chaperone still remains an area of active research. Therefore, the elucidation of α-synuclein amyloidogenesis is crucial for the understanding of its interaction with different partners in PD conditions.

1.10 Thesis motivation and perspective

Parkinson's disease is the second most common neurodegenerative disease after Alzheimer's disease and many treatments are geared towards the motor dysfunction symptoms in patients. In Parkinson's disease, the deposition of α-synuclein amyloids along with many other proteins were detected in the dopaminergic neurons projecting from the substantia nigra pars compacta that results in neuronal death. α-Synuclein is an intrinsically disordered protein; the rate of amyloid formation of α-synuclein and the species formed during the course of aggregation are believed to dictate the onset of Parkinson's diseases progression. Therefore, it is of significant interest to comprehend the molecular details of α-synuclein interaction with various partners which may lead to amyloid formation.

This thesis aims at uncovering the underlying molecular mechanism of interaction of α-synuclein with distinct partners using a wide array of biophysical techniques. α-Synuclein is known to bind with synaptic vesicles for the neurotransmitter release in the presynaptic terminal of neurons. In chapter 2, we utilized time-resolved fluorescence spectroscopy to gain the site-specific structural and dynamical insights of membrane-bound α-synuclein. Our time-resolved measurements allowed us to quantify the translational diffusion of α-synuclein on synthetic lipid membranes and also provided insights into the subtle alterations in the dynamics of membrane-bound α-synuclein, as a function of phospholipid head-group chemistry and membrane curvature (chapter 2). We believe that this interplay of membrane properties and α-synuclein diffusion might be of prime importance for its regulatory role in neurotransmitter release as well as in the etiology of PD progression (chapter 2). Additionally, the conformational plasticity of α-synuclein allows it to interact with tau protein (an amyloidogenic IDP, implicated in Alzheimer's disease) and form pathological amyloids in many neurodegenerative diseases. In chapter 3, we demonstrate the heterotypic association of early and late interaction of α-synuclein and tau (chapter 3) in the pathologically relevant condition. In chapter 4, we shed light into the amyloid dissociation regulated in the presence of molecular chaperons. We embarked upon understanding the effect of chaperones on α-synuclein aggregation to overcome the detrimental effect of amyloids (chapter 4). I believe that the work embodied in this thesis will improve our current understanding towards the α-synuclein interaction with multiple partners which might trigger the amyloid formation and provide molecular insights for the designing of therapeutic agents to combat the deadly neurodegenerative diseases.

1.11 References:

1. Dobson, C. M.; Šali, A.; Karplus, M., Protein Folding: A Perspective from Theory and Experiment. *Angewandte Chemie International Edition* **1998,** *37* (7), 868-893.

2. Udgaonkar, J. B., Multiple routes and structural heterogeneity in protein folding. *Annu Rev Biophys* **2008,** *37*, 489-510.

3. Wolynes, P. G.; Onuchic, J. N.; Thirumalai, D., Navigating the folding routes. *Science* **1995,** *267* (5204), 1619-20.

4. Dill, K. A.; Chan, H. S., From Levinthal to pathways to funnels. *Nat Struct Biol* **1997,** *4* (1), 10-9.

5. Jahn, T. R.; Radford, S. E., The Yin and Yang of protein folding. *Febs J* **2005,** *272* (23), 5962-70.

6. Hartl, F. U.; Hayer-Hartl, M., Converging concepts of protein folding in vitro and in vivo. *Nat Struct Mol Biol* **2009,** *16* (6), 574-81.

7. Nussinov, R.; Udgaonkar, J. B., Editorial overview: Folding and binding: Dynamic conformational heterogeneity is pivotal to cell life. *Curr Opin Struct Biol* **2016,** *36* (10), 9.

8. Dobson, C. M., Protein folding and misfolding. *Nature* **2003,** *426* (6968), 884-90.

9. Hartl, F. U., Molecular chaperones in cellular protein folding. *Nature* **1996,** *381* (6583), 571-9.

10. Chiti, F.; Dobson, C. M., Protein misfolding, functional amyloid, and human disease. *Annu Rev Biochem* **2006,** *75*, 333-66.

11. Hartl, F. U.; Bracher, A.; Hayer-Hartl, M., Molecular chaperones in protein folding and proteostasis. *Nature* **2011,** *475* (7356), 324-32.

12. Chaari, A.; Hoarau-Vechot, J.; Ladjimi, M., Applying chaperones to protein-misfolding disorders: molecular chaperones against alpha-synuclein in Parkinson's disease. *Int J Biol Macromol* **2013,** *60*, 196-205.

13. Morris, A. M.; Watzky, M. A.; Finke, R. G., Protein aggregation kinetics, mechanism, and curve-fitting: a review of the literature. *Biochim Biophys Acta* **2009,** *3*, 375-97.

14. Miranker, A. D., Unzipping the mysteries of amyloid fiber formation. *Proc Natl Acad Sci U S A* **2004,** *101* (13), 4335-6.

15. Eisenberg, D.; Jucker, M., The amyloid state of proteins in human diseases. *Cell* **2012,** *148* (6), 1188-203.

16. Rochet, J.-C.; Lansbury, P. T., Amyloid fibrillogenesis: themes and variations. *Current Opinion in Structural Biology* **2000,** *10* (1), 60-68.

17. Chiti, F.; Dobson, C. M., Protein Misfolding, Amyloid Formation, and Human Disease: A Summary of Progress Over the Last Decade. *Annu Rev Biochem* **2017,** *86*, 27-68.

18. Soto, C., Unfolding the role of protein misfolding in neurodegenerative diseases. *Nat Rev Neurosci* **2003,** *4* (1), 49-60.

19. Greenwald, J.; Riek, R., Biology of Amyloid: Structure, Function, and Regulation. *Structure* **2010,** *18* (10), 1244-1260.

20. Westermark, G. T.; Johnson, K. H.; Westermark, P., Staining methods for identification of amyloid in tissue. *Methods Enzymol* **1999,** *309*, 3-25.

21. Tuttle, M. D.; Comellas, G.; Nieuwkoop, A. J.; Covell, D. J.; Berthold, D. A.; Kloepper, K. D.; Courtney, J. M.; Kim, J. K.; Barclay, A. M.; Kendall, A.; Wan, W.; Stubbs, G.; Schwieters, C. D.; Lee, V. M.; George, J. M.; Rienstra, C. M., Solid-state NMR structure of a pathogenic fibril of full-length human alpha-synuclein. *Nat Struct Mol Biol* **2016,** *23* (5), 409-15.

22. Wälti, M. A.; Orts, J.; Riek, R., Quenched hydrogen-deuterium exchange NMR of a disease-relevant Aβ(1-42) amyloid polymorph. *PLOS ONE* **2017,** *12* (3), e0172862.

23. Gremer, L.; Scholzel, D.; Schenk, C.; Reinartz, E.; Labahn, J.; Ravelli, R. B. G.; Tusche, M.; Lopez-Iglesias, C.; Hoyer, W.; Heise, H.; Willbold, D.; Schroder, G. F., Fibril structure of amyloid-beta(1-42) by cryo-electron microscopy. *Science* **2017,** *358* (6359), 116-119.

24. Sunde, M.; Serpell, L. C.; Bartlam, M.; Fraser, P. E.; Pepys, M. B.; Blake, C. C., Common core structure of amyloid fibrils by synchrotron X-ray diffraction. *J Mol Biol* **1997,** *273* (3), 729-39.

25. Chen, M.; Margittai, M.; Chen, J.; Langen, R., Investigation of alpha-synuclein fibril structure by site-directed spin labeling. *J Biol Chem* **2007,** *282* (34), 24970-9.

26. Iwata, K.; Fujiwara, T.; Matsuki, Y.; Akutsu, H.; Takahashi, S.; Naiki, H.; Goto, Y., 3D structure of amyloid protofilaments of β₂-microglobulin fragment probed by solid-state NMR. *Proceedings of the National Academy of Sciences* **2006,** *103* (48), 18119-18124.

27. Shewmaker, F.; McGlinchey, R. P.; Wickner, R. B., Structural insights into functional and pathological amyloid. *J Biol Chem* **2011,** *286* (19), 16533-40.

28. Petkova, A. T.; Buntkowsky, G.; Dyda, F.; Leapman, R. D.; Yau, W. M.; Tycko, R., Solid state NMR reveals a pH-dependent antiparallel beta-sheet registry in fibrils formed by a beta-amyloid peptide. *J Mol Biol* **2004,** *335* (1), 247-60.

29. Perutz, M. F.; Finch, J. T.; Berriman, J.; Lesk, A., Amyloid fibers are water-filled nanotubes. *Proceedings of the National Academy of Sciences of the United States of America* **2002,** *99* (8), 5591-5595.

30. Krishnan, R.; Lindquist, S. L., Structural insights into a yeast prion illuminate nucleation and strain diversity. *Nature* **2005,** *435*, 765.

31. Liu, Y.; Gotte, G.; Libonati, M.; Eisenberg, D., A domain-swapped RNase A dimer with implications for amyloid formation. *Nature Structural Biology* **2001,** *8*, 211.

32. Ferrone, F., Analysis of protein aggregation kinetics. *Methods Enzymol* **1999,** *309*, 256-74.

33. Oosawa, F.; Kasai, M., A theory of linear and helical aggregations of macromolecules. *J Mol Biol* **1962,** *4*, 10-21.

34. Invernizzi, G.; Papaleo, E.; Sabate, R.; Ventura, S., Protein aggregation: mechanisms and functional consequences. *Int J Biochem Cell Biol* **2012,** *44* (9), 1541-54.

35. Frieden, C., Protein aggregation processes: In search of the mechanism. *Protein Sci* **2007,** *16* (11), 2334-44.

36. Dovidchenko, N. V.; Leonova, E. I.; Galzitskaya, O. V., Mechanisms of amyloid fibril formation. *Biochemistry* **2014,** *79* (13), 1515-27.

37. Carulla, N.; Caddy, G. L.; Hall, D. R.; Zurdo, J.; Gairi, M.; Feliz, M.; Giralt, E.; Robinson, C. V.; Dobson, C. M., Molecular recycling within amyloid fibrils. *Nature* **2005,** *436* (7050), 554-8.

38. Baglioni, S.; Casamenti, F.; Bucciantini, M.; Luheshi, L. M.; Taddei, N.; Chiti, F.; Dobson, C. M.; Stefani, M., Prefibrillar amyloid aggregates could be generic toxins in higher organisms. *J Neurosci* **2006,** *26* (31), 8160-7.

39. Campioni, S.; Mannini, B.; Zampagni, M.; Pensalfini, A.; Parrini, C.; Evangelisti, E.; Relini, A.; Stefani, M.; Dobson, C. M.; Cecchi, C.; Chiti, F., A causative link between the structure of aberrant protein oligomers and their toxicity. *Nat Chem Biol* **2010,** *6* (2), 140-7.

40. McLean, C. A.; Cherny, R. A.; Fraser, F. W.; Fuller, S. J.; Smith, M. J.; Beyreuther, K.; Bush, A. I.; Masters, C. L., Soluble pool of Abeta amyloid as a determinant of severity of neurodegeneration in Alzheimer's disease. *Ann Neurol* **1999,** *46* (6), 860-6.

41. Shankar, G. M.; Li, S.; Mehta, T. H.; Garcia-Munoz, A.; Shepardson, N. E.; Smith, I.; Brett, F. M.; Farrell, M. A.; Rowan, M. J.; Lemere, C. A.; Regan, C. M.; Walsh, D. M.; Sabatini, B. L.; Selkoe, D. J., Amyloid β-Protein Dimers Isolated Directly from Alzheimer Brains Impair Synaptic Plasticity and Memory. *Nature medicine* **2008,** *14* (8), 837-842.

42. Cheng, I. H.; Scearce-Levie, K.; Legleiter, J.; Palop, J. J.; Gerstein, H.; Bien-Ly, N.; Puolivali, J.; Lesne, S.; Ashe, K. H.; Muchowski, P. J.; Mucke, L., Accelerating amyloid-beta fibrillization reduces oligomer levels and functional deficits in Alzheimer disease mouse models. *J Biol Chem* **2007,** *282* (33), 23818-28.

43. Dueholm, M. S.; Albertsen, M.; Otzen, D.; Nielsen, P. H., Curli Functional Amyloid Systems Are Phylogenetically Widespread and Display Large Diversity in Operon and Protein Structure. *PLOS ONE* **2012,** *7* (12), e51274.

44. Blanco, L. P.; Evans, M. L.; Smith, D. R.; Badtke, M. P.; Chapman, M. R., Diversity, biogenesis and function of microbial amyloids. *Trends in Microbiology* **2012,** *20* (2), 66-73.

45. Kushnirov, V. V.; Vishnevskaya, A. B.; Alexandrov, I. M.; Ter-Avanesyan, M. D., Prion and Nonprion Amyloids: A Comparison Inspired by the Yeast Sup35 Protein. *Prion* **2007,** *1* (3), 179-184.

46. Fowler, D. M.; Koulov, A. V.; Alory-Jost, C.; Marks, M. S.; Balch, W. E.; Kelly, J. W., Functional amyloid formation within mammalian tissue. *PLoS Biol* **2006,** *4* (1), 0040006.

47. Fusco, G.; Chen, S. W.; Williamson, P. T. F.; Cascella, R.; Perni, M.; Jarvis, J. A.; Cecchi, C.; Vendruscolo, M.; Chiti, F.; Cremades, N.; Ying, L.; Dobson, C. M.; De Simone, A., Structural basis of membrane disruption and cellular toxicity by alpha-synuclein oligomers. *Science* **2017,** *358* (6369), 1440-1443.

48. Chen, S. W.; Drakulic, S.; Deas, E.; Ouberai, M.; Aprile, F. A.; Arranz, R.; Ness, S.; Roodveldt, C.; Guilliams, T.; De-Genst, E. J.; Klenerman, D.; Wood, N. W.; Knowles, T. P.; Alfonso, C.; Rivas, G.; Abramov, A. Y.; Valpuesta, J. M.; Dobson, C. M.; Cremades, N., Structural characterization of toxic oligomers that are kinetically trapped during alpha-synuclein fibril formation. *Proc Natl Acad Sci U S A* **2015,** *112* (16), 8.

49. Kriwacki, R. W.; Hengst, L.; Tennant, L.; Reed, S. I.; Wright, P. E., Structural studies of p21Waf1/Cip1/Sdi1 in the free and Cdk2-bound state: conformational disorder mediates binding diversity. *Proc Natl Acad Sci U S A* **1996,** *93* (21), 11504-9.

50. Wright, P. E.; Dyson, H. J., Intrinsically unstructured proteins: re-assessing the protein structure-function paradigm. *J Mol Biol* **1999,** *293* (2), 321-31.

51. Uversky, V. N.; Gillespie, J. R.; Fink, A. L., Why are "natively unfolded" proteins unstructured under physiologic conditions? *Proteins* **2000,** *41* (3), 415-27.

52. Dunker, A. K.; Obradovic, Z.; Romero, P.; Garner, E. C.; Brown, C. J., Intrinsic protein disorder in complete genomes. *Genome Inform Ser Workshop Genome Inform* **2000,** *11*, 161-71.

53. Dunker, A. K.; Brown, C. J.; Lawson, J. D.; Iakoucheva, L. M.; Obradovic, Z., Intrinsic disorder and protein function. *Biochemistry* **2002,** *41* (21), 6573-82.

54. Tompa, P., Intrinsically unstructured proteins. *Trends Biochem Sci* **2002,** *27* (10), 527-33.

55. Ward, J. J.; Sodhi, J. S.; McGuffin, L. J.; Buxton, B. F.; Jones, D. T., Prediction and functional analysis of native disorder in proteins from the three kingdoms of life. *J Mol Biol* **2004,** *337* (3), 635-45.

56. Fink, A. L., Natively unfolded proteins. *Curr Opin Struct Biol* **2005,** *15* (1), 35-41.

57. Dyson, H. J.; Wright, P. E., Intrinsically unstructured proteins and their functions. *Nat Rev Mol Cell Biol* **2005,** *6* (3), 197-208.

58. Gsponer, J.; Babu, M. M., The rules of disorder or why disorder rules. *Prog Biophys Mol Biol* **2009,** *99* (2-3), 94-103.

59. Dunker, A. K.; Babu, M. M.; Barbar, E.; Blackledge, M.; Bondos, S. E.; Dosztányi, Z.; Dyson, H. J.; Forman-Kay, J.; Fuxreiter, M.; Gsponer, J.; Han, K.-H.; Jones, D. T.; Longhi, S.; Metallo, S. J.; Nishikawa, K.; Nussinov, R.; Obradovic, Z.; Pappu, R. V.; Rost, B.; Selenko, P.; Subramaniam, V.; Sussman, J. L.; Tompa, P.; Uversky, V. N., What's in a name? Why these proteins are intrinsically disordered: Why these proteins are intrinsically disordered. *Intrinsically Disordered Proteins* **2013,** *1* (1), e24157.

60. Tompa, P., Intrinsically disordered proteins: a 10-year recap. *Trends Biochem Sci* **2012,** *37* (12), 509-16.

61. Uversky, V. N.; Dunker, A. K., Understanding protein non-folding. *Biochim Biophys Acta* **2010,** *6* (64), 1.

62. Forman-Kay, Julie D.; Mittag, T., From Sequence and Forces to Structure, Function, and Evolution of Intrinsically Disordered Proteins. *Structure 21* (9), 1492-1499.

63. Theillet, F.-X.; Binolfi, A.; Frembgen-Kesner, T.; Hingorani, K.; Sarkar, M.; Kyne, C.; Li, C.; Crowley, P. B.; Gierasch, L.; Pielak, G. J.; Elcock, A. H.; Gershenson, A.; Selenko, P., Physicochemical Properties of Cells and Their Effects on Intrinsically Disordered Proteins (IDPs). *Chemical reviews* **2014,** *114* (13), 6661-6714.

64. Xie, H.; Vucetic, S.; Iakoucheva, L. M.; Oldfield, C. J.; Dunker, A. K.; Uversky, V. N.; Obradovic, Z., Functional anthology of intrinsic disorder. 1. Biological processes and functions of proteins with long disordered regions. *J Proteome Res* **2007,** *6* (5), 1882-98.

65. Burger, M. V.; Gurry, T.; Stultz, M. C., Intrinsically Disordered Proteins: Where Computation Meets Experiment. *Polymers* **2014,** *6* (10).

66. Babu, M. M.; van der Lee, R.; de Groot, N. S.; Gsponer, J., Intrinsically disordered proteins: regulation and disease. *Curr Opin Struct Biol* **2011,** *21* (3), 432-40.

67. Uversky, V. N., Intrinsic disorder-based protein interactions and their modulators. *Curr Pharm Des* **2013,** *19* (23), 4191-213.

68. Gsponer, J.; Futschik, M. E.; Teichmann, S. A.; Babu, M. M., Tight Regulation of Unstructured Proteins: From Transcript Synthesis to Protein Degradation. *Science* **2008,** *322* (5906), 1365-1368.

69. van der Lee, R.; Buljan, M.; Lang, B.; Weatheritt, R. J.; Daughdrill, G. W.; Dunker, A. K.; Fuxreiter, M.; Gough, J.; Gsponer, J.; Jones, D. T.; Kim, P. M.; Kriwacki, R. W.; Oldfield, C. J.; Pappu, R. V.; Tompa, P.; Uversky, V. N.; Wright, P. E.; Babu, M. M., Classification of Intrinsically Disordered Regions and Proteins. *Chemical reviews* **2014,** *114* (13), 6589-6631.

70. Mori, F.; Tanji, K.; Yoshimoto, M.; Takahashi, H.; Wakabayashi, K., Demonstration of alpha-synuclein immunoreactivity in neuronal and glial cytoplasm in normal human brain tissue using proteinase K and formic acid pretreatment. *Exp Neurol* **2002,** *176* (1), 98-104.

71. Yap, T. L.; Pfefferkorn, C. M.; Lee, J. C., Residue-specific fluorescent probes of alpha-synuclein: detection of early events at the N- and C-termini during fibril assembly. *Biochemistry* **2011,** *50* (12), 1963-5.

72. Pfefferkorn, C. M.; Jiang, Z.; Lee, J. C., Biophysics of α-synuclein membrane interactions. *Biochimica et Biophysica Acta (BBA) - Biomembranes* **2012,** *1818* (2), 162-171.

73. Deleersnijder, A.; Gerard, M.; Debyser, Z.; Baekelandt, V., The remarkable conformational plasticity of alpha-synuclein: blessing or curse? *Trends Mol Med* **2013,** *19* (6), 368-77.

74. Souza, J. M.; Giasson, B. I.; Lee, V. M.; Ischiropoulos, H., Chaperone-like activity of synucleins. *FEBS Lett* **2000,** *474* (1), 116-9.

75. Kim, T. D.; Paik, S. R.; Yang, C. H., Structural and functional implications of C-terminal regions of alpha-synuclein. *Biochemistry* **2002,** *41* (46), 13782-90.

76. Allison, J. R.; Rivers, R. C.; Christodoulou, J. C.; Vendruscolo, M.; Dobson, C. M., A relationship between the transient structure in the monomeric state and the aggregation propensities of alpha-synuclein and beta-synuclein. *Biochemistry* **2014,** *53* (46), 7170-83.

77. Allison, J. R.; Varnai, P.; Dobson, C. M.; Vendruscolo, M., Determination of the Free Energy Landscape of α-Synuclein Using Spin Label Nuclear Magnetic Resonance Measurements. *Journal of the American Chemical Society* **2009,** *131* (51), 18314-18326.

78. Watson, J. B.; Hatami, A.; David, H.; Masliah, E.; Roberts, K.; Evans, C. E.; Levine, M. S., Alterations in corticostriatal synaptic plasticity in mice overexpressing human alpha-synuclein. *Neuroscience* **2009,** *159* (2), 501-13.

79. Cooper, A. A.; Gitler, A. D.; Cashikar, A.; Haynes, C. M.; Hill, K. J.; Bhullar, B.; Liu, K.; Xu, K.; Strathearn, K. E.; Liu, F.; Cao, S.; Caldwell, K. A.; Caldwell, G. A.;

Marsischky, G.; Kolodner, R. D.; Labaer, J.; Rochet, J. C.; Bonini, N. M.; Lindquist, S., Alpha-synuclein blocks ER-Golgi traffic and Rab1 rescues neuron loss in Parkinson's models. *Science* **2006,** *313* (5785), 324-8.

80. Nath, A.; Rhoades, E., A flash in the pan: dissecting dynamic amyloid intermediates using fluorescence. *FEBS Lett* **2013,** *587* (8), 1096-105.

81. Goedert, M., Alpha-synuclein and neurodegenerative diseases. *Nat Rev Neurosci* **2001,** *2* (7), 492-501.

82. Xu, L.; Ma, B.; Nussinov, R.; Thompson, D., Familial Mutations May Switch Conformational Preferences in alpha-Synuclein Fibrils. *ACS Chem Neurosci* **2017,** *8* (4), 837-849.

83. Ono, K.; Ikeda, T.; Takasaki, J.; Yamada, M., Familial Parkinson disease mutations influence alpha-synuclein assembly. *Neurobiol Dis* **2011,** *43* (3), 715-24.

84. Proukakis, C.; Dudzik, C. G.; Brier, T.; MacKay, D. S.; Cooper, J. M.; Millhauser, G. L.; Houlden, H.; Schapira, A. H., A novel α-synuclein missense mutation in Parkinson disease. *Neurology* **2013,** *80* (11), 1062-1064.

85. Fredenburg, R. A.; Rospigliosi, C.; Meray, R. K.; Kessler, J. C.; Lashuel, H. A.; Eliezer, D.; Lansbury, P. T., Jr., The impact of the E46K mutation on the properties of alpha-synuclein in its monomeric and oligomeric states. *Biochemistry* **2007,** *46* (24), 7107-18.

86. Ghosh, D.; Mondal, M.; Mohite, G. M.; Singh, P. K.; Ranjan, P.; Anoop, A.; Ghosh, S.; Jha, N. N.; Kumar, A.; Maji, S. K., The Parkinson's disease-associated H50Q mutation accelerates alpha-Synuclein aggregation in vitro. *Biochemistry* **2013,** *52* (40), 6925-7.

87. Fares, M. B.; Ait-Bouziad, N.; Dikiy, I.; Mbefo, M. K.; Jovicic, A.; Kiely, A.; Holton, J. L.; Lee, S. J.; Gitler, A. D.; Eliezer, D.; Lashuel, H. A., The novel Parkinson's disease linked mutation G51D attenuates in vitro aggregation and membrane binding of alpha-synuclein, and enhances its secretion and nuclear localization in cells. *Hum Mol Genet* **2014,** *23* (17), 4491-509.

88. Rajagopalan, S.; Andersen, J. K., Alpha synuclein aggregation: is it the toxic gain of function responsible for neurodegeneration in Parkinson's disease? *Mech Ageing Dev* **2001,** *122* (14), 1499-510.

89. Uversky, V. N.; Eliezer, D., Biophysics of Parkinson's disease: structure and aggregation of alpha-synuclein. *Curr Protein Pept Sci* **2009,** *10* (5), 483-99.

90. Luk, K. C.; Song, C.; O'Brien, P.; Stieber, A.; Branch, J. R.; Brunden, K. R.; Trojanowski, J. Q.; Lee, V. M.-Y., Exogenous α-synuclein fibrils seed the formation of Lewy

body-like intracellular inclusions in cultured cells. *Proceedings of the National Academy of Sciences* **2009,** *106* (47), 20051-20056.

91. Bernstein, S. L.; Liu, D.; Wyttenbach, T.; Bowers, M. T.; Lee, J. C.; Gray, H. B.; Winkler, J. R., Alpha-synuclein: stable compact and extended monomeric structures and pH dependence of dimer formation. *J Am Soc Mass Spectrom* **2004,** *15* (10), 1435-43.

92. Uversky, V. N.; Li, J.; Fink, A. L., Metal-triggered structural transformations, aggregation, and fibrillation of human alpha-synuclein. A possible molecular NK between Parkinson's disease and heavy metal exposure. *J Biol Chem* **2001,** *276* (47), 44284-96.

93. Uversky, V. N.; Yamin, G.; Munishkina, L. A.; Karymov, M. A.; Millett, I. S.; Doniach, S.; Lyubchenko, Y. L.; Fink, A. L., Effects of nitration on the structure and aggregation of alpha-synuclein. *Brain Res Mol Brain Res* **2005,** *134* (1), 84-102.

94. Glaser, C. B.; Yamin, G.; Uversky, V. N.; Fink, A. L., Methionine oxidation, alpha-synuclein and Parkinson's disease. *Biochim Biophys Acta* **2005,** *17* (2), 157-69.

95. Fujiwara, H.; Hasegawa, M.; Dohmae, N.; Kawashima, A.; Masliah, E.; Goldberg, M. S.; Shen, J.; Takio, K.; Iwatsubo, T., alpha-Synuclein is phosphorylated in synucleinopathy lesions. *Nat Cell Biol* **2002,** *4* (2), 160-4.

96. Necula, M.; Chirita, C. N.; Kuret, J., Rapid anionic micelle-mediated alpha-synuclein fibrillization in vitro. *J Biol Chem* **2003,** *278* (47), 46674-80.

97. Flagmeier, P.; Meisl, G.; Vendruscolo, M.; Knowles, T. P. J.; Dobson, C. M.; Buell, A. K.; Galvagnion, C., Mutations associated with familial Parkinson's disease alter the initiation and amplification steps of α-synuclein aggregation. *Proceedings of the National Academy of Sciences of the United States of America* **2016,** *113* (37), 10328-10333.

98. Manecka, D.-L.; Vanderperre, B.; Fon, E. A.; Durcan, T. M., The Neuroprotective Role of Protein Quality Control in Halting the Development of Alpha-Synuclein Pathology. *Frontiers in Molecular Neuroscience* **2017,** *10*, 311.

99. Burre, J.; Sharma, M.; Tsetsenis, T.; Buchman, V.; Etherton, M. R.; Sudhof, T. C., Alpha-synuclein promotes SNARE-complex assembly in vivo and in vitro. *Science* **2010,** *329* (5999), 1663-7.

100. Burre, J.; Sharma, M.; Sudhof, T. C., alpha-Synuclein assembles into higher-order multimers upon membrane binding to promote SNARE complex formation. *Proc Natl Acad Sci U S A* **2014,** *111* (40), 22.

101. Lai, Y.; Kim, S.; Varkey, J.; Lou, X.; Song, J.-K.; Diao, J.; Langen, R.; Shin, Y.-K., Nonaggregated α-Synuclein Influences SNARE-Dependent Vesicle Docking via Membrane Binding. *Biochemistry* **2014,** *53* (24), 3889-3896.

102. Lee, H. J.; Choi, C.; Lee, S. J., Membrane-bound alpha-synuclein has a high aggregation propensity and the ability to seed the aggregation of the cytosolic form. *J Biol Chem* **2002,** *277* (1), 671-8.

103. Davidson, W. S.; Jonas, A.; Clayton, D. F.; George, J. M., Stabilization of alpha-synuclein secondary structure upon binding to synthetic membranes. *J Biol Chem* **1998,** *273* (16), 9443-9.

104. Bussell, R., Jr.; Eliezer, D., A structural and functional role for 11-mer repeats in alpha-synuclein and other exchangeable lipid binding proteins. *J Mol Biol* **2003,** *329* (4), 763-78.

105. Jao, C. C.; Der-Sarkissian, A.; Chen, J.; Langen, R., Structure of membrane-bound alpha-synuclein studied by site-directed spin labeling. *Proc Natl Acad Sci U S A* **2004,** *101* (22), 8331-6.

106. Chandra, S.; Chen, X.; Rizo, J.; Jahn, R.; Sudhof, T. C., A broken alpha -helix in folded alpha -Synuclein. *J Biol Chem* **2003,** *278* (17), 15313-8.

107. Bisaglia, M.; Trolio, A.; Bellanda, M.; Bergantino, E.; Bubacco, L.; Mammi, S., Structure and topology of the non-amyloid-β component fragment of human α-synuclein bound to micelles: Implications for the aggregation process. *Protein Science : A Publication of the Protein Society* **2006,** *15* (6), 1408-1416.

108. Ulmer, T. S.; Bax, A.; Cole, N. B.; Nussbaum, R. L., Structure and dynamics of micelle-bound human alpha-synuclein. *J Biol Chem* **2005,** *280* (10), 9595-603.

109. Robotta, M.; Braun, P.; van Rooijen, B.; Subramaniam, V.; Huber, M.; Drescher, M., Direct Evidence of Coexisting Horseshoe and Extended Helix Conformations of Membrane-Bound Alpha-Synuclein. *ChemPhysChem* **2011,** *12* (2), 267-269.

110. Bodner, C. R.; Dobson, C. M.; Bax, A., Multiple tight phospholipid-binding modes of alpha-synuclein revealed by solution NMR spectroscopy. *J Mol Biol* **2009,** *390* (4), 775-90.

111. Braun, A. R.; Sevcsik, E.; Chin, P.; Rhoades, E.; Tristram-Nagle, S.; Sachs, J. N., α-Synuclein Induces Both Positive Mean Curvature and Negative Gaussian Curvature in Membranes. *Journal of the American Chemical Society* **2012,** *134* (5), 2613-2620.

112. Ouberai, M. M.; Wang, J.; Swann, M. J.; Galvagnion, C.; Guilliams, T.; Dobson, C. M.; Welland, M. E., alpha-Synuclein senses lipid packing defects and induces lateral expansion of lipids leading to membrane remodeling. *J Biol Chem* **2013,** *288* (29), 20883-95.

113. Pandey, A. P.; Haque, F.; Rochet, J. C.; Hovis, J. S., alpha-Synuclein-induced tubule formation in lipid bilayers. *J Phys Chem B* **2011,** *115* (19), 5886-93.

114. Varkey, J.; Isas, J. M.; Mizuno, N.; Jensen, M. B.; Bhatia, V. K.; Jao, C. C.; Petrlova, J.; Voss, J. C.; Stamou, D. G.; Steven, A. C.; Langen, R., Membrane curvature induction and tubulation are common features of synucleins and apolipoproteins. *J Biol Chem* **2010,** *285* (42), 32486-93.

115. Nuscher, B.; Kamp, F.; Mehnert, T.; Odoy, S.; Haass, C.; Kahle, P. J.; Beyer, K., Alpha-synuclein has a high affinity for packing defects in a bilayer membrane: a thermodynamics study. *J Biol Chem* **2004,** *279* (21), 21966-75.

116. Miller, L. M.; Bourassa, M. W.; Smith, R. J., FTIR spectroscopic imaging of protein aggregation in living cells. *Biochim Biophys Acta* **2013,** *10* (46), 25.

117. Giehm, L.; Svergun, D. I.; Otzen, D. E.; Vestergaard, B., Low-resolution structure of a vesicle disrupting α-synuclein oligomer that accumulates during fibrillation. *Proc Natl Acad Sci U S A* **2011,** *108* (8), 3246-51.

118. Serpell, L. C.; Berriman, J.; Jakes, R.; Goedert, M.; Crowther, R. A., Fiber diffraction of synthetic alpha-synuclein filaments shows amyloid-like cross-beta conformation. *Proc Natl Acad Sci U S A* **2000,** *97* (9), 4897-902.

119. Heise, H.; Hoyer, W.; Becker, S.; Andronesi, O. C.; Riedel, D.; Baldus, M., Molecular-level secondary structure, polymorphism, and dynamics of full-length alpha-synuclein fibrils studied by solid-state NMR. *Proc Natl Acad Sci U S A* **2005,** *102* (44), 15871-6.

120. Der-Sarkissian, A.; Jao, C. C.; Chen, J.; Langen, R., Structural organization of alpha-synuclein fibrils studied by site-directed spin labeling. *J Biol Chem* **2003,** *278* (39), 37530-5.

121. Xu, L.; Nussinov, R.; Ma, B., Coupling of the non-amyloid-component (NAC) domain and the KTK(E/Q)GV repeats stabilize the alpha-synuclein fibrils. *Eur J Med Chem* **2016,** *121*, 841-850.

122. de Oliveira, G. A.; Marques, M. A.; Cruzeiro-Silva, C.; Cordeiro, Y.; Schuabb, C.; Moraes, A. H.; Winter, R.; Oschkinat, H.; Foguel, D.; Freitas, M. S.; Silva, J. L., Structural basis for the dissociation of alpha-synuclein fibrils triggered by pressure perturbation of the hydrophobic core. *Sci Rep* **2016,** *6* (37990).

123. Rodriguez, J. A.; Ivanova, M. I.; Sawaya, M. R.; Cascio, D.; Reyes, F. E.; Shi, D.; Sangwan, S.; Guenther, E. L.; Johnson, L. M.; Zhang, M.; Jiang, L.; Arbing, M. A.; Nannenga, B. L.; Hattne, J.; Whitelegge, J.; Brewster, A. S.; Messerschmidt, M.; Boutet, S.; Sauter, N. K.; Gonen, T.; Eisenberg, D. S., Structure of the toxic core of alpha-synuclein from invisible crystals. *Nature* **2015,** *525* (7570), 486-90.

124. Horvath, I.; Wittung-Stafshede, P., Cross-talk between amyloidogenic proteins in type-2 diabetes and Parkinson's disease. *Proc Natl Acad Sci U S A* **2016,** *113* (44), 12473-12477.

125. Giasson, B. I.; Forman, M. S.; Higuchi, M.; Golbe, L. I.; Graves, C. L.; Kotzbauer, P. T.; Trojanowski, J. Q.; Lee, V. M., Initiation and synergistic fibrillization of tau and alpha-synuclein. *Science* **2003,** *300* (5619), 636-40.

126. Moussaud, S.; Jones, D. R.; Moussaud-Lamodiere, E. L.; Delenclos, M.; Ross, O. A.; McLean, P. J., Alpha-synuclein and tau: teammates in neurodegeneration? *Mol Neurodegener* **2014,** *9* (43), 1750-1326.

127. Esposito, A.; Dohm, C. P.; Kermer, P.; Bahr, M.; Wouters, F. S., alpha-Synuclein and its disease-related mutants interact differentially with the microtubule protein tau and associate with the actin cytoskeleton. *Neurobiol Dis* **2007,** *26* (3), 521-31.

128. Waxman, E. A.; Giasson, B. I., Induction of intracellular tau aggregation is promoted by alpha-synuclein seeds and provides novel insights into the hyperphosphorylation of tau. *J Neurosci* **2011,** *31* (21), 7604-18.

129. Lee, V. M.; Giasson, B. I.; Trojanowski, J. Q., More than just two peas in a pod: common amyloidogenic properties of tau and alpha-synuclein in neurodegenerative diseases. *Trends Neurosci* **2004,** *27* (3), 129-34.

130. Jensen, P. H.; Hager, H.; Nielsen, M. S.; Hojrup, P.; Gliemann, J.; Jakes, R., alpha-synuclein binds to Tau and stimulates the protein kinase A-catalyzed tau phosphorylation of serine residues 262 and 356. *J Biol Chem* **1999,** *274* (36), 25481-9.

131. Li, Z.; Srivastava, P., Heat-shock proteins. *Curr Protoc Immunol* **2004,** *1* (10).

132. Moon, S.; Cho, S.; Kim, H., Organization and evolution of mitochondrial gene clusters in human. *Genomics* **2008,** *92* (2), 85-93.

133. Hartl, F. U. In *The Role of Molecular Chaperones Hsp70 And Hsp60 in Protein Folding*, Post-transcriptional Control of Gene Expression, Berlin, Heidelberg, 1996//; Resnekov, O.; von Gabain, A., Eds. Springer Berlin Heidelberg: Berlin, Heidelberg, 1996; pp 193-206.

134. Mayer, M. P.; Bukau, B., Hsp70 chaperones: cellular functions and molecular mechanism. *Cell Mol Life Sci* **2005,** *62* (6), 670-84.

135. McCarty, J. S.; Buchberger, A.; Reinstein, J.; Bukau, B., The role of ATP in the functional cycle of the DnaK chaperone system. *J Mol Biol* **1995,** *249* (1), 126-37.

136. Laloraya, S.; Dekker, P. J.; Voos, W.; Craig, E. A.; Pfanner, N., Mitochondrial GrpE modulates the function of matrix Hsp70 in translocation and maturation of preproteins. *Molecular and Cellular Biology* **1995,** *15* (12), 7098-7105.

137. Hennessy, F.; Nicoll, W. S.; Zimmermann, R.; Cheetham, M. E.; Blatch, G. L., Not all J domains are created equal: implications for the specificity of Hsp40-Hsp70 interactions. *Protein Sci* **2005,** *14* (7), 1697-709.

138. Kampinga, H. H.; Craig, E. A., The HSP70 chaperone machinery: J proteins as drivers of functional specificity. *Nat Rev Mol Cell Biol* **2010,** *11* (8), 579-92.

139. Liu, Q.; Krzewska, J.; Liberek, K.; Craig, E. A., Mitochondrial Hsp70 Ssc1: role in protein folding. *J Biol Chem* **2001,** *276* (9), 6112-8.

140. Craig, E. A.; Kramer, J.; Shilling, J.; Werner-Washburne, M.; Holmes, S.; Kosic-Smithers, J.; Nicolet, C. M., SSC1, an essential member of the yeast HSP70 multigene family, encodes a mitochondrial protein. *Mol Cell Biol* **1989,** *9* (7), 3000-8.

141. Ebrahimi-Fakhari, D.; Wahlster, L.; McLean, P. J., Molecular chaperones in Parkinson's disease--present and future. *J Parkinsons Dis* **2011,** *1* (4), 299-320.

142. Recasens, A.; Dehay, B., Alpha-synuclein spreading in Parkinson's disease. *Frontiers in Neuroanatomy* **2014,** *8* (159).

143. Xu, L.; Pu, J., Alpha-Synuclein in Parkinson's Disease: From Pathogenetic Dysfunction to Potential Clinical Application. *Parkinson's Disease* **2016,** *2016*, 1720621.

144. Nakamura, K., alpha-Synuclein and mitochondria: partners in crime? *Neurotherapeutics* **2013,** *10* (3), 391-9.

145. Hsu, L. J.; Sagara, Y.; Arroyo, A.; Rockenstein, E.; Sisk, A.; Mallory, M.; Wong, J.; Takenouchi, T.; Hashimoto, M.; Masliah, E., alpha-synuclein promotes mitochondrial deficit and oxidative stress. *Am J Pathol* **2000,** *157* (2), 401-10.

146. Xie, W.; Chung, K. K., Alpha-synuclein impairs normal dynamics of mitochondria in cell and animal models of Parkinson's disease. *J Neurochem* **2012,** *122* (2), 404-14.

147. Kilpatrick, K.; Novoa, J. A.; Hancock, T.; Guerriero, C. J.; Wipf, P.; Brodsky, J. L.; Segatori, L., Chemical induction of Hsp70 reduces alpha-synuclein aggregation in neuroglioma cells. *ACS Chem Biol* **2013,** *8* (7), 1460-8.

148. Auluck, P. K.; Chan, H. Y.; Trojanowski, J. Q.; Lee, V. M.; Bonini, N. M., Chaperone suppression of alpha-synuclein toxicity in a Drosophila model for Parkinson's disease. *Science* **2002,** *295* (5556), 865-8.

149. Klucken, J.; Shin, Y.; Masliah, E.; Hyman, B. T.; McLean, P. J., Hsp70 Reduces alpha-Synuclein Aggregation and Toxicity. *J Biol Chem* **2004,** *279* (24), 25497-502.

150. Butler, E. K.; Voigt, A.; Lutz, A. K.; Toegel, J. P.; Gerhardt, E.; Karsten, P.; Falkenburger, B.; Reinartz, A.; Winklhofer, K. F.; Schulz, J. B., The Mitochondrial Chaperone Protein TRAP1 Mitigates α-Synuclein Toxicity. *PLOS Genetics* **2012,** *8* (2), e1002488.

151. Pridgeon, J. W.; Olzmann, J. A.; Chin, L. S.; Li, L., PINK1 protects against oxidative stress by phosphorylating mitochondrial chaperone TRAP1. *PLoS Biol* **2007,** *5* (7), 19.

Diffusion of α-Synuclein on the Lipid Membranes

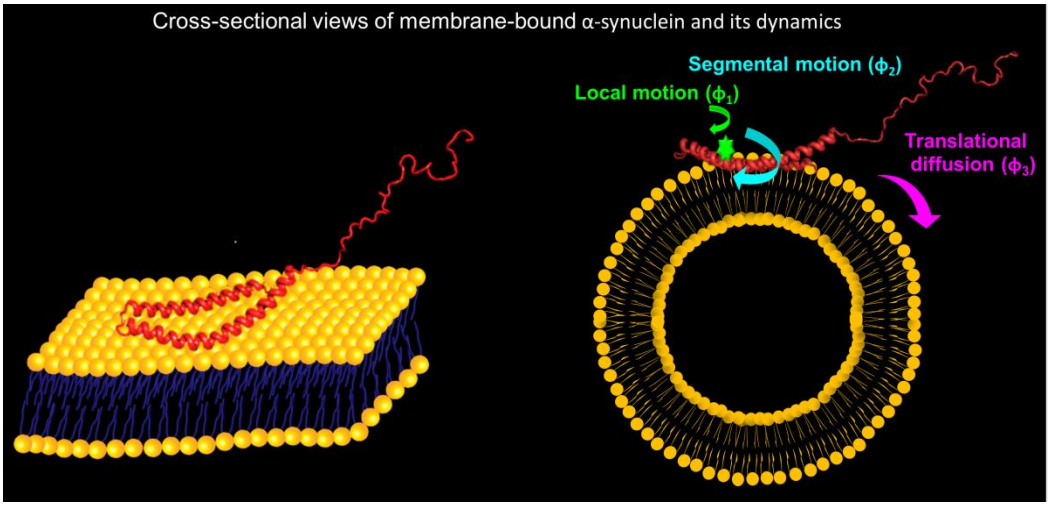

2.1 Introduction

The diffusion of proteins on the lipid membranes plays an indispensable role in many vital processes, including energy conversion, signaling, chemotaxis, cell division, protein insertion, and secretion.[1] Therefore, quantitative measurements of protein diffusion on the membranes can be of prime importance. For our studies, we utilized α-synuclein (α-syn), an intrinsically disordered protein (IDP), expressed in the presynaptic terminal of the neurons. Aberrant folding and aggregation of α-synuclein is implicated in Parkinson's disease as well as in a number of other neurodegenerative disorders.[2-5] However, the precise physiological function of α-synuclein still remains elusive. Several evidences suggest that α-synuclein exhibits eclectic behavior and helps in maintaining synaptic plasticity, regulating vesicle trafficking and several others functions.[6-8] It is also known to interact with a SNARE (soluble N-ethyl maleimide sensitive factor attachment protein receptors) complex protein known as synaptobrevin, which helps in neurotransmitter release into the presynaptic cleft of the neurons.[9-11] α-Synuclein is composed of three distinct domains: the positively charged N-terminal segments that initiates interactions with negatively charged membranes, the central hydrophobic NAC domain that forms the amyloid core of α-synuclein aggregates and the negatively charged C-terminal segment that interacts with ions such as calcium ions and modulates neurotransmitter release (Figures 2.1A and 2.1B).[12-14]

α-Synuclein undergoes a profound structural transition from a disordered to an ordered α-helical state upon interaction with negatively charged membranes.[15-16] A body of evidence has suggested that the N-terminal of α-synuclein initiates interaction with the membrane, followed by the NAC domain and forms an amphipathic helical structure, whereas the C-terminal does not interact with the membrane and remains unstructured.[17-18] Solution-state NMR and EPR studies have shown that upon interaction with membrane mimetic, sodium dodecyl sulfate (SDS) micelles and anionic small unilamellar vesicles (SUV), α-synuclein can predominantly adopt two different conformations, namely, the extended helix made up of the first 100 amino acids and the broken horseshoe conformation comprised of two short α-helices connected by a well ordered, extended linker.[19-24] Studies using double electron-electron resonance-based inter-spin measurements of LUV (large unilamellar vesicles)-bound α-synuclein reported the presence of both extended and broken helices.[25] Hence, there is a consensus that multiple conformations of α-synuclein can coexist on the membrane and undergo energetically favorable inter-conversions.[25-27] The interaction of α-synuclein with membranes is believed to play a crucial role in modulating both the

functional as well as pathological roles of α-syn. Not only does the membrane induce a disorder-to-order transition of α-syn, thereby, mediating its proposed cellular function of synaptic vesicle clustering during neurotransmitter release, it also induces aggregation of α-synuclein into amyloid fibrils.

Biological membranes are diverse in nature and their physicochemical properties vary from one cell (or organelle) to the other.[28-30] Membranes have varied curvature, different phospholipid head-group chemistry, different acyl chain composition, fluidity, etc. Interaction with negatively charged membranes leads to the binding-induced folding of α-synuclein on the membrane, which affects the stability of the membranes resulting in membrane remodeling.[31-34] Also, membranes are fluidic in nature,[35] by virtue of which different proteins, carbohydrates and signaling molecules are transported across membranes through diffusion, to maintain proper cellular homeostasis. Thus, in order to gain insights into the functional as well pathological aspects of α-synuclein, it is imperative to study its dynamics and diffusion on the membrane. In this work, we have utilized depolarization kinetics measurements using picosecond time-resolved fluorescence spectroscopy to capture the different modes of rotational dynamics of α-synuclein on the membrane in a site-specific manner. We have shown that dynamics of α-synuclein on membrane is altered depending upon membrane curvature as well as phospholipid head-group chemistry and have also estimated the translational diffusion coefficients of α-synuclein on synthetic lipid membranes.

2.2 Experimental Section

2.2.1 Materials

Chloroform solutions of POPG (1-palmitoyl-2-oleoyl-snglycero-3-phospho (1'-rac-glycerol) (sodium salt)), POPA (1-palmitoyl-2-oleoyl-snglycero-3-phosphate (sodium salt)) and POPS (1-palmitoyl-2-oleoyl-snglycero-3-phospho-L-serine (sodium salt)) were purchased from Avanti Polar Lipids and used without any further purification. IAEDANS was purchased from Invitrogen. Q (quaternary ammonium) sepharose fast flow resin was purchased from GE Healthcare. All the other chemicals required for expression and purification were purchased from Sigma Aldrich.

2.2.2 α-syn expression, purification and mutagenesis

Wild-type and Single cysteine (Cys) variants of α-syn were purified using a reported protocol.[36] The pT7-7 plasmid with α-synuclein gene was transformed in BL21 (DE3) strain

of *Escherichia coli* cells. The purity of the protein was assayed by SDS-PAGE (SDS - polyacrylamide gel electrophoresis) and the pure fractions were dialyzed in a dialysis buffer (20 mM Tris, 50 mM NaCl, pH 7.4). The purified protein was stored at -80 ºC. The Cys variants of α-syn were purified in the presence of 1 mM DTT. Prior to every experiment, all the protein solutions were concentrated using 3 kDa AMICON and filtered through 50 kDa AMICON to remove any oligomers.

2.2.3 Preparation of SUVs and LUVs

Small unilamellar vesicles (SUVs) from anionic POPG, POPA and POPS were prepared using a reported protocol.[37] Briefly, appropriate amount of the respective chloroform solution was taken in a round bottom flask and purged with a gentle stream of nitrogen for 2 h followed by vacuum desiccation for 2 hours to ensure complete removal of the residual organic solvent. The dried lipid film was hydrated in DPBS (Dulbecco's phosphate buffer saline: 2.67 mM KCl, 1.47 mM KH_2PO_4, 138 mM NaCl, and 8.06 mM Na_2HPO_4, pH 7.4) buffer with intermittent vortex for 1 hour to a final lipid concentration of 10 mM. This resulted in a turbid solution having MLVs (multilamellar vesicles). These MLVs were divided into two volumes. One volume was used to prepare SUVs and others to prepare LUVs. To obtain LUVs, extrusion technique was utilized whereby the vesicular suspension was extruded 11 times through a polycarbonate membrane filter of 100 nm pore size using a mini-extruder kit (Avanti Polar Lipids, Inc.). For SUVs, MLVs were subjected to 5 freeze-thaw cycles, alternating between liquid nitrogen and water bath (preset at 42 °C) for one minute. The MLVs were then sonicated in a bath sonicator for 1 hour at 40 °C using 37 Hz pulse rate to obtain SUVs. The size of the SUVs (35 nm ± 10 nm) and LUVs (120 nm ± 10 nm) were confirmed by dynamic light scattering measurements on a Malvern Zetasizer Nano ZS90 instrument (Malvern, UK). A He-Ne laser (632 nm) was used for exciting the samples. We measured the hydrodynamic radius of α-syn with SUVs and LUVs.

2.2.4 Dynamical light scattering

The size of the SUVs (35 nm ± 10 nm) and LUVs (120 nm ± 10 nm) were confirmed by dynamic light scattering measurements on a Malvern Zetasizer Nano ZS90 instrument (Malvern, UK). A He-Ne laser (632 nm) was used for exciting the samples. We measured the hydrodynamic radius of α-syn with SUVs and LUVs.

2.2.5 Fluorescence labeling of α-syn with IAEDANS

The labeling of the single Cys in α-syn with IAEDANS was carried in DPBS buffer (pH 7.4) according to the protocol described previously.[38] Briefly, IAEDANS and α-syn were mixed in a 10: 1 molar ratio and allowed to stir in the dark for 2 h at room temperature. Stock solutions of IAEDANS (in dimethyl sulfoxide (DMSO)) were prepared freshly. The labelled protein was then passed through a PD-10 column to remove any unreacted dye. The concentration of the labeled protein was estimated using ε_{337} = 6100 M^{-1} cm^{-1} for AEDANS.[39]

2.2.6 CD measurements

The far UV CD spectra were collected on Chirascan CD spectrometer (Applied Photophysics, UK) using 1 mm pathlength quartz cuvette at room temperature. The concentration of wild-type and Cys variants of α-syn were fixed at 25 μM. CD spectra in the absence and in the presence of different lipids (1 mM) in DPBS buffer were collected with a scan rate of 1 nm/s and averaged over 3 scans. The scan range was fixed from 200 nm to 260 nm. All the spectra were buffer subtracted and smoothened using Chirascan 'ProData viewer' software provided with the instrument.

2.2.7 Steady-state fluorescence measurements

All steady-state experiments were carried out on Fluoromax-4 (Horiba Jobin Yvon, NJ) using 10 mm x 2 mm quartz cuvette at room temperature. The final concentration of α-syn and lipids were maintained at 50 μM and 2 mM, respectively. For measuring AEDANS fluorescence, the samples were excited at 340 nm and the emission spectra were background subtracted and corrected. The steady-state fluorescence anisotropies were measured at the emission maxima of AEDANS fluorescence spectra. The steady-state fluorescence anisotropy (r_{ss}) is given by the following relationship:

$$r_{ss} = (I_{\parallel} - GI_{\perp}) / (I_{\parallel} + 2GI_{\perp}) \text{--------(1)}$$

where, $I_{\parallel}$ and $I_{\perp}$ are fluorescence intensities collected using parallel (VV) and perpendicular geometry (VH), respectively and G is an instrument and wavelength dependent correction factor to compensate for the polarization bias of the detection system. The perpendicular components were always corrected using a G-factor and it was determined by measuring the HV and HH fluorescence intensities and the ratio of HV to HH was used as a G-factor.

2.2.8 Time-resolved fluorescence measurements

The time-resolved fluorescence decays of the samples (in the absence and presence of Trp variants in POPG) were collected using a Ti:sapphire laser coupled to a time-correlated single- photon-counting setup. The laser wavelength of 885 nm frequency tripled to obtain an excitation wavelength of 295 nm and fluorescence decays were collected at 350 nm with a bandpass of 10 nm. In order to obtain a good signal-to noise ratio, 10,000 counts were collected at the peak using a microchannel plate photomultiplier (model 2809u; Hamamatsu, Hamamatsu City, Japan). All the experiments were carried out at room temperature.

Time-resolved fluorescence decay measurements of the samples were performed using a time-correlated single photon counting (TCSPC) setup (Fluorocube; Horiba Jobin–Yvon, NJ). The samples were excited using a 375-nm laser diode (LD) (for AEDANS) having instrument response of ~200 ps. Fluorescence was detected at the steady-state emission maxima of AEDANS fluorescence emission spectra with band pass of 12 nm. The time-resolved decay of fluorescence intensity was collected at the magic angle (54.7 º) with respect to the polarization of incident light. The photon counts at the peaks were at least 10,000. The intensity decays were deconvoluted with respect to the instrument response function and were analyzed using the equation:

$$I(t) = \sum_{i=1}^{3} \alpha_i e^{-\frac{t}{\tau_i}} \text{ --------(2)}$$

where, α_i and τ_i represent the contributions and lifetime, respectively, of the different lifetime components and were used in the anisotropy decay analysis.

For fluorescence anisotropy decay measurements, the time-dependent decay of fluorescence were collected at 0º [$I_{\parallel}(t)$] and 90º [$I_{\perp}(t)$] with respect to the excitation polarization, and the anisotropy decays were analyzed by globally fitting $I_{\parallel}(t)$ and $I_{\perp}(t)$ as described in our previous reports.[40]

$I_{\parallel}(t) = I(t)[1+2r(t)]/3$ --------(3)

$I_{\perp}(t) = I(t)[1-r(t)]/3$ --------(4)

where, G is an instrument and wavelength dependent correction factor to compensate for the polarization bias of the detection system. $I_{\perp}(t)$ was always corrected with the G-factor that was estimated independently using free dye ANS in ethanol. The time-resolved anisotropy decays [r(t)] can be described as a bi or a tri-exponential decay models as follows:

$$r(t)= r_0 \sum_{i=1}^{3} \beta_i e^{-\frac{t}{\phi_i}} \quad \text{--------(5)}$$

where r_0 represents the initial anisotropy of AEDANS, and ϕ_i are rotational correlation times and β_i are the corresponding amplitudes. In order to estimate the anisotropy decay parameters, the analyses were performed by floating all the parameters. Subsequently, to assess the robustness of the recovered rotational correlation times, one rotational correlation time was fixed at different values, whereas the other parameters were floated. In each case, the goodness of fit was assessed by reduced χ^2 values, randomness of residuals, and autocorrelation analysis as described previously.[40]

2.3 Results

2.3.1 Conformational and dynamical changes of the membrane-bound state of α-synuclein

α-Synuclein is present in the presynaptic terminal of the neurons and possibly helps in neurotransmitter release, hence, we utilized SUVs of ~30 nm diameter which are comparable in size to the synaptic vesicles in which neurotransmitters are encapsulated. Using far-UV circular dichroism (CD), we first monitored the conformational change of α-synuclein upon

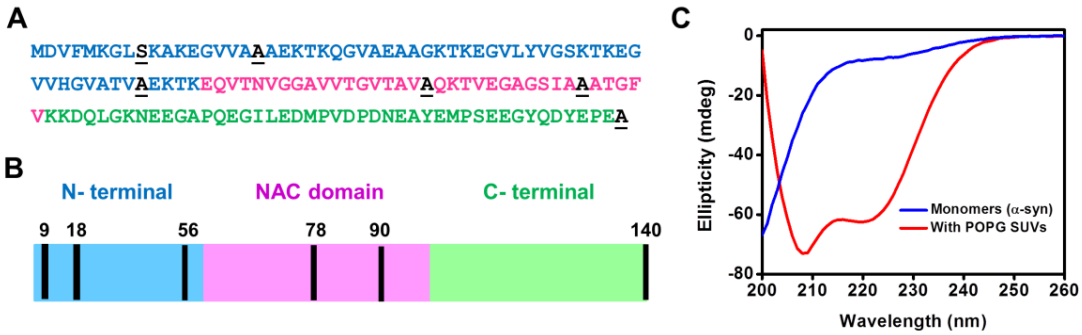

Figure 2.1 (A) Amino acid sequence of α-synuclein: N-terminal (blue), NAC domain (pink) and C-terminal (green) (Cys mutational sites are black in color and are underscored). (B) Various regions of the protein: N-terminal, NAC domain and C-terminal. Cys positions are indicated in black. (C) CD spectra of wild-type α-synuclein in the free and in the POPG SUVs bound state.

interaction with the POPG SUVs, where we observed a conformational transition from a random coil structure to an ordered helical structure (Figure 2.1C). Dynamic light scattering measurements also pointed towards a slight increase in the hydrodynamic diameter of α-synuclein-SUV complex as compared to SUVs only (Figure 2.2).

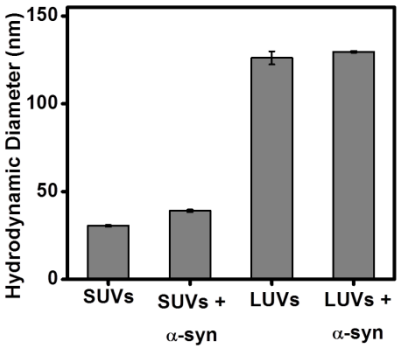

Figure 2.2 Hydrodynamic diameter obtained using dynamic light scattering experiments.

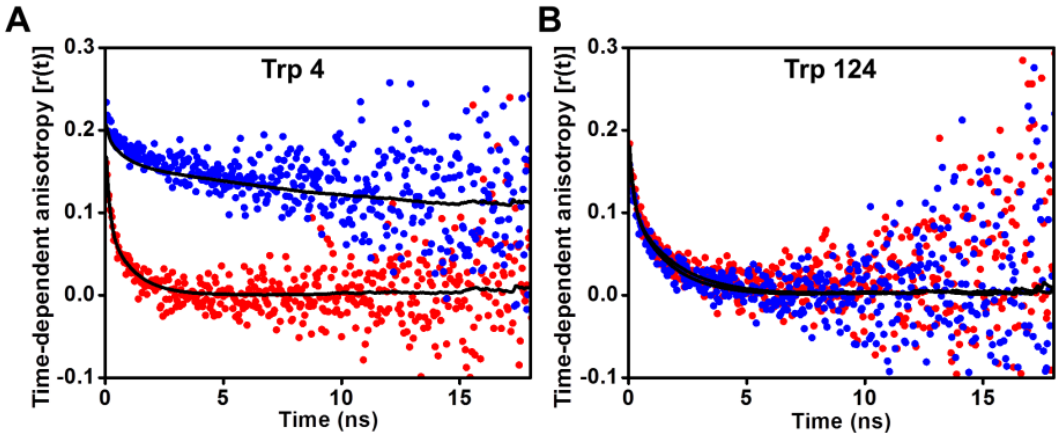

Figure 2.3 Time-resolved fluorescence anisotropy decays of single Trp variants of α-synuclein in the monomeric state (red solid circles) and in the POPG SUVs bound state (blue solid circles). The fits are indicated by black solid lines. (A) Trp4. (B) Trp124.

Next, in order to probe the residue-specific dynamics of α-synuclein on the membrane, we took advantage of the absence of tryptophan (Trp) residue in the protein and used our single Trp variants at the N-terminal (Trp 4) and C-terminal (Trp 124) segment of α-synuclein. These mutations did not alter the structural attributes of the protein and behaved similarly to wild type α-synuclein as reported previously.[36, 40] In order to delineate the different modes of rotational relaxation occurring in monomeric as well as in membrane-bound α-synuclein, we carried out the picosecond time-resolved fluorescence anisotropy measurements that allow us

to discern the timescales and contributions of various rotational relaxation modes. The time-resolved fluorescence anisotropy decay curves for monomeric free α-synuclein exhibited atypical bi-exponential kinetics. The early sub-nanosecond component (~ 0.1 ns) represents the local dynamics of Trp sidechain, whereas, the slower component (~ 1.4 ns) arises due to the backbone segmental mobility of the disordered polypeptide chain (Figure 2.3; Table 2.1), as described in our previous work.[40] In the presence of POPG SUVs, the N-terminal position (Trp 4) exhibited much slower depolarization kinetics consisting of a much longer correlation time (~ 45 ns) indicating significant dampening of the rotational motion around this region in the presence of membrane (Figure 2.3). On the contrary, residue position 124 did not exhibit any dampening in the rotational dynamics indicating the C-terminal segment of α-synuclein does not interact with the membrane. This result is in line with previous reports.[18, 36, 41-43] We then asked the question: what is the molecular origin of the long rotational correlation time component (> 30 ns) that we observe for the N-terminal segment of lipid-bound α-syn? Is this

Table 2.1

Typical parameters associated with the time-resolved fluorescence intensity and anisotropy decays of Trp4 and Trp124 variants of α-synuclein in the monomeric state and in the POPG SUVs bound state. The standard errors estimated from multiple data acquisition and analysis.

Trp Variants of α-Synuclein (Conditions)	Fluorescence Lifetime in ns (amplitude)			Mean Lifetime in ns	Rotational Correlation time in ns (amplitude)	
	τ_1 (α_1)	τ_2 (α_2)	τ_3 (α_3)		ϕ_1(β_1)	ϕ_2(β_2)
Trp 4 (Monomers)	4.13 (0.37)	1.9 (0.43)	0.51 (0.20)	2.4	1.1 (0.44)	0.13 (0.56)
Trp 4 (Membrane-bound)	3.9 (0.50)	1.61 (0.36)	0.39 (0.14)	2.6	44.8 (0.76)	0.56 (0.24)
Trp 124 (Monomers)	3.51 (0.34)	1.87 (0.44)	0.65 (0.22)	2.16	1.56 (0.53)	0.14 (0.47)
Trp 124 (Membrane-bound)	4.14 (0.20)	2.2 (0.56)	0.65 (0.24)	2.22	1.32 (0.52)	0.15 (0.48)

correlation time connected to coupled protein and membrane dynamics? Since Trp has a short average excited-state lifetime of ~ 3 ns, it is not an appropriate fluorescent reporter to capture the process occurring on a much longer time scale compared to its fluorescence lifetime. A more accurate quantification of the rotational correlation time was required to decipher the molecular origin of the slow dynamics of lipid-bound α-synuclein, therefore, we used a long lifetime thiol-active fluorophore, such as IAEDANS that can exhibit much longer

fluorescence lifetime (> 10 ns) that will allow us to accurately estimate the longer rotational correlation time component.

2.3.2 Residue-specific structural change of α-synuclein on the lipid membrane surface

Next, in order to monitor the residue-specific dynamics of membrane-bound α-synuclein using a long lifetime fluorophore, IAEDANS, we took advantage of the nonoccurrence of Cys and incorporated single Cys at the residue positions 9, 18, 56, 78, 90 and 140 encompassing the entire polypeptide length. The residue positions 9, 18, 56, 90 and 140 were chosen based on the earlier reports[24-25, 44] and we made an additional mutation at residue

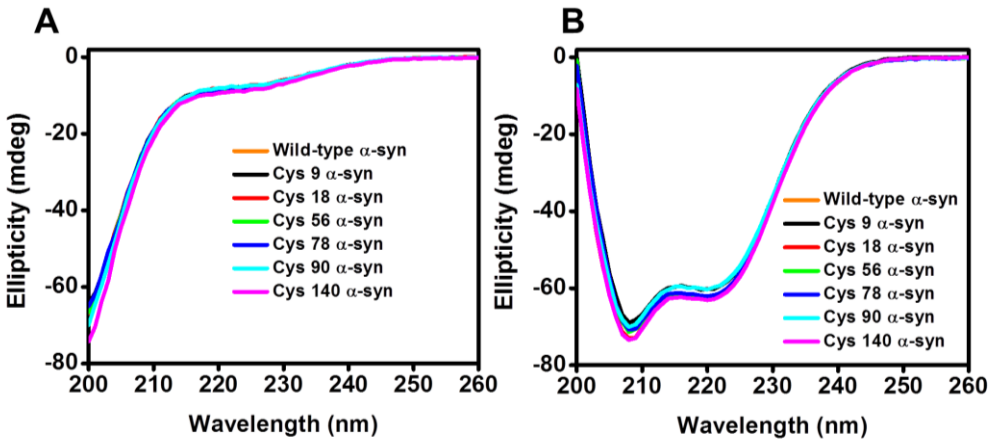

Figure 2.4. CD spectra of wild-type and single cysteine mutants of α-synuclein showed structural transition from the disordered to the helical state (A) in the monomeric state and (B) in the presence of

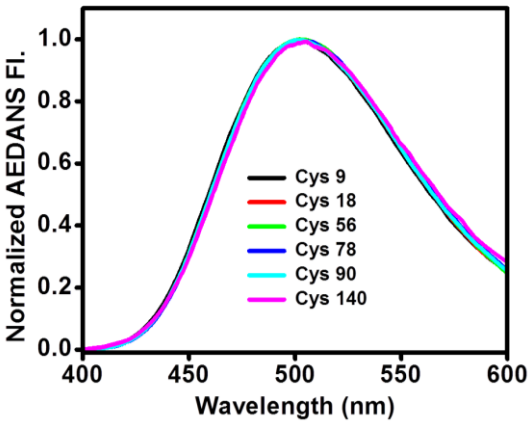

Figure 2.5 Fluorescence spectra of AEDANS labeled Cys mutants of α-synuclein in the monomeric state.

POPG SUVs position 78. α-synuclein is known to adopt a range of structural conformations on the membrane including a pair of anti-parallel α-helices (residues 3–37 and 45–92) and a single extended α-helix (residues 9–89) obtained from NMR studies. Cysteine mutations which we have created encompasses these regions of the protein.[22, 45-46] All of these variants did not alter the structural attributes of the protein and behaved similar to wild-type α-syn, both in the free monomeric state as well as in the membrane-bound state (Figure 2.4). The single Cys constructs were then covalently labeled with the long lifetime fluorophore, IAEDANS. As a prelude to the picosecond time-resolved fluorescence studies, we carried out steady-state fluorescence experiments with IAEDANS labeled Cys variants. For all the residue position, the AEDANS exhibited highly red-shifted emission maxima (~ 500 nm) as expected for solvent exposed locations in the free disordered state (Figure 2.5). Upon binding to POPG SUVs, different locations showed a varied extent of blue-shift (Figure 2.6A). N-terminal positions, 9 and 18, showed emission maxima at ~ 493 nm and 480 nm, respectively. The residues near and within the NAC domain showed emission maxima at ~ 486 nm, 491 nm and 498 nm for 56, 78, and 90, respectively. There was no detectable spectral shift

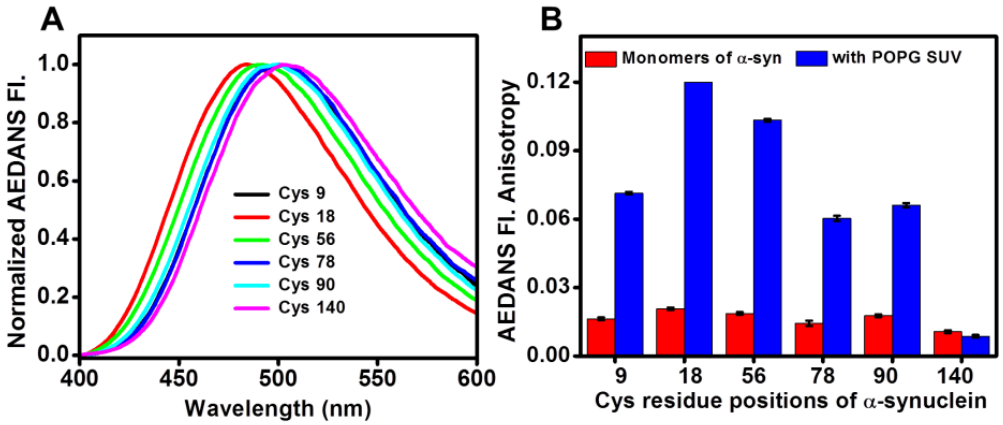

Figure 2.6 Steady-state fluorescence of AEDANS labeled single cysteine constructs of α-synuclein. (A) AEDANS fluorescence spectra of α-synuclein bound to POPG SUVs. (B) AEDANS fluorescence anisotropy of monomeric α-synuclein (red) and upon binding to POPG SUVs (blue). Error bars are obtained from at least three independent measurements.

observed in the C-terminal residue, 140, that is known not to interact with the membrane surface. These results revealed different microenvironment of various locations and corroborated our Trp previous fluorescence data.[37] Next, we investigated the rotational mobility of the fluorophore at a given residue position using steady-state fluorescence

anisotropy measurements of AEDANS. In the unbound form, anisotropy was low (r_{ss} ~ 0.02) for all the positions of α-synuclein indicating high flexibility that is expected for disordered monomeric α-synuclein (Figure 2.6B). In the membrane-bound state, dampening in the rotational dynamics was observed for the residue positions in

the N-terminal segment and in the NAC domain indicating that these regions of α-synuclein are closely interacting with the lipid membrane. Whereas, the C-terminal location did not show any significant increase in the anisotropy since this part does not participate in membrane interaction (Figure 2.6B). These results are in line with the previous studies on the residue-specific structural organization of membrane-bound α-syn.[15, 20, 26-27, 36] These steady-state fluorescence experiments, however, do not allow us to discern the different modes of protein dynamics on the lipid membrane.

2.3.3 Dynamics of α-synuclein on the membrane

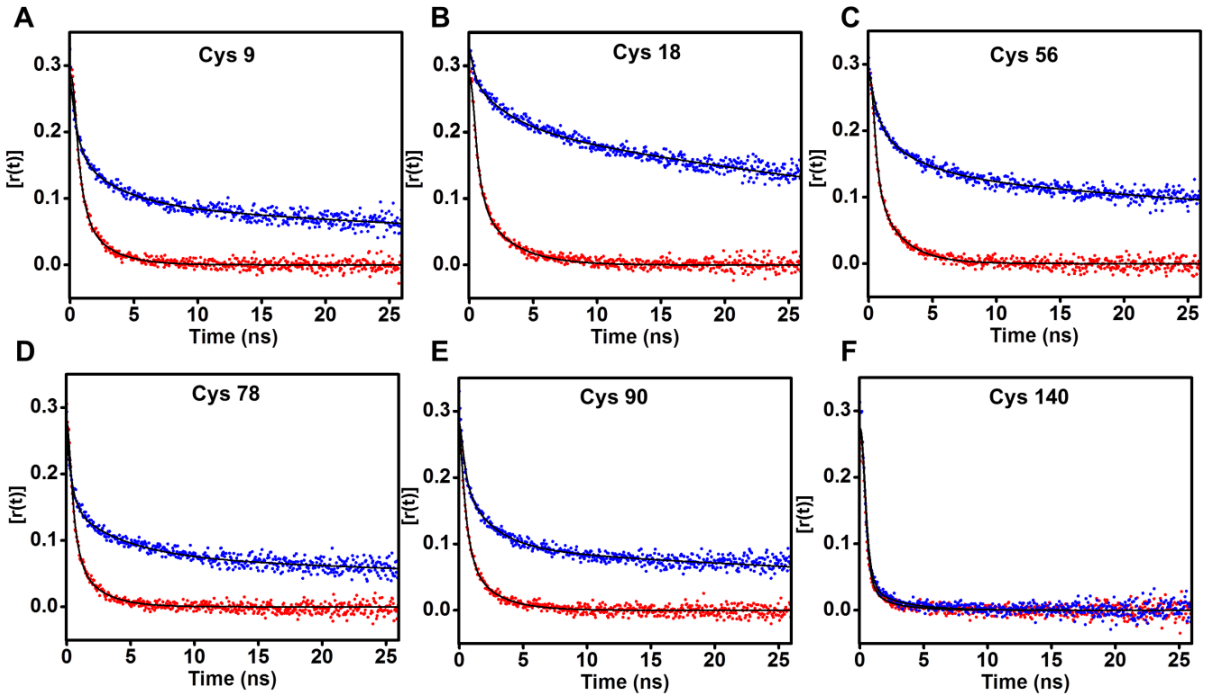

Figure 2.7 Time-resolved fluorescence anisotropy decays of AEDANS labeled single Cys mutants of α-synuclein in the monomeric state (red solid circles) and in the POPG SUVs bound state (blue solid circles). (A) Cys9. (B) Cys18. (C) Cys56. (D) Cys78. (E) Cys90 and (F) Cys140. The fits are indicated by black solid lines.

Next, in order to obtain dynamical insights into membrane-bound α-syn, we monitored the fluorescence depolarization kinetics using picosecond time-resolved fluorescence anisotropy measurements. Our time-resolved fluorescence anisotropy data for AEDANS showed a typical bi-exponential decay profile for the monomers of α-syn, similar to what was observed using Trp fluorescence (Figure 2.7). The faster correlation time (~ 0.45 ns), with significantly high amplitude (~ 70 %), arises due to the local rotational mobility of the dye having a longer linker. The slower correlation time (~ 2.2 ns) represents the backbone segmental fluctuations. We then recorded the fluorescence anisotropy decays at various residue locations of α-synuclein bound to POPG SUVs. A comparison of the anisotropy decay profiles of AEDANS and Trp revealed that the signal-to-noise ratio in the longer time-window is far superior for AEDANS due to longer fluorescence lifetime compared to Trp (Figures 2.3 and 2.7). Therefore, AEDANS anisotropy decays allow us to estimate the timescale of slower events much more accurately compared to Trp anisotropy. The obtained decay profiles for all the residue positions, except 140, could be adequately described by a tri-exponential decay law, as evident from the reduced χ^2 and the randomness of residuals (Table 2.2; Figure 2.8). We recovered three rotational correlation times from our analysis for all residue positions, except140, which exhibited a bi-exponential decay. The tri-exponential anisotropy decay profiles obtained in our measurements could arise due to three well-separated independent motions: a fast (local) wobbling-in-cone motion of the dye (ϕ_1 ~ 0.5 ns); (ii) the segmental mobility of the polypeptide chain (ϕ_2 ~ 3 ns); (iii) a slow rotational correlation time (ϕ_3 ~ 60 ns). The slow rotational correlation time component was nearly independent of the locations that interact with the lipid membrane. We next asked the question: What is the molecular origin of this slow rotational correlation time? There are three possibilities: (i) the global tumbling of the α-synuclein-SUV complex; (ii) the global reorientation of only α-synuclein within the membrane; (iii) the translation diffusion of α-synuclein on the curved membrane surface that could potentially contribute to fluorescence depolarization. We set out to explore all these three possibilities to decipher the origin of this slow dynamics.

From our DLS data, we estimated the hydrodynamic radius of the SUV-protein complex (R_h ~39 nm) and using the Stokes-Einstein relationship (Eq. 7), we calculated the rotational correlational time (ϕ_{calc}) associated with the global tumbling of the protein-SUV complex:

$$\phi_{calc} = \frac{4}{3}\pi R_h^3 \eta / k_B T \text{ --------(7)}$$

where η is the viscosity, k_B is the Boltzmann constant, and T is the absolute temperature.

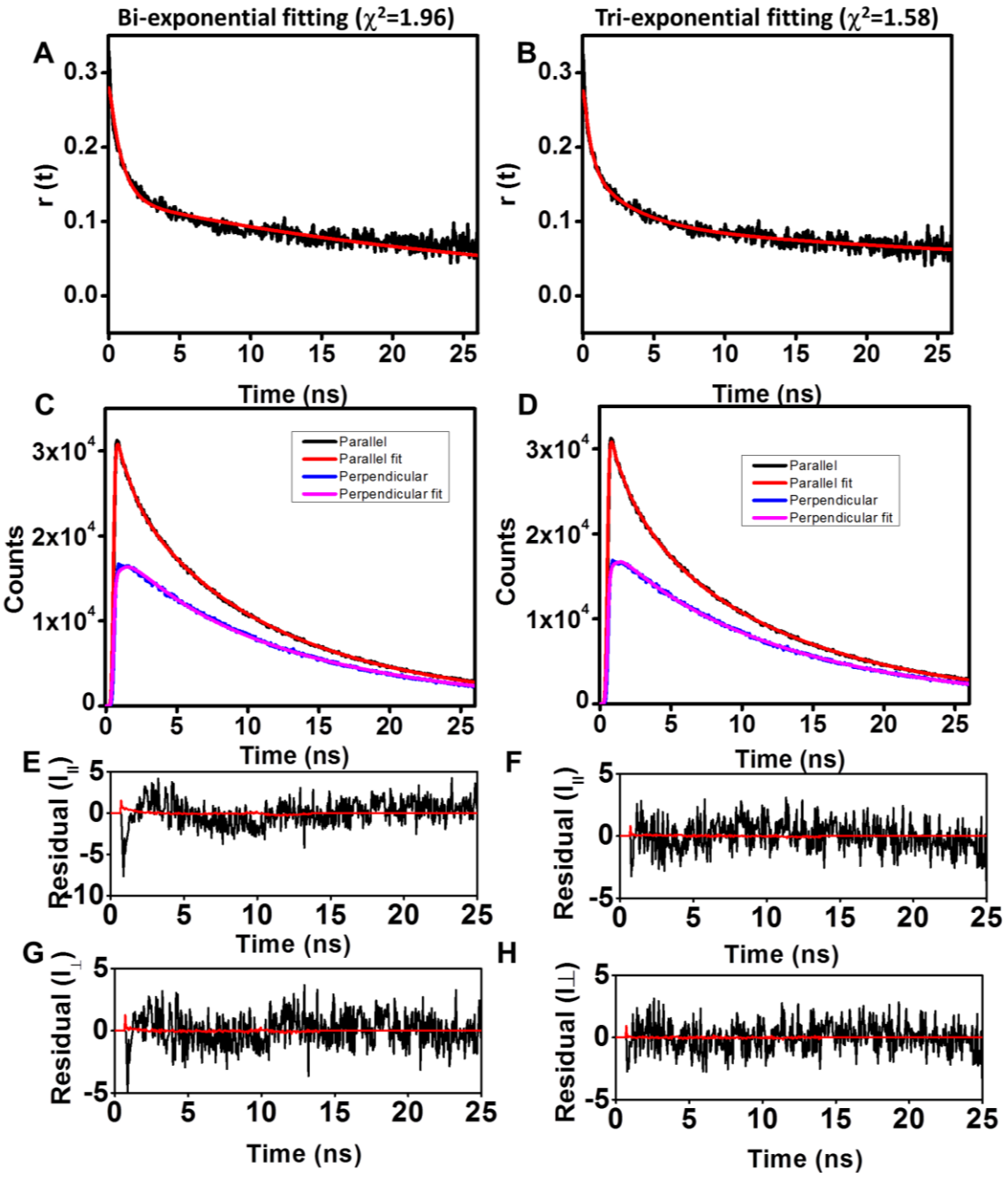

Figure 2.8 The time-resolved fluorescence anisotropy decay analysis for AEDANS labeled Cys9 variant of α-synuclein. The bi-exponential (A) and tri-exponential (B) fit of the raw anisotropy data indicated by black line, whereas, the fitted decay shown by red line. The bi-exponential (C) and tri-exponential (D) fit of the global analysis of $I_{||}(t)$ (black) and $I_{\perp}(t)$ (blue) and corresponding fits shown using red and pink color, respectively. (E) and (F) represent the residual plots of $I_{||}(t)$ for bi-exponential and tri-exponential fits, respectively. (G) and (H) represents the residual plots of $I_{\perp}(t)$ for bi-exponential and tri-exponential fits, respectively.

Table 2.2

The time-resolved fluorescence intensity and anisotropy decays parameters of AEDANS labeled single Cys variants of α-synuclein in the monomeric state and in the POPG SUVs bound state. The standard errors estimated from multiple data acquisition and analysis.

Cys Variants of α-Synuclein (Conditions)		Fluorescence Lifetime in ns (amplitude)		Rotational Correlation time in ns (amplitude)		
		τ_1 (α_1)	τ_2 (α_2)	ϕ_1(β_1)	ϕ_2(β_2)	ϕ_3(β_3)
Cys 9	Monomer	13±0.2 (0.87±0.03)	2.5±0.5 (0.13±0.03)	0.45±0.05 (0.72±0.04)	2±0.3 (0.28±0.03)	
	with POPG SUVs	13±0.1 (0.82±0.02)	4.9±0.2 (0.19±0.03)	0.45±0.05 (0.4±0.03)	3±0.3 (0.3±0.05)	65±10 (0.33±0.02)
Cys 18	Monomer	13.8±0.1 (0.85±0.06)	4.5±0.5 (0.12±0.03)	0.45±0.06 (0.65±0.05)	2.5±0.5 (0.32±0.05)	
	with POPG SUVs	17.1±0.1 (0.91±0.1)	4.2±0.5 (0.09±0.01)	0.43±0.05 (0.15±0.04)	3.4±0.8 (0.22±0.01)	58.8±4.4 (0.63±0.03)
Cys 56	Monomer	13.3±0.3 (0.87±0.04)	4.8±0.6 (0.12±0.03)	0.38±0.03 (0.65±0.03)	2.3±0.5 (0.35±0.03)	
	with POPG SUVs	14.9±0.1 (0.88±0.03)	5.5±0.5 (0.11±0.02)	0.55±0.05 (0.28±0.02)	3±0.3 (0.26±0.02)	65±10 (0.47±0.02)
Cys 78	Monomer	13±0.1 (0.88±0.01)	4.7±0.3 (0.12±0.01)	0.38±0.03 (0.72±0.03)	2.3±0.5 (0.28±0.03)	
	with POPG SUVs	13.9±0.1 (0.87±0.02)	4.8±0.3 (0.13±0.02)	0.45±0.05 (0.45±0.04)	3±0.5 (0.21±0.03)	65±10 (0.31±0.02)
Cys 90	Monomer	13.1±0.1 (0.9±0.02)	4.8±0.3 (0.1±0.02)	0.45±0.05 (0.69±0.03)	2.2±0.2 (0.3±0.03)	
	with POPG SUVs	14.5±0.2 (0.84±0.02)	4.9±0.3 (0.16±0.02)	0.4±0.05 (0.4±0.02)	3±0.3 (0.3±0.03)	65±10 (0.32±0.02)

Cys 140	Monomer	11.3±0.1 (0.58±0.02)	5.2±0.2 (0.42±0.02)	0.25±0.05 (0.88±0.02)	2±0.3 (0.1±0.02)
	with POPG SUVs	11.5±0.1 (0.7±0.02)	5.2±0.2 (0.3±0.03)	0.25±0.05 (0.8±0.03)	2±0.5 (0.2±0.02)

The calculated rotational correlational time for the protein-SUV complex is ~7.2 μs, which is over two orders of magnitude slower than the observed rotational correlation time (ϕ_3 ~ 60 ns). Therefore, the observed slow rotational correlation time cannot represent the global tumbling of the protein-SUV complex.

Next, we considered whether the slow dynamics (ϕ_3) could arise due to the global reorientation of the protein within the membrane. In order to examine this possibility, we chose to measure the depolarization kinetics of α-synuclein on large unilamellar vesicles (LUVs) that have larger hydrodynamic radius (R_h ~100 nm) (Figure 2.2). If the slower component (ϕ_3) arises due to the global reorientation of the protein within the membrane, we expect to see similar long rotational correlational times. In other words, the curvature of membrane should not affect the reorientation timescale of α-synuclein on the membrane.

2.3.4 The effect of membrane curvature

We first performed CD measurements to monitor the secondary structural change in α-synuclein on the POPG LUVs surface (Figure 2.9). α-Synuclein showed conformational transition from random coil to helical structure in the presence of POPG LUVs. For performing further experiments, AEDANS labeled at Cys18 of α-synuclein was chosen on

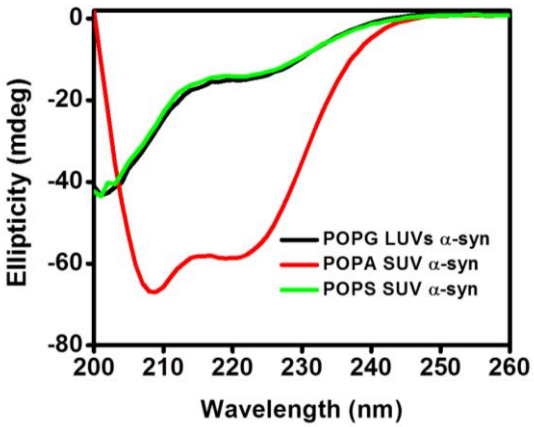

Figure 2.9 CD spectra of wild-type α-synuclein in the presence of POPG LUVs (black), POPA SUVs (red) and POPS SUVs (green).

account of the strongest binding of this region α-synuclein to the membrane. The steady-state fluorescence emission spectra of AEDANS showed emission maxima at ~ 493 nm on LUVs surface as opposed to ~ 480 nm on the SUV surface (Figure 2.10A). This suggested that residue 18 is more solvent exposed in the membrane-bound state of LUVs as compared to SUVs. Our above result was also supported by AEDANS steady-state fluorescence anisotropy measurements, which demonstrated that the anisotropy was ~ 0.07 in LUV-bound state and ~ 0.12 in the SUV-bound state (Figure 2.10B). Therefore, we expect that the rotational mobility of AEDANS labeled α-synuclein would be more on the LUVs as compared to SUVs. The different conformations adopted by α-synuclein on the highly curved surface (predominantly horseshoe broken helix conformation) and less curved surface (predominantly extended helix conformation) might contribute to the variation in the lipid-protein interaction.[21, 24] Next, we investigated the time-resolved fluorescence anisotropy of the fluorophore on the POPG LUVs. Our time-resolved anisotropy data for AEDANS showed that the amplitude of the fast correlation time (ϕ_1) increased from 15 % for SUV-bound α-synuclein to 25 % for LUV-bound α-synuclein also supported more rotational mobility of the dye in the fluorescence depolarization kinetics (Figure 2.10C). Interestingly, the slow correlation time (ϕ_3) showed a sharp increase from ~ 60 ns in the case of POPG SUVs to ~ 285 ns for POPG LUVs (Table 2.3). Significant dampening in the slower component (ϕ_3) of the AEDANS labeled α-synuclein bound to LUVs suggested that the slow rotational correlational time cannot arise due to the global reorientation of α-synuclein on the membrane surface. Hence, we ruled out the second possibility as well. These results indicated that the slower rotational correlation time component of membrane-bound α-synuclein could possibly arise due to the translational diffusion of α-synuclein on the membrane that causes the angular displacement of transition dipole leading to the slow depolarization. The wobbling-in-cone dynamic model coupled with the translational diffusion of the fluorophore on spherical surfaces has been observed for the micelle-dye complexes.[47-49]

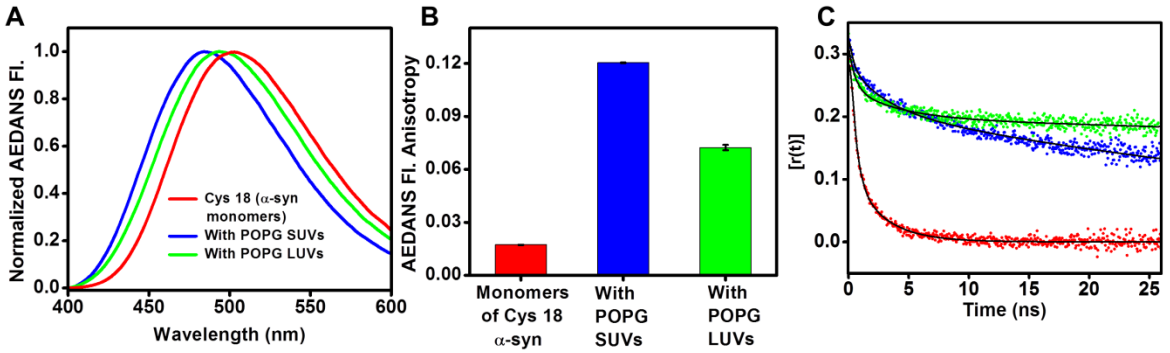

Figure 2.10 AEDANS labeled single Cys of α-synuclein in the monomeric state (red), in the POPG SUVs bound state (blue) and in the POPG LUVs bound state (green). (A) AEDANS fluorescence spectra. (B) AEDANS fluorescence anisotropy. Error bars are obtained from at least three independent measurements. (C) Time-resolved fluorescence anisotropy decays. The fits are indicated by black solid lines. (Data for monomeric and POPG SUVs bound α-synuclein again shown here for comparison)

2.3.5 Influence of the lipid head-group chemistry on the diffusion of α-synuclein

In order to establish that the slow rotational correlation time of α-synuclein on the membrane represents the translational diffusion of α-synuclein on the membrane, we used vesicles from a variety of negatively charged lipids. Our previous studies showed that α-synuclein binding affinity depends on the lipid headgroup chemistry and follows the order: POPA > POPG > POPS.[37] Also, our previous results on single Trp experiments with different membranes

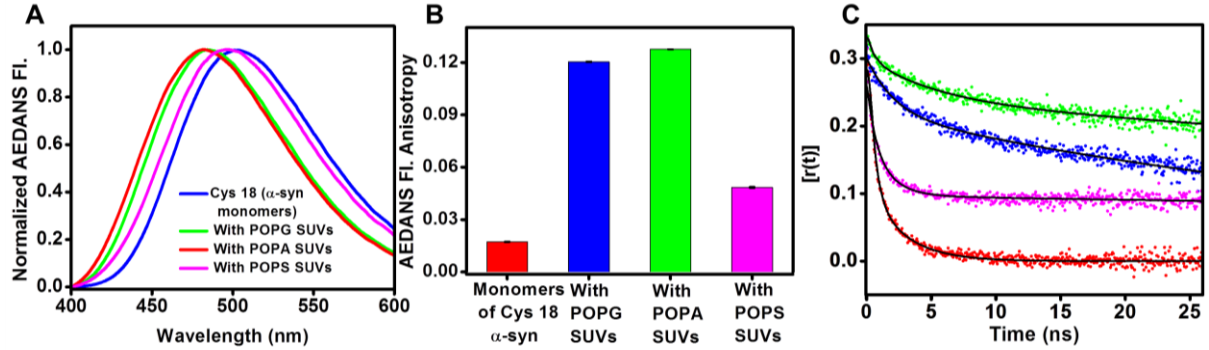

Figure 2.11 AEDANS labeled single Cys of α-synuclein in the monomeric state (red), in the POPG SUVs bound state (blue), in the POPA SUVs bound state (green) and in the POPS SUVs bound state (pink). (A) AEDANS fluorescence spectra. (B) AEDANS fluorescence anisotropy. Error bars are obtained from at least three independent measurements. (C) Time-resolved fluorescence anisotropy decays. The fits are indicated by black solid lines. (Data for monomeric and POPG SUVs bound α-synuclein again shown here for comparison).

suggested that α-synuclein immersion is into the outer leaflet of the membrane containing ordered water layer.[36] However, on the POPA membrane, α-synuclein penetrates further inside into the hydrophobic region of the bilayer.[36] If the slow rotational correlational time

Table 2.3

Typical parameters associated with the time-resolved fluorescence intensity and anisotropy decays of AEDANS labeled single Cys variants of α-synuclein in the presence of POPG LUVs, POPA SUVs and POPS SUVs. The standard errors estimated from multiple data acquisition and analysis.

Cys 18 Variants of α-Synuclein in the Presence of Different Lipids	Fluorescence Lifetime in ns (amplitude)		Rotational Correlation time in ns (amplitude)		
	τ_1 (α_1)	τ_2 (α_2)	ϕ_1(β_1)	ϕ_2(β_2)	ϕ_3(β_3)
POPG LUV	16.2±0.3 (0.91±0.2)	3±0.6 (0.1±0.02)	0.45±0.09 (0.25±0.03)	3.3±0.5 (0.16±0.02)	285±45 (0.6±0.03)
POPA SUV	16±0.2 (0.89±0.1)	2.7±0.5 (0.1±0.01)	0.44±0.06 (0.22±0.05)	6.1±0.99 (0.18±0.02)	182±42 (0.60±0.03)
POPS SUV	14.21±0.2 (0.88±0.2)	3.1±0.75 (0.12±0.02)	0.45±0.08 (0.36±0.08)	1.61±0.29 (0.32±0.07)	365±161 (0.32±0.03)

arises due to the translational diffusion of α-synuclein on the membrane, we would expect to see more dampened slow rotational correlation time (ϕ_3) in the presence of POPA membrane since it interacts more strongly with α-synuclein. As a prelude we first performed CD measurements that indicate a conformational switch in α-synuclein from an intrinsically disordered state to a helical state upon binding to POPA and POPS SUVs (Figure 2.9). The steady-state AEDANS fluorescence emission spectra showed an emission maximum at ~ 497 nm in the presence of POPS, indicating that residue 18 is more exposed to water, that is in accordance with our previous work [36] (Figure 2.11A). However, α-synuclein on the POPA exhibited an emission maximum at ~ 482 nm which is similar to what we observed for POPG (Figure 2.11A). Our steady-state anisotropy data were also in agreement with our steady-state fluorescence emission data (Figure 2.11 B). These results are in agreement with our previous results showing the interaction of α-synuclein with the membrane is dependent on lipid headgroup and follows the order: POPA > POPG > POPS. Next, we embarked upon fluorescence depolarization measurements. Analysis of the time-resolved anisotropy data for

AEDANS (Table 2.3) revealed that the amplitudes of the fast correlation time were 36 % and 22 % in the presence of POPS and POPA, respectively, depicting increased local conformational flexibility on both the lipid surfaces (Figure 2.11C). The recovered values of the long rotational correlation times (ϕ_3) correlated well with the extent of binding of α-synuclein, as a function of phospholipid headgroup chemistry. The stronger binding of α-synuclein to POPA in comparison to POPG was evident from their slow rotational correlation times (ϕ_3 ~ 180 ns for POPA and ~ 60 ns for POPG), both having significantly high amplitudes (~ 60 %). Although, the value of ϕ_3 also showed a prominent increase to ~ 365 ns for the POPS SUVs, the estimation may not be accurate on account of the significantly low amplitude (~ 30 %) associated with it. The dampening of slow rotational correlation time (ϕ_3) associated with stronger binding of α-synuclein to the membrane established that the slow

Table 2.4

Values of parameters derived from fluorescence anisotropy measurements for calculating the translational diffusion coefficient of α-synuclein.

Cys 18 Variants of α-Synuclein in the Presence of Different Lipids	Rotational Correlation time in ns (amplitude)			τ_D (ns)	D_t X 10^{-10} (m^2/s)
	$\phi_1(\beta_1)$	$\phi_2(\beta_2)$	$\phi_3(\beta_3)$		
POPG SUV	0.43±0.05 (0.15±0.04)	3.4±0.8 (0.22±0.01)	58.8±4.4 (0.63±0.03)	61	8.71 ± 0.06
POPA SUV	0.44±0.06 (0.22±0.05)	6.1±0.99 (0.18±0.02)	182±42 (0.60±0.03)	190	2.92 ± 0.06

rotational dynamics primarily arises due to translational diffusion lipid-bound α-synuclein on the curved membrane surface. These results also raised the possibility of estimating the diffusion coefficient of α-synuclein on the POPG and POPA SUVs since the high amplitude (~ 60 %) allows us to accurately estimation the diffusion coefficient from the slow rotational correlation time (ϕ_3). The translational diffusion coefficient (D_t) is given by:

$$D_t = r_M^2 / 6\phi_3 \text{ -------(8)}$$

where r_M is the radius of the protein-SUV complex and ϕ_3 is the slow rotational correlational time associated with translation diffusion. The translational diffusion coefficient of α-synuclein on the POPG and POPA membrane were estimated to be ~ 8.71 x 10^{-10} m^2/s and 2.92 x 10^{-10} m^2/s (Table 2.4). These results are in agreement with all of the above results and suggest that α-synuclein on the POPG surface diffuses faster than on the POPA surface due to weaker lipid-protein interaction. Taken together, our results suggest the fluorescence depolarization kinetics reports on local dynamics, segmental mobility and the translational diffusion of α-synuclein on the membrane. Our findings allowed us to depict a model that shows the dynamical events of membrane-bound α-synuclein (Figure 2.12).

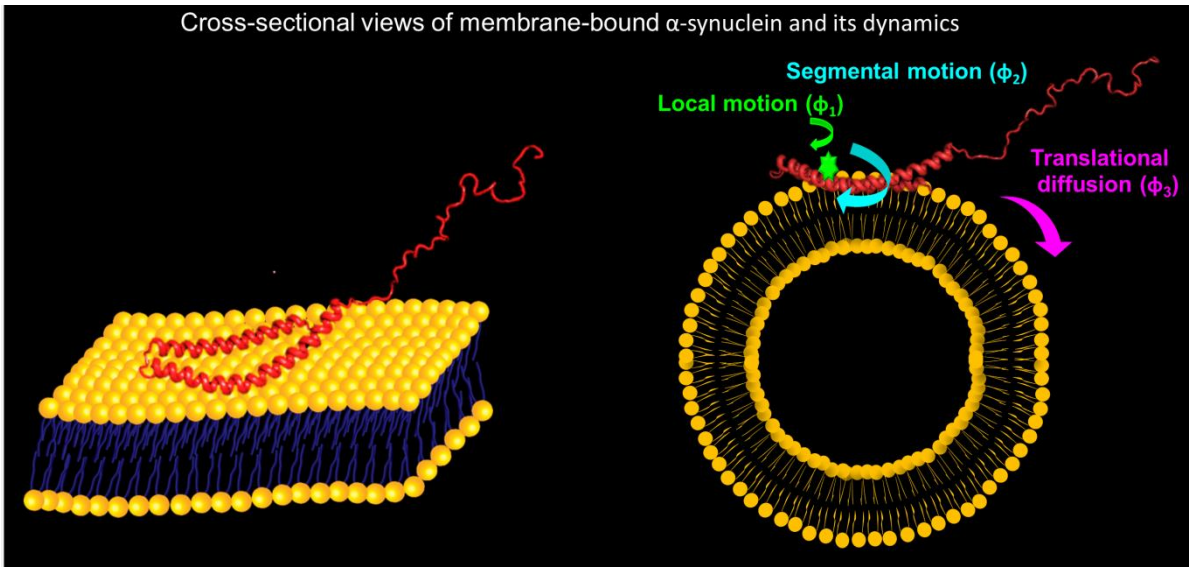

Figure 2.12 A proposed model of membrane-bound α-synuclein dynamics contributed from three dynamically distinct types of motions. The three representative motions of α-synuclein, the wobbling-in-cone motion of the fluorophore (φ_1), the segmental motion of the protein (φ_2) and translational diffusion of protein on the membrane surface (φ_3) is shown on the cross-section of a SUV. The structure of α-synuclein (red) was taken from the protein database (PDB: 1XQ8)[22] and generated using PyMOL (Version 1.8, Schrödinger, LLC, New York).

2.4 Discussion

The α-synuclein and membrane interaction has relevance in both functional and pathological contexts. Our CD data showed the disorder-to-helix conformational switch of α-synuclein upon interaction with the negatively charged synthetic lipid membranes. We utilized the long lifetime fluorophore IAEDANS, covalently attached to α-synuclein, to discern the different dynamical modes of α-synuclein on the membranes in a residue-specific manner. We have

established that the N-terminal and NAC domains bind strongly while the C-terminal remains free from the membrane, which is also in line with previous reports.[15-17, 20, 22, 24] Our results from AEDANS data of membrane-bound α-synuclein are largely consistent with the EPR experiments and Trp fluorescence experiments, where a helical wheel model of α-synuclein–membrane was proposed.[20, 36] Our picosecond time-resolved anisotropy decay results of AEDANS labeled to different single Cys variants of α-synuclein showed three dynamically distinct rotational correlational times for the N-terminal and NAC domain residues. Our results allowed us to establish that the slow rotational correlational time of ~ 60 ns arises due to the translational diffusion of α-synuclein on the membrane. However, the C-terminal residue does not sense this diffusion dynamics because it does not interact with the membrane and undergoes rapid depolarization similar to free monomeric α-synuclein.

Our results reveal subtle differences in the structural and dynamical features of membrane-bound α-synuclein, as a function of vesicles curvature. Our biophysical measurements also suggest higher binding affinity and lower conformational flexibility of α-synuclein when bound to POPG SUVs as opposed to POPG LUVs. These results indicated that the membrane curvature plays a critical role in determining the extent of binding of α-synuclein to the membrane, which is in also in agreement with the previous FCS data on interaction of α-synuclein with GUVs and FRET measurements of α-synuclein interacting with micelles/LUVs.[41, 50] The FCS and FRET data suggest that both curvature as well as lipid composition of the vesicles modulate the extent of binding and the preferred conformation of α-synuclein on the membrane. Although multiple conformations of α-synuclein can coexist on the membrane and undergo energetically favorable inter-conversions, the differences in the recovered rotational correlation times associated with translational diffusion of α-synuclein on SUVs and LUVs might stem from the different conformational preference in the presence of respective membrane surfaces.

The other important feature of our work lies in the fact that our depolarization measurements on membrane-bound α-synuclein can provide insights into the different dynamics of α-synuclein on the negatively charged membrane surfaces as a function of phospholipid headgroup chemistry (POPG, POPA and POPS). The estimated diffusion coefficient of α-synuclein on the POPG membrane (~ 8.4 x 10^{-10} m^2/s) is nearly three times faster than on POPA membranes (~ 2.7 x 10^{-10} m^2/s) which clearly points towards a stronger binding of α-synuclein to POPA SUVs. The slower diffusion of α-synuclein on POPA also corroborates our previous finding that α-synuclein penetrates deeper into the hydrophobic core region of POPA SUVs as compared to other negatively charged lipid vesicles.[37]

Interestingly, the diffusion of any peripheral or transmembrane protein is of prime importance for modulating the signaling between the cells and within the cells. Around 70 % of signaling molecules are unstructured in eukaryotic cells.[51-52] Typical lipid diffusion is occurring on the timescale ~ 10^{-12} m^2/s. The diffusion coefficient of free α-syn in solution as obtained from NMR as well as FCS measurements is ~ 10^{-10} m^2/s.[53-54] The translational diffusion coefficients estimated from our experiments in membrane-bound α-syn is in the order of ~ 10^{-10} m^2/s. The translation diffusion of lipids is 100 times slower than the estimated timescale of α-syn diffusion both in the absence and presence of membranes. The translational diffusion coefficient of α-syn on POPG SUVs, obtained from our time-resolved fluorescence measurements, is also in reasonable agreement with the polymer surfactant aggregates, where using time-resolved fluorescence anisotropy decay, translation diffusion of polymer was observed in the range 1-5 x 10^{-10} m^2/s.[55] All these results suggest that fluorescence depolarization kinetics measurements offer a reliable methodology to estimate the translational diffusion coefficient of membrane-associated proteins.

In summary, our work highlights the studies performed by time-resolved fluorescence anisotropy decay experiments in combination with the other spectroscopic measurements and demonstrates the dynamics of α-synuclein on the negatively charged membranes having distinct headgroup chemistry and membrane curvature. Additionally, our results also illustrate that the curvature of the membrane plays an important role in the structure and dynamics of α-syn. The structural and dynamical modulation in α-syn, upon interaction with membranes, also has an impact on membrane topology and lipid packing which could potentially help in the fusion of vesicles in the presynaptic terminal of the neurons. The translational diffusion of α-synuclein on membrane also has the ability to modulate the local/temporal concentration of the protein on the membrane which can potentially trigger pathological amyloid formation. Therefore, the translational diffusion of α-synuclein on a membrane surface could be of prime importance for elucidating its physiological function as well as its role in Parkinson's diseases progression.

2.5 References:

1. Jensen, R. B.; Wang, S. C.; Shapiro, L., Dynamic localization of proteins and DNA during a bacterial cell cycle. *Nat Rev Mol Cell Biol* **2002,** *3* (3), 167-76.

2. Goedert, M., NEURODEGENERATION. Alzheimer's and Parkinson's diseases: The prion concept in relation to assembled Abeta, tau, and alpha-synuclein. *Science* **2015,** *349* (6248), 1255555.

3. Chiti, F.; Dobson, C. M., Protein Misfolding, Amyloid Formation, and Human Disease: A Summary of Progress Over the Last Decade. *Annu Rev Biochem* **2017,** *86*, 27-68.

4. Waxman, E. A.; Giasson, B. I., Molecular mechanisms of α-synuclein neurodegeneration. *Biochimica et Biophysica Acta (BBA) - Molecular Basis of Disease* **2009,** *1792* (7), 616-624.

5. Breydo, L.; Wu, J. W.; Uversky, V. N., Alpha-synuclein misfolding and Parkinson's disease. *Biochim Biophys Acta* **2012,** *2*, 261-85.

6. Maroteaux, L.; Campanelli, J. T.; Scheller, R. H., Synuclein: a neuron-specific protein localized to the nucleus and presynaptic nerve terminal. *J Neurosci* **1988,** *8* (8), 2804-15.

7. Deleersnijder, A.; Gerard, M.; Debyser, Z.; Baekelandt, V., The remarkable conformational plasticity of alpha-synuclein: blessing or curse? *Trends Mol Med* **2013,** *19* (6), 368-77.

8. Cooper, A. A.; Gitler, A. D.; Cashikar, A.; Haynes, C. M.; Hill, K. J.; Bhullar, B.; Liu, K.; Xu, K.; Strathearn, K. E.; Liu, F.; Cao, S.; Caldwell, K. A.; Caldwell, G. A.; Marsischky, G.; Kolodner, R. D.; Labaer, J.; Rochet, J. C.; Bonini, N. M.; Lindquist, S., Alpha-synuclein blocks ER-Golgi traffic and Rab1 rescues neuron loss in Parkinson's models. *Science* **2006,** *313* (5785), 324-8.

9. Burre, J.; Sharma, M.; Tsetsenis, T.; Buchman, V.; Etherton, M. R.; Sudhof, T. C., Alpha-synuclein promotes SNARE-complex assembly in vivo and in vitro. *Science* **2010,** *329* (5999), 1663-7.

10. Burre, J.; Sharma, M.; Sudhof, T. C., alpha-Synuclein assembles into higher-order multimers upon membrane binding to promote SNARE complex formation. *Proc Natl Acad Sci U S A* **2014,** *111* (40), 22.

11. Lai, Y.; Kim, S.; Varkey, J.; Lou, X.; Song, J. K.; Diao, J.; Langen, R.; Shin, Y. K., Nonaggregated alpha-synuclein influences SNARE-dependent vesicle docking via membrane binding. *Biochemistry* **2014,** *53* (24), 3889-96.

12. Drescher, M.; Huber, M.; Subramaniam, V., Hunting the chameleon: structural conformations of the intrinsically disordered protein alpha-synuclein. *Chembiochem* **2012,** *13* (6), 761-8.

13. Ullman, O.; Fisher, C. K.; Stultz, C. M., Explaining the structural plasticity of alpha-synuclein. *J Am Chem Soc* **2011,** *133* (48), 19536-46.

14. Uversky, V. N., A protein-chameleon: conformational plasticity of alpha-synuclein, a disordered protein involved in neurodegenerative disorders. *J Biomol Struct Dyn* **2003,** *21* (2), 211-34.

15. Pfefferkorn, C. M.; Jiang, Z.; Lee, J. C., Biophysics of α-synuclein membrane interactions. *Biochimica et Biophysica Acta (BBA) - Biomembranes* **2012,** *1818* (2), 162-171.

16. Nath, A.; Rhoades, E., A flash in the pan: dissecting dynamic amyloid intermediates using fluorescence. *FEBS Lett* **2013,** *587* (8), 1096-105.

17. Bartels, T.; Ahlstrom, L. S.; Leftin, A.; Kamp, F.; Haass, C.; Brown, M. F.; Beyer, K., The N-terminus of the intrinsically disordered protein alpha-synuclein triggers membrane binding and helix folding. *Biophys J* **2010,** *99* (7), 2116-24.

18. Vamvaca, K.; Volles, M. J.; Lansbury, P. T., Jr., The first N-terminal amino acids of alpha-synuclein are essential for alpha-helical structure formation in vitro and membrane binding in yeast. *J Mol Biol* **2009,** *389* (2), 413-24.

19. Bussell, R., Jr.; Eliezer, D., A structural and functional role for 11-mer repeats in alpha-synuclein and other exchangeable lipid binding proteins. *J Mol Biol* **2003,** *329* (4), 763-78.

20. Jao, C. C.; Der-Sarkissian, A.; Chen, J.; Langen, R., Structure of membrane-bound alpha-synuclein studied by site-directed spin labeling. *Proc Natl Acad Sci U S A* **2004,** *101* (22), 8331-6.

21. Chandra, S.; Chen, X.; Rizo, J.; Jahn, R.; Sudhof, T. C., A broken alpha -helix in folded alpha -Synuclein. *J Biol Chem* **2003,** *278* (17), 15313-8.

22. Ulmer, T. S.; Bax, A.; Cole, N. B.; Nussbaum, R. L., Structure and dynamics of micelle-bound human alpha-synuclein. *J Biol Chem* **2005,** *280* (10), 9595-603.

23. Bisaglia, M.; Tessari, I.; Pinato, L.; Bellanda, M.; Giraudo, S.; Fasano, M.; Bergantino, E.; Bubacco, L.; Mammi, S., A topological model of the interaction between alpha-synuclein and sodium dodecyl sulfate micelles. *Biochemistry* **2005,** *44* (1), 329-39.

24. Bussell, R., Jr.; Ramlall, T. F.; Eliezer, D., Helix periodicity, topology, and dynamics of membrane-associated alpha-synuclein. *Protein Sci* **2005,** *14* (4), 862-72.

25. Robotta, M.; Braun, P.; van Rooijen, B.; Subramaniam, V.; Huber, M.; Drescher, M., Direct evidence of coexisting horseshoe and extended helix conformations of membrane-bound alpha-synuclein. *Chemphyschem* **2011,** *12* (2), 267-9.

26. Ferreon, A. C.; Gambin, Y.; Lemke, E. A.; Deniz, A. A., Interplay of alpha-synuclein binding and conformational switching probed by single-molecule fluorescence. *Proc Natl Acad Sci U S A* **2009,** *106* (14), 5645-50.

27. Bodner, C. R.; Dobson, C. M.; Bax, A., Multiple tight phospholipid-binding modes of alpha-synuclein revealed by solution NMR spectroscopy. *J Mol Biol* **2009,** *390* (4), 775-90.

28. Epand, R. M., Lipid polymorphism and protein-lipid interactions. *Biochim Biophys Acta* **1998,** *10* (3), 353-68.

29. van Meer, G.; Voelker, D. R.; Feigenson, G. W., Membrane lipids: where they are and how they behave. *Nat Rev Mol Cell Biol* **2008,** *9* (2), 112-24.

30. Engelman, D. M., Membranes are more mosaic than fluid. *Nature* **2005,** *438* (7068), 578-80.

31. Pandey, A. P.; Haque, F.; Rochet, J. C.; Hovis, J. S., alpha-Synuclein-induced tubule formation in lipid bilayers. *J Phys Chem B* **2011,** *115* (19), 5886-93.

32. Varkey, J.; Isas, J. M.; Mizuno, N.; Jensen, M. B.; Bhatia, V. K.; Jao, C. C.; Petrlova, J.; Voss, J. C.; Stamou, D. G.; Steven, A. C.; Langen, R., Membrane curvature induction and tubulation are common features of synucleins and apolipoproteins. *J Biol Chem* **2010,** *285* (42), 32486-93.

33. Ouberai, M. M.; Wang, J.; Swann, M. J.; Galvagnion, C.; Guilliams, T.; Dobson, C. M.; Welland, M. E., alpha-Synuclein senses lipid packing defects and induces lateral expansion of lipids leading to membrane remodeling. *J Biol Chem* **2013,** *288* (29), 20883-95.

34. Braun, A. R.; Sevcsik, E.; Chin, P.; Rhoades, E.; Tristram-Nagle, S.; Sachs, J. N., alpha-Synuclein induces both positive mean curvature and negative Gaussian curvature in membranes. *J Am Chem Soc* **2012,** *134* (5), 2613-20.

35. Engelman, D. M., Membranes are more mosaic than fluid. *Nature* **2005,** *438*, 578.

36. Jain, N.; Bhasne, K.; Hemaswasthi, M.; Mukhopadhyay, S., Structural and Dynamical Insights into the Membrane-Bound α-Synuclein. *PLOS ONE* **2013,** *8* (12), e83752.

37. Drescher, M.; Veldhuis, G.; van Rooijen, B. D.; Milikisyants, S.; Subramaniam, V.; Huber, M., Antiparallel arrangement of the helices of vesicle-bound alpha-synuclein. *J Am Chem Soc* **2008,** *130* (25), 7796-7.

38. Wang, R.; Sun, S.; Bekos, E. J.; Bright, F. V., Dynamics Surrounding Cys-34 in Native, Chemically Denatured, and Silica-Adsorbed Bovine Serum Albumin. *Analytical Chemistry* **1995,** *67* (1), 149-159.

39. Hudson, E. N.; Weber, G., Synthesis and characterization of two fluorescent sulfhydryl reagents. *Biochemistry* **1973,** *12* (21), 4154-4161.

40. Jain, N.; Narang, D.; Bhasne, K.; Dalal, V.; Arya, S.; Bhattacharya, M.; Mukhopadhyay, S., Direct Observation of the Intrinsic Backbone Torsional Mobility of Disordered Proteins. *Biophysical Journal 111* (4), 768-774.

41. Trexler, A. J.; Rhoades, E., Alpha-synuclein binds large unilamellar vesicles as an extended helix. *Biochemistry* **2009,** *48* (11), 2304-2306.

42. Eliezer, D.; Kutluay, E.; Bussell, R., Jr.; Browne, G., Conformational properties of alpha-synuclein in its free and lipid-associated states. *J Mol Biol* **2001,** *307* (4), 1061-73.

43. Wang, G. F.; Li, C.; Pielak, G. J., 19F NMR studies of alpha-synuclein-membrane interactions. *Protein Sci* **2010,** *19* (9), 1686-91.

44. Bertoncini, C. W.; Jung, Y.-S.; Fernandez, C. O.; Hoyer, W.; Griesinger, C.; Jovin, T. M.; Zweckstetter, M., Release of long-range tertiary interactions potentiates aggregation of natively unstructured α-synuclein. *Proceedings of the National Academy of Sciences of the United States of America* **2005,** *102* (5), 1430-1435.

45. Fusco, G.; De Simone, A.; Arosio, P.; Vendruscolo, M.; Veglia, G.; Dobson, C. M., Structural Ensembles of Membrane-bound α-Synuclein Reveal the Molecular Determinants of Synaptic Vesicle Affinity. *Scientific Reports* **2016,** *6*, 27125.

46. Lokappa, S. B.; Ulmer, T. S., Alpha-synuclein populates both elongated and broken helix states on small unilamellar vesicles. *J Biol Chem* **2011,** *286* (24), 21450-7.

47. Krishna, M. M. G.; Das, R.; Periasamy, N.; Nityananda, R., Translational diffusion of fluorescent probes on a sphere: Monte Carlo simulations, theory, and fluorescence anisotropy experiment. *The Journal of Chemical Physics* **2000,** *112* (19), 8502-8514.

48. Maiti, N. C.; Krishna, M. M. G.; Britto, P. J.; Periasamy, N., Fluorescence Dynamics of Dye Probes in Micelles. *The Journal of Physical Chemistry B* **1997,** *101* (51), 11051-11060.

49. Krishna, M. M.; Srivastava, A.; Periasamy, N., Rotational dynamics of surface probes in lipid vesicles. *Biophys Chem* **2001,** *90* (2), 123-33.

50. Middleton, E. R.; Rhoades, E., Effects of Curvature and Composition on α-Synuclein Binding to Lipid Vesicles. *Biophysical Journal* **2010,** *99* (7), 2279-2288.

51. Sigalov, A. B., Protein intrinsic disorder and oligomericity in cell signaling. *Mol Biosyst* **2010,** *6* (3), 451-61.

52. Iakoucheva, L. M.; Brown, C. J.; Lawson, J. D.; Obradovic, Z.; Dunker, A. K., Intrinsic disorder in cell-signaling and cancer-associated proteins. *J Mol Biol* **2002,** *323* (3), 573-84.

53. Nath, S.; Meuvis, J.; Hendrix, J.; Carl, S. A.; Engelborghs, Y., Early aggregation steps in alpha-synuclein as measured by FCS and FRET: evidence for a contagious conformational change. *Biophys J* **2010,** *98* (7), 1302-11.

54. Wang, Y.; Benton, L. A.; Singh, V.; Pielak, G. J., Disordered Protein Diffusion under Crowded Conditions. *The Journal of Physical Chemistry Letters* **2012,** *3* (18), 2703-2706.

55. Sen, S.; Sukul, D.; Dutta, P.; Bhattacharyya, K., Fluorescence Anisotropy Decay in Polymer−Surfactant Aggregates. *The Journal of Physical Chemistry A* **2001,** *105* (32), 7495-7500.

Synergistic Amyloid Switch Triggered by Early Heterotypic Oligomerization of Intrinsically Disordered α-Synuclein and Tau

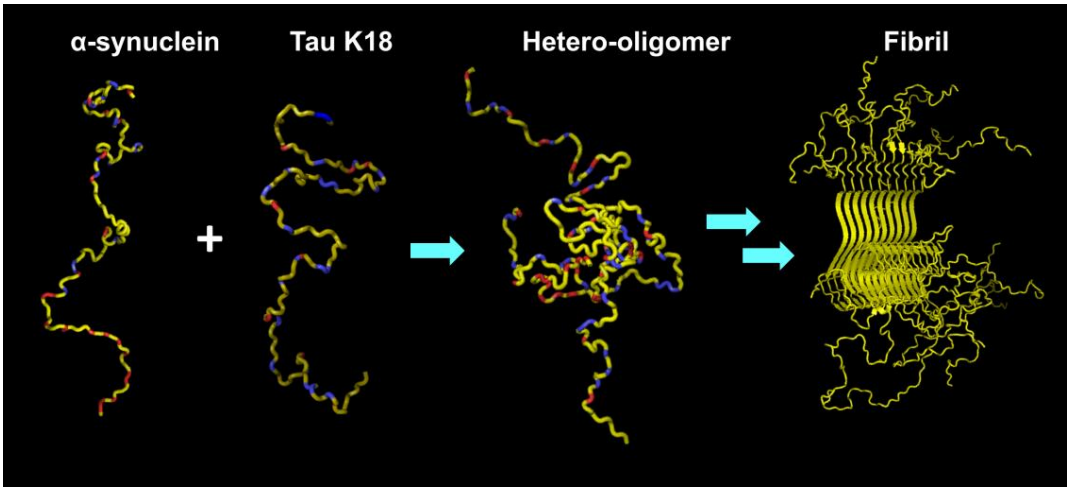

3.1 Introduction

Amyloids represent exquisite protein nanoaggregates that are constituted by characteristic cross-β structure and are implicated in a variety of devastating neurodegenerative diseases.[1-5] Many of the amyloidogenic proteins are intrinsically disordered in their monomeric form and convert into highly ordered amyloid fibrils through a complex cascade of conformational changes and assembly events. For instance, α-synuclein (α-syn) is a small (14.5 kDa) intrinsically disordered protein (IDP), amyloid formation of which is associated with Parkinson's disease (PD).[6-9] α-synuclein is predominantly found in the cytosol of presynaptic terminals.[10] The precise function of α-synuclein remains elusive and is proposed to be involved in functions such as vesicle localization, neurotransmitter release, maintaining neuronal plasticity etc.[11-13] α-synuclein is divided into three distinct regions: the positively charged N-terminal region (1-60 amino acids) which initiates the membrane-binding; the hydrophobic amino acid rich central region (61-95 amino acids) known as NAC (non-amyloid β-component of Alzheimer's amyloid) domain which forms the amyloid core; the C-terminal end (96-140 amino acids) is highly negatively charged because of the presence of ten glutamates and five aspartates[14-16] (Figure 3.1A). The acidic C-terminal segment binds to calcium and other cations and plays an important role in chaperone functioning.[17-19] The conformational plasticity of α-synuclein allows it to interact with a wide range of partners including membranes and different proteins.[14, 20-21] The molecular structure of α-synuclein amyloid fibrils is poorly understood. However, several studies using infrared spectroscopy[22], small angle X-ray scattering[23-24], nuclear magnetic resonance[25-26] and electronic paramagnetic resonance[27-28] provide insights into the structure of the fibrils and suggest that the NAC domain forms the solvent-protected core of amyloids.[29-30] Recent high-resolution structural studies revealed the architecture of the toxic core comprising 11-residue peptide segment of the NAC domain of α-synuclein.[31] PD linked point mutations, including A30P, E46K, and A53T have been shown to alter the fibrillization kinetics.[32-33]

Tau is also an amyloidogenic IDP that is found mostly in the central- and the peripheral nervous systems.[34-35] It is a highly soluble microtubule binding protein, which interacts with tubulin and stabilizes the polymerization of tubulin.[36] Hyper-phosphorylation of tau at specific residues result in self-assembly of tau into tangled paired helical filaments that are implicated in Alzheimer's disease (AD).[37] In human brain tissues, six different isoforms of tau are formed by alternative mRNA splicing, which differs in the number of microtubule binding domains.[38] Among six different isoforms, Tau K18 is consists of four repeats (Figure

3.1B) and fails to aggregate for a considerably long period of time under physiological conditions. Tau K18 aggregation is catalyzed in the presence of polyanionic cofactors, such as heparin, RNA, polyglutamate, fatty acids, etc. and it exhibits faster aggregation kinetics as compared to full-length tau under similar aggregation condition (in the presence of cofactor) and forms the amyloid core.[39-42] A remarkable conformational plasticity of tau K18 allows it to form liquid droplets in a phosphorylation-specific manner and showed a phase-separated state.[43] Therefore, the behavior of the tau K18 fragment is under intense scrutiny. Recent studies have shown that human brain tau acts as a ligand for α-synuclein and that they co-localize in axons.[44] This intermolecular interaction is known to modulate the phosphorylation of tau and can potentially affect a variety of signaling pathways. Recent evidences suggest that tau and α-synuclein interact to form pathological co-amyloids that are localized in different regions of the brain and are associated with several neurological diseases such as PD, AD, Down syndrome, multiple system atrophy etc.[45-48]

Inspite of the broad acceptance of the α-synuclein and tau interaction, little is known about the early intermolecular interactions that govern oligomerization and amyloid formation. In this work, we investigated the heterotypic early interactions of α-synuclein and tau K18 at the residue-specific level. Recent studies have shown that oligomeric intermediate species are more toxic than the high molecular weight aggregates such as ordered amyloid fibrils.[49-52] Our studies allowed us to construct the conformational dynamics map as well as to elucidate the early (oligomeric state) and late (amyloid state) intermolecular association of α-synuclein and tau K18. We found that α-synuclein and tau K18 co-aggregate with a significantly shorter lag phase by rapid conformational sequestration within the oligomers that mature into amyloid fibrils. A more profound effect was observed in the case of a familial PD mutant, A30P α-synuclein that is known to aggregate with a long lag phase that allows accumulation of toxic oligomeric intermediates.[52-53] Interestingly, the interaction between A30P α-synuclein and tau K18 result in a more efficient aggregation process by significantly shortening the lag phase. Therefore, the critical early intermolecular interaction could potentially play a protective role under physiological condition by rapid recruitment of the toxic oligomers into less-toxic matured amyloid fibrils.

3.2 Experimental Section

3.2.1 Materials

IAEDANS (1,5-IAEDANS, 5-((((2-Iodoacetyl) amino) ethyl) amino) Naphthalene-1-Sulfonic Acid), AlexaFluor 488 C_5-maleimide and AlexaFluor 594 C_5-maleimide were purchased from Invitrogen. All the other chemicals were procured from Sigma Aldrich (St. Louis, MO). Protein concentrators and filters were obtained from Merck Millipore. Q Sepharose resin, SP Sepharose resin and PD-10 column were procured from GE Healthcare Life Sciences (USA).

3.2.2 Mutagenesis, expression and purification of α-synuclein and tau K18

Human α-synuclein and tau K18 were cloned in pT7.7 and pET23a vectors, respectively. Both the plasmids were transformed in E.coli BL21(DE3). The single Trp mutants of α-synuclein (F4W, A27W, Y39W, A56W, A69W, A78W, A90W, A107W, A124W, and A140W) used for the experiments were same as mentioned in Jain et.al 2013.[21] Single point mutation at S9C and A30P α-synuclein were created using site-directed mutagenesis kit, Quick Change, purchased from Stratagene. Following primers were used for creating the mutations.

A30P F: 5'-GGGTGTGGCAGAAGCACCAGGAAAGACAAAAGAGGG-3'
A30P R: 5'-CCCTCTTTTGTCTTTCCTGGTGCTTCTGCCACACCC-3'
S9C F: 5'-CATGAAAGGACTTTGTAAGGCCAAGGAGGG-3'
S9C R: 5'-CCCTCCTTGGCCTTACAAAGTCCTTTCATG-3'

Mutations were confirmed by DNA sequencing. Wild-type and variants of α-synuclein were expressed and purified using the reported protocol[21] with slight modification. Briefly, the grown culture was induced with 800 µM Isopropyl β-D-1-thiogalactopyranoside at 30 °C for 8 hours for better induction. The cells were lysed using lysis buffer (50 mM Tris, 150 mM NaCl, 10 mM EDTA, pH 8 containing 50 µL protease inhibitor cocktail) and boiled at 95 °C for 30 mins followed by centrifugation at 12,000 rpm for 30 min at 4 °C. The supernatant was mixed with 136 µL/mL of 10 % streptomycin sulphate and 228 µL/mL of glacial acetic acid for precipitating DNA. After DNA removal, equal volume of saturated ammonium sulphate was added and kept at 4 °C with an intermittent mixing for 1 hour for precipitated protein. The protein pellet was washed with ammonium acetate and ethanol in equal ratio. The pellet was suspended in equilibrating buffer (10 mM Tris, pH 7.4) and further purified by FPLC

(fast performance liquid chromatography) on a Q Sepharose column. The purity of the collected fractions was assessed by SDS-PAGE (Figure 3.2). The pure fractions were dialyzed in a dialysis buffer (20 mM Tris, 50 mM NaCl, pH 7.4) and stored at -80 °C. Required amount of protein were taken out and filtered through 50 kDa filter and monomeric protein was used for the experiments. The purification protocol for tau K18 was similar to α-synuclein with minor changes. The equilibrating buffer for tau K18 was 20 mM MES (2-(N-morpholino) ethanesulfonic acid), 1 mM EDTA, 2 mM DTT, 1 mM $MgCl_2$, pH6.8. SP Sepharose column was used and the purity of the collected fractions was assessed by SDS-PAGE (Figure 3.2). The pure fractions were dialyzed in a dialysis buffer (MES 20 mM, $MgCl_2$ 1 mM, DTT 2 mM and EDTA 1 mM, pH 6.8) and stored at -80 °C.

3.2.3 α-synuclein and tau K18 co-aggregation kinetics

α-Synuclein and tau K18 co-aggregation was carried out using monomeric proteins in varied concentrations on a POLARstar Omega Plate Reader Spectrophotometer (BMG LABTECH, Germany) using 96 well plate. The aggregation reaction of 150 μL with a 3 mm glass bead was setup in 14 mM MES, pH 6.8 with 600 rpm orbital shaking and temperature was set at 37 ºC. The ThT concentration used for the aggregation was 20 μM. The aggregation reactions were allowed to reach saturation and the lag time from the data was extracted using nucleation-dependent polymerization model[54] and plotted using Origin software. Standard deviations were calculated from three or more repeats.

3.2.4 Steady-state fluorescence

Aggregates of α-synuclein Trp mutants were prepared in the presence and absence tau K18 in the aggregation buffer (in 14 mM MES, pH 6.8). The Trp emission spectra and anisotropy were collected at 0 h and in the saturation phase (aggregates were separated using centrifugation at 15,000 rpm for 10 min at 25 ºC). The concentrations of α-synuclein and tau K18 were fixed at 20 μM and 50 μM in all the experiments, until mentioned otherwise.

All steady state experiments were carried out on a Fluoromax-4 (Horiba Jobin Yvon, NJ) using 10 mm quartz cuvette at 25 ºC. The aggregates were stirred using magnetic bead while collecting the data. Following parameters were adjusted for collecting Trp emission spectra: λ_{ex} = 295 nm and λ_{em} (scan range) = 310 nm to 400 nm with the integration time of 1 s. The excitation and emission bandpass were adjusted to 1 nm and 3 nm, respectively. All the

spectra were buffer subtracted and intensity-normalized at the peak maximum to visualize the spectral-shifts using OriginPro Version 8.5 software. The steady-state anisotropy is given by:

$r = (I_{||}-GI_{\perp}) / (I_{||}+2GI_{\perp})$,

where, $I_{||}$ and $I_{\perp}$ are fluorescence intensities collected using parallel (VV) and perpendicular geometry (VH), respectively and G is an instrument and wavelength dependent correction factor to compensate for the polarization bias of the detection system. The perpendicular components were always corrected using a G-factor and it was determined by measuring the HV and HH fluorescence intensities and the ratio of HV to HH was used as a G-factor.

For Trp anisotropy measurements, excitation wavelength and bandpass were fixed to 295 nm and 2 nm, respectively, whereas emission wavelength was fixed at 346 nm with a bandpass of 5 nm. The integration time was fixed as 3 s.

For FRET measurements, the two native Cys of tau K18 were randomly labeled with IAEDANS in native buffer condition (MES 14 mM, pH6.8) and free dye was removed using desalting PD-10 column (GE Healthcare). Trp and AEDANS were used as a FRET pair and efficiency was estimated using the following equation:

$E = 1 - F_{DA}/F_D$

Where, F_{DA} and F_D are the fluorescence of the donor (Trp) in presence and absence of acceptor (AEDANS), respectively.[55] The direct fluorescence of the acceptor was subtracted from the data.

3.2.5 Dynamic light scattering

The sizes of the proteins at the early oligomeric state were determined using Malvern Zetasizer Nano-ZS90 instrument. A He-Ne laser (632 nm) was used for exciting the samples. All the buffers and solutions were filtered through 0.02 μm filters (Anatop 10 filter; Whatman).[56] Monomeric α-synuclein (20 μM), tau K18 (50 μM) and mixture of both were used for the measurements.

3.2.6 Glutaraldehyde crosslinking assay

Glutaraldehyde crosslinking assay was performed to characterize the oligomers. The monomeric α-synuclein, tau K18 and the mixture of both were used (10 μM each). We treated the sample with 0.05 % of glutaraldehyde for 15 mins at 25 ºC followed by quenching with 0.05 M sodium borohydride for 15 min. The samples were run on the SDS−PAGE and visualized by Coomassie blue staining.[57]

3.2.7 CD experiments

The far-UV CD spectra were recorded on a Chirascan CD spectrometer (Applied Photophysics, UK) at room temperature. The monomeric α-synuclein, monomeric tau K18 and mixtures of both were taken in 1 mm path length quartz cuvette. The secondary structural changes were recorded in the range of 205-260 nm. For the co-aggegates of α-synuclein and tau K18, monomers were removed by centrifugation and CD spectra were collected in 10 mm cuvette. The final spectrum was averaged over three scans, was corrected with buffer baseline subtraction and plotted using Origin Software.

3.2.8 AFM imaging

Freshly cleaved mica (muscovite grade V-4 mica from SPI, PA) was washed with MQ water and 10 μL of undiluted sample was deposited on it for 10 mins drying followed by washing with 500 μL of MQ water. After wash, the sample was kept under mild stream of nitrogen gas for 30 mins for drying. The images were acquired using Innova (Bruker) AFM in tapping mode. The collected images were processed and analyzed by using WSxM 5.0.[58]

3.2.9 Stopped-flow fluorescence

Stopped-flow mixing experiments were carried out on a spectrometer (Chirascan, Applied Photophysics) connected to a stopped-flow apparatus (SF.3, Applied Photophysics) as reported in our previous studies.[59] Monomeric α-synuclein and tau K18 were mixed in the buffer (MES 14 mM, pH 6.8) in 1:10 ratio, with the final concentration of α-synuclein and tau K18 were 20 μM and 50 μM, respectively. The deadtime of mixing was ~ 3 ms. For the Trp fluorescence studies, Trp 4 and Trp 124 variants of α-synuclein were used with the excitation at 295 nm and fluorescence was collected using 320 nm log pass filter. The kinetic traces were collected for 1 sec with 1000 time points and were averaged over 10 datasets to get a better single to noise ratio. The datasets of Trp 4 and Trp 124 of α-synuclein in the presence and absence of tau K18 were averaged and plotted using Origin software.

3.2.10 Salt-dependent studies of α-synuclein and tau K18

For the monomeric interaction of α-synuclein and tau K18, Trp 4 and Trp 124 variants of α-synuclein were used and Trp anisotropy was measured in the presence of increasing salt concentration. The aggregation kinetics of α-synuclein (20 μM) and tau K18 (50 μM) was

performed in plate reader at different concentrations of NaCl (5 mM, 10 mM, 20 mM, 50 mM, 100 mM, 150 mM and 200 mM). The lag time from the data was extracted using nucleation-dependent polymerization model[54] and plotted using Origin software.

3.2.11 Confocal imaging of α-synuclein-tau K18 fibrils

S9C α-synuclein was labeled with AlexaFluor 594 C_5-maleimide and the two native Cys residues of tau K18 were randomly labeled using AlexaFluor 488 C_5-maleimide in native buffer condition and free dye was removed using PD-10 column followed by filtration with 3 kDa MWCO filter. The aggregation kinetics of α-synuclein and tau K18 was performed as mentioned above. In the saturation phase, 10 µl aliquot was placed on the glass slide, mounted with coverslip and imaged under the confocal microscope. Images were collected on a Zeiss LSM 780 (Carl Zeiss, Germany) confocal laser scanning microscope. Images were then analyzed in ImageJ (NIH, Bethesda, MD, USA) software.[60]

3.3 Results and discussion

3.3.1 Synergistic effect in α-synuclein and tau K18 aggregation

In order to discern the synergistic effect of α-synuclein and tau K18, we initiated our studies by monitoring the aggregation kinetics of α-synuclein, tau K18 and their different stoichiometric mixtures using a well-known amyloid marker namely, thioflavin-T (ThT).[55] α-Synuclein and tau K18 were expressed, purified and purity was checked by SDS-PAGE

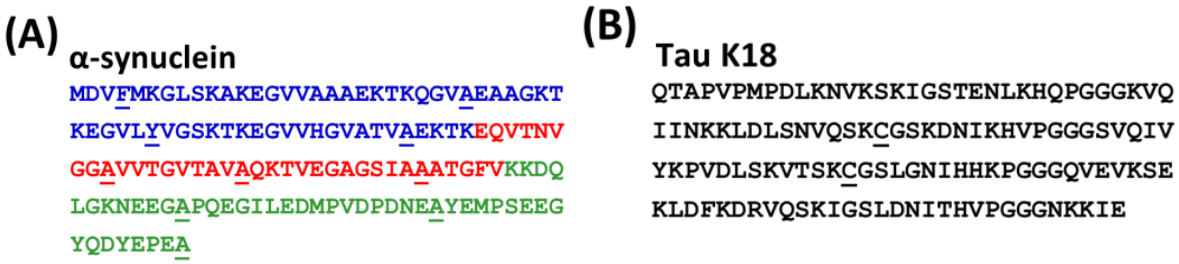

Figure 3.1 (A) Amino acid sequence of α-synuclein: N-terminal (blue), NAC domain (red) and C-terminal (green) (Trp mutational sites are underscored). (B) Amino acid sequence of tau K18 (black) (Native Cys are underscored).

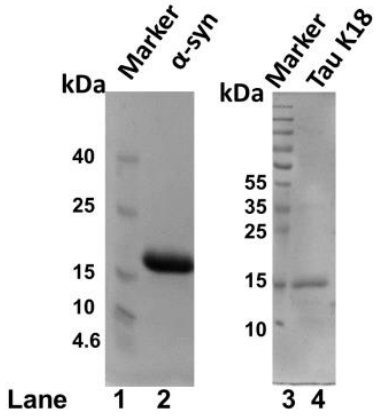

Figure 3.2 15% SDS-PAGE purified α-synuclein and tau K18, markers (lane 1 and 4), α-synuclein (lane 2), and tau K18 (lane 4).

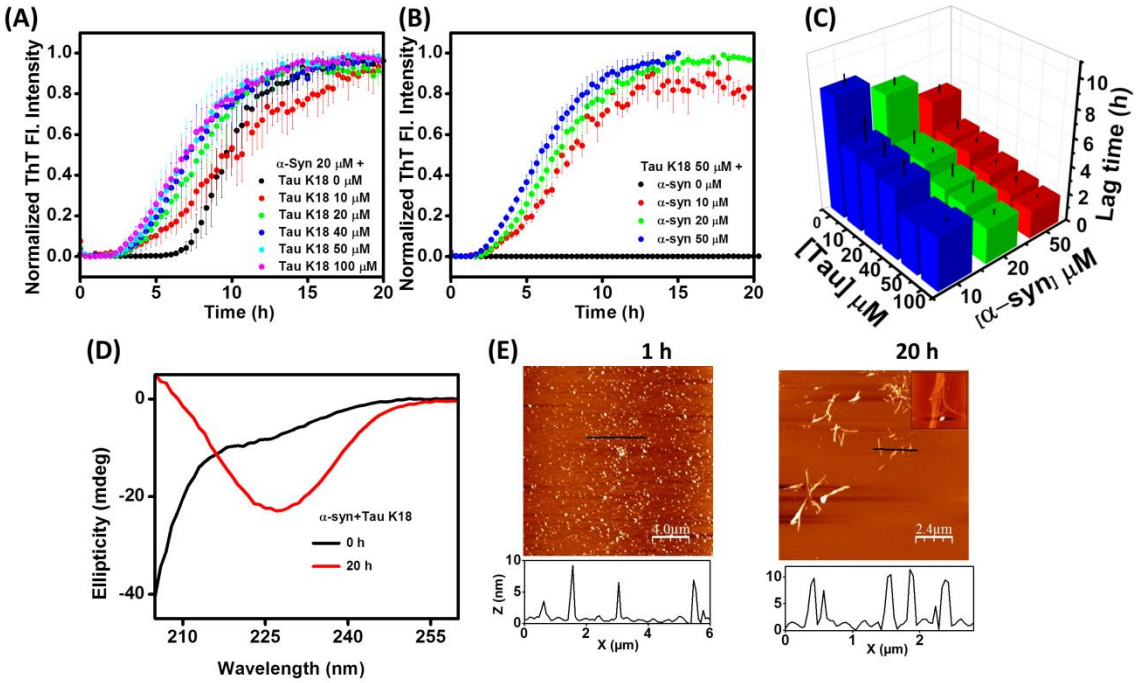

Figure 3.3 (A) Normalized ThT fluorescence aggregation kinetics of α-synuclein (20 μM) in the presence of different concentrations of tau K18 (0-100 μM). The solid lines are the fits obtained using the nucleation-dependent polymerization model (55). (B) Aggregation kinetics of Tau K18 (50 μM) in the presence of different concentrations of α-synuclein (0-50 μM). (C) Bar plots of lag time recovered from the fits from the aggregation kinetics of α-synuclein at 10 μM (blue), 20 μM (green) and 50 μM (red) in the presence of varied concentrations of tau K18 (0-100 μM). (D) Far-UV CD spectra of α-synuclein and tau K18 aggregates at 0 h (black) and 20 h (red). (E) AFM images of α-synuclein (20 μM) and tau K18 (50 μM) aggregates showing a transition from spherical oligomers (1 h) to straight fibril (20 h). Error bars are obtained from at least three independent measurements.

(Figure 3.2). The time-course of α-synuclein aggregation exhibited a typical nucleation-dependent kinetics comprising a lag phase. The lag phase became shorter, when we added tau K18 to α- synuclein (Figure 3.3A). For instance, α-synuclein (20 μM) exhibited a lag phase of ~ 7.5 h that was shortened to ~3 h in the presence 50 μM tau K18. Under the same aggregation condition, tau K18 alone did not aggregate on this timescale. Upon addition of α-synuclein, we observed nucleation-dependent aggregation kinetics of tau K18 (Figure 3.4).

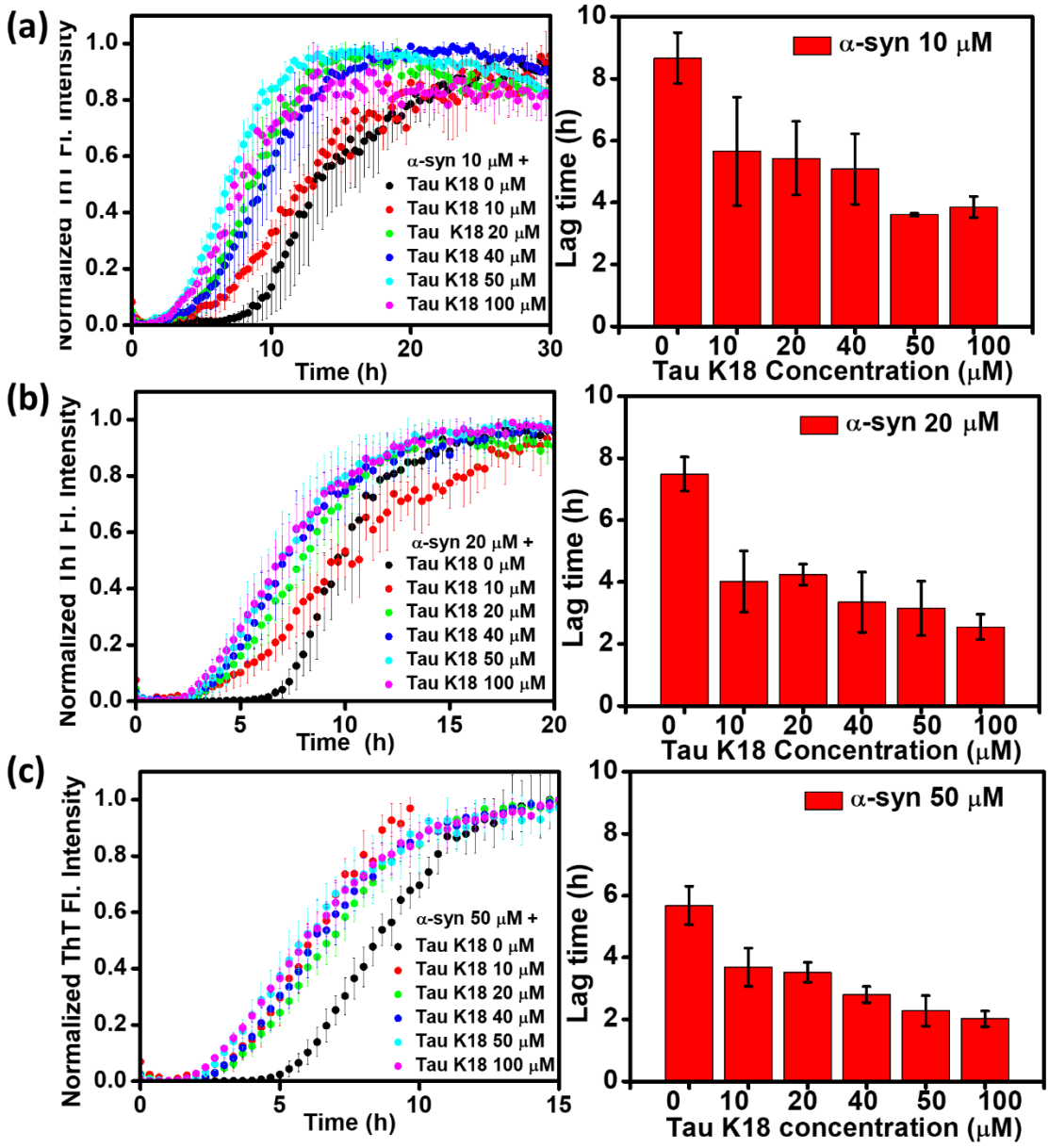

Figure 3.4 Concentration titration of α-synuclein and tau K18 aggregation. (A) α-synuclein (10 μM) and tau K18 (0-100 μM). (B) α-synuclein (20 μM) and tau K18 (0-100 μM). (C) α-synuclein (50 μM) and tau K18 (0-100 μM). The bar plots showed the lag time of aggregation kinetics. Error bars indicate SDs from three or more repeats.

Table 3.1

Lag time extracted from concentration titration of α-synucleinand tau K18 aggregation kinetics. Data was fitted using the equation mentioned in Arora et.al [54].

S.No.	Aggregation Condition	Lag time (h)
1	α-synuclein (10 μM)	8.67 ± 0.82
2	α-synuclein (20 μM)	7.49 ± 0.55
3	α-synuclein (50 μM)	5.68 ± 0.62
4	α-synuclein (10 μM) + Tau K18 (10 μM)	5.65 ± 1.75
5	α-synuclein (10 μM) + Tau K18 (20 μM)	5.43 ± 1.19
6	α-synuclein (10 μM) + Tau K18 (40 μM)	5.08 ± 1.14
7	α-synuclein (10 μM) + Tau K18 (50 μM)	3.61 ± 0.04
8	α-synuclein (10 μM) + Tau K18 (100 μM)	3.86 ± 0.34
9	α-synuclein (20 μM) + Tau K18 (10 μM)	4.02 ± 0.99
10	α-synuclein (20 μM) + Tau K18 (20 μM)	4.24 ± 0.34
11	α-synuclein (20 μM) + Tau K18 (40 μM)	3.35 ± 0.97
12	α-synuclein (20 μM) + Tau K18 (50 μM)	3.15 ± 0.88
13	α-synuclein (20 μM) + Tau K18 (100 μM)	2.55 ± 0.41
14	α-synuclein (50 μM) + Tau K18 (10 μM)	3.69 ± 0.62
15	α-synuclein (50 μM) + Tau K18 (20 μM)	3.52 ± 0.32
16	α-synuclein (50 μM) + Tau K18 (40 μM)	2.8 ± 0.262
17	α-synuclein (50 μM) + Tau K18 (50 μM)	2.28 ± 0.49
18	α-synuclein (50 μM) + Tau K18 (100 μM)	2.02 ± 0.25
19	A30P α-synuclein (20 μM)	20.64 ± 1.83

20	A30P α-synuclein(20 μM) + Tau K18 (50 μM)	3.34 ± 0.28

We next carried out a series of aggregation reactions by keeping the α-synuclein concentration constant and changing the tau K18 concentration and vice-versa (Figure 3.3) and the average lag times were extracted by fitting using the nucleation-dependent polymerization model[54] (Table 3.1). A 3D plot of lag times constructed from the kinetic analysis of the concentration titration experiments is shown in Figure 3.3C. Our preliminary kinetic analysis indicated a synergistic effect between α-synuclein and tau K18 aggregation. In order to structurally characterize the α-synuclein-tau K18 co-aggregates, we used circular dichroism spectroscopy that showed a structural transition from the disordered state to a β-rich aggregated state that is expected for amyloids (Figure 3.3D). In order to visualize the morphological transitions during aggregation, we utilized atomic force microscopy (AFM). Our AFM images showed the formation of spherical oligomers that matured into ordered amyloid fibrils (Figure 3.3E). This set of results showed that α-synuclein and tau K18 together aggregate at a much faster rate compared to the individual proteins. Our next goal was to delineate the molecular origin of acceleration in aggregation kinetics in the presence of both α-synuclein and tau K18.

3.3.2 The early intermolecular interactions and hetero-oligomerization

In order to characterize the early intermolecular interactions between α-syn and tau K18, we first performed the glutaraldehyde crosslinking assay that indicated the formation of heterodimer (Figure 3.5A). In order to quantify these early intermediates, we utilized dynamic light scattering measurements to obtain the size information. Monomeric α-synuclein and tau K18 showed hydrodynamic radius of ~ 3 nm (Figure 3.5B). Upon mixing these proteins there was an increase in hydrodynamic radius ~ 4 nm indicating the formation of initial obligatory heterotypic oligomers (Figure 3.5B). Our CD results showed that there was no gain in the secondary structural content upon mixing of α-synuclein and tau k18 (Figure 3.3D). These results indicated the formation of unstructured early hetero-oligomers of α-synuclein and tau K18. In order to discern the region-specific insights into hetero-oligomerization, we embarked on site-specific tryptophan (Trp) fluorescence studies. We took advantage of the fact that α-synuclein is devoid of any Trp and used single Trp mutants created along the sequence of α-synuclein. Our previous results showed that these mutations did not affect the overall properties of α-synuclein.[21, 61] Trp fluorescence spectra for all of the residue positions demonstrated a red-shifted emission peak in the monomeric form, as

expected (Figure 3.6). We also monitored the Trp fluorescence (polarization) anisotropy of each residue position that provides information about the local chain flexibility.

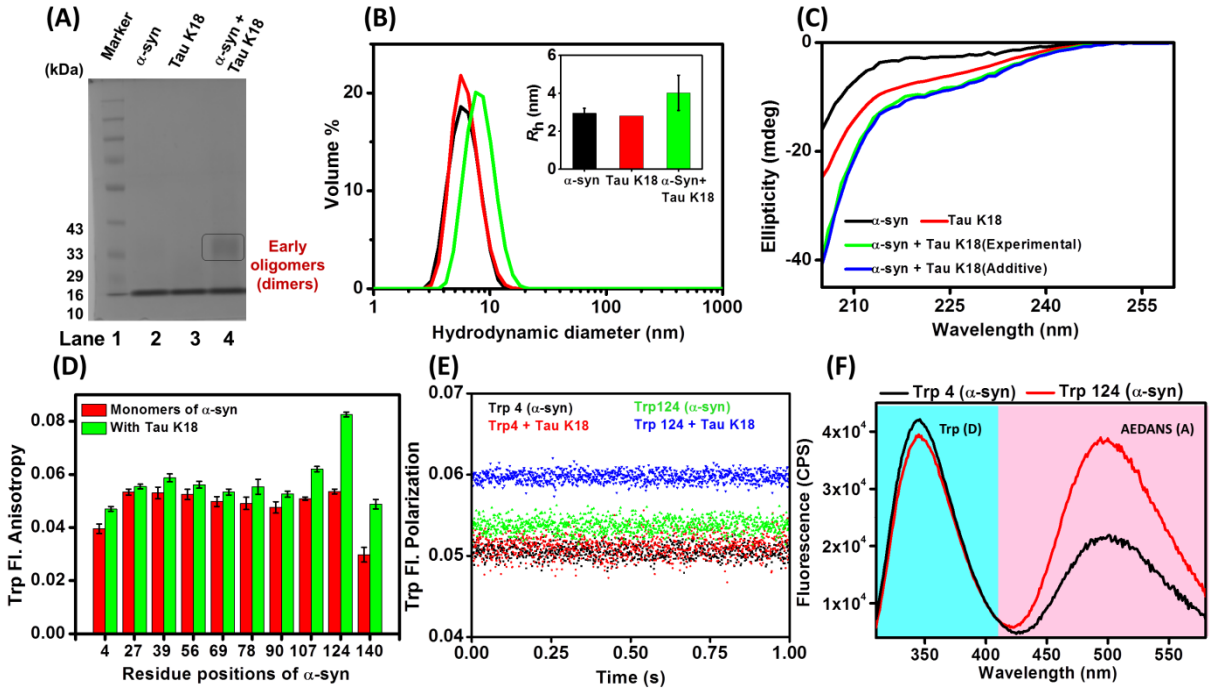

Figure 3.5 Characterization of early heterotypic oligomers of α-synuclein and tau K18. (a) Glutaraldehyde cross-linking assay analyzed on SDS PAGE; protein marker (lane 1), α-synuclein (lane 2), tau K18 (lane 3) and after mixing (lane 4). The concentrations of α-synuclein and tau K18 were fixed at 10 μM and samples were treated with 0.05 % glutaraldehyde. (b) Size distribution by dynamic light scattering measurements of α-synuclein (black), tau K18 (red) and after mixing α-synuclein and tau K18 (green) (inset shows the bar graph of hydrodynamic radius of α-synuclein (black), tau K18 (red) and after mixing (green)). (c) Far-UV CD spectra of α-synuclein(black), tau K18 (red), after mixing (green) and additive spectra of α-synuclein and tau K18 (blue) (d) Trp fluorescence anisotropy of α-synuclein in the monomeric (red) and upon mixing with tau K18 (green). Error bars are obtained from at least three independent measurements. (e) Stopped-flow Trp fluorescence polarization kinetics of α-synuclein: Trp 4 (black) and Trp 124 (green) in the monomeric state, and Trp 4 (red) and Trp 124 (blue) upon mixing with tau K18. (f) Fluorescence spectra showing intermolecular FRET between Trp (donor: D) of α-synuclein and AEDANS (acceptor: A) labeled tau K18 (Trp 4 α-synuclein: black; Trp 124 α-synuclein: red).

All of the residue positions in α-synuclein showed low anisotropy (≤ 0.05) that is consistent with its disordered state in the monomeric form.[21, 61] Upon addition of tau K18, Trp fluorescence anisotropy of α-synuclein was nearly similar at the N-terminal and the NAC domain residues but showed an increase at the C-terminal residues. Residue position 124 demonstrated the highest anisotropy (0.08), hence lower flexibility, which suggested that the

C-terminal segment of α-synuclein interacts with tau K18 (Figure 3.5C). In order to understand the kinetics of α-synuclein-tau K18 interaction, we then performed the stopped-flow fluorescence polarization experiments using Trp 124 α-synuclein and tau K18 to monitor the early oligomerization kinetics (Figure 3.5D). Our results show that the increase in the polarization due to hetero-oligomerization is much faster than the deadtime of our stopped-flow mixer (~ 3 ms) therefore, the oligomerization occurs faster than 3 ms. The N-terminal residue (Trp 4) did not show any change in the polarization value. These results suggested that the C-terminal segment of α-synuclein rapidly binds to tau K18 to form early hetero-oligomers.

To further support this observation, we performed intermolecular fluorescence resonance energy transfer (FRET) between α-syn and tau K18. In these experiments, we used Trp as the donor and IAEDANS (1,5-IAEDANS, 5-((((2-Iodoacetyl) amino) ethyl) amino) Naphthalene-1-Sulfonic Acid) labeled at Cysteines (Cys) as the acceptor. We first chose Trp 124 variant from the C-terminal segment of α-synuclein as the donor and labeled the native Cys residues of tau K18 with AEDANS. Our intermolecular FRET experiments with 20 µM α-synuclein and 50 µM tau K18 showed a FRET efficiency of ~ 40 %. On the contrary, the FRET efficiency between an N-terminal residue of α-synuclein (Trp 4) and tau K18-AEDANS was much lower (~ 22 %) (Figure 3.5E) and might be the result of polypeptide chain fluctuation. Our FRET data along with our residue-specific fluorescence anisotropy data suggested that the early hetero-oligomerization between α-synuclein and tau K18 is promoted by the C-terminal segment of α-synuclein. Since the C-terminal segment of α-synuclein is negatively charged and tau K18 is primarily positively charged, we conjectured that this heterotypic interaction could be electrostatically driven.[36, 44]

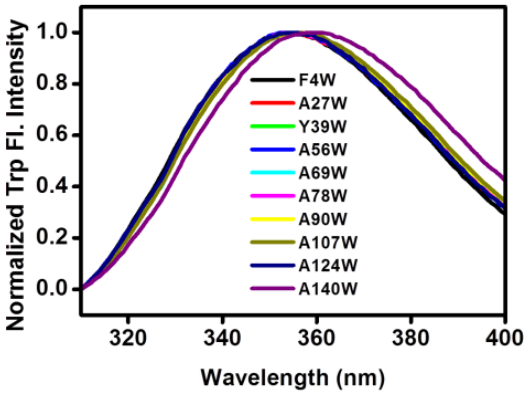

Figure 3.6 Trp fluorescence spectra of all α-synuclein mutants at the monomeric state.

3.3.3 Electrostatic interaction governs the early intermolecular contacts in hetero-oligomers

In order to establish that the interaction is electrostatically driven, we varied the ionic strength by adding salt (NaCl 0-200 mM) and monitored the fluorescence anisotropy of residues at both N- and C-terminal segments. The higher ionic strength is expected to weaken the electrostatic interaction. We indeed observed that the anisotropy of Trp 124 in the presence of tau K18 dropped as a function of the salt concentrations, whereas, Trp 4 did not show any significant change (Figure 3.7A). Additionally, we performed aggregation kinetics at different salt concentrations and observed the elongation of lag time at higher salt concentrations (Figure 3.7B). Under the physiological salt concentration, α-synuclein and tau K18 co-assemble to form amyloid fibrils (Figure 3.7C). The aggregation is decelerated upon addition of salt presumably because the early oligomerization is inhibited at higher ionic strength. The early disordered (heterotypic) oligomers of α-syn and tau K18 serve as precursors to ordered amyloid fibrils. These results established that the early interaction between α-syn and tau K18 is predominantly driven by electrostatic interactions as described before. [36, 44]

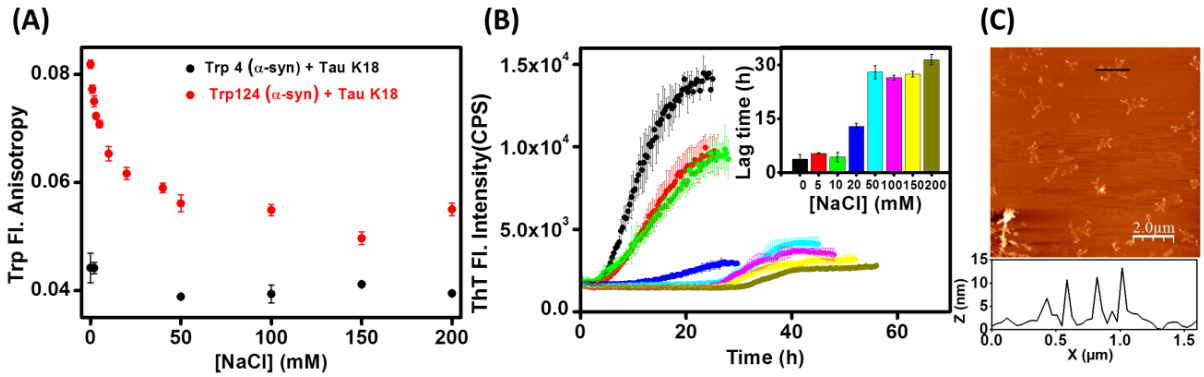

Figure 3.7 Electrostatic interaction between α-synuclein and tau K18. (a) Trp fluorescence anisotropy of Trp 4 (N-terminal) and Trp 124 (C-terminal) of α-synuclein in the presence of tau K18 as a function of NaCl concentration (0-200 mM). Error bars indicate SDs. (b) ThT fluorescence kinetics of α-synuclein-tau K18 aggregation as a function of NaCl concentration (0-200 mM) (Inset shows the lag time recovered from the aggregation kinetics fit at different NaCl concentrations). Error bars are obtained from at least three independent measurements. (c) AFM image of α-synuclein-tau K18 aggregates at physiological salt concentration (150 mM).

3.3.4 Structural insights into the heterotypic amyloids

Next, we asked the question: Is the overall arrangement of α-synuclein aggregates in the presence of tau K18 similar to that formed in the absence of tau K18? This is an important aspect because the structural arrangement of protein molecules within the amyloid fold has been linked to amyloid toxicity.[62] As a prelude, we first established that α-synuclein and tau K18 separately formed fibrils under our aggregation condition and captured the spectroscopic signatures of matured fibrils of individual proteins (Figure 3.8).

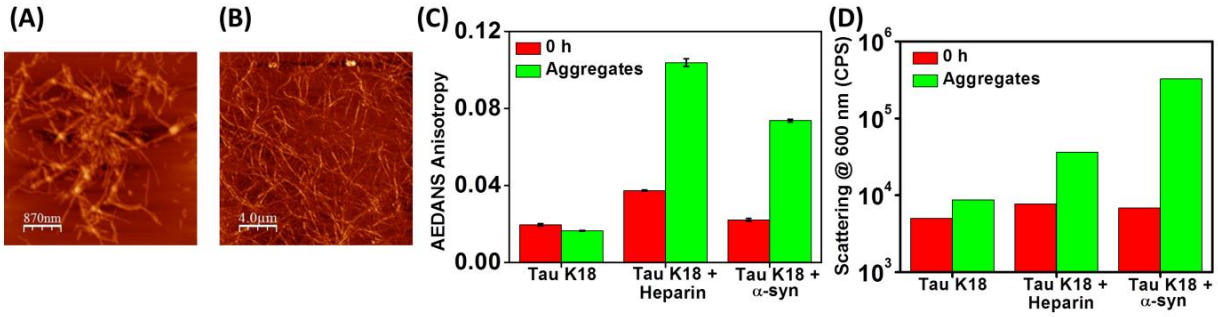

Figure 3.8 (a) AFM image of α-synuclein fibrils in the aggregation buffer. (b) AFM image of tau K18 fibrils in the presence of heparin in the aggregation buffer. (c) Native Cys of tau K18 (50 μM) labeled with AEDANS. The AEDANS fluorescence anisotropy of tau K18 in absence of heparin, in the presence of heparin (12.5 μM) and in the presence of α-synuclein(20 μM) at the early oligomeric state (red) and in the aggregated state (green). (d) Scattering at the early oligomeric state (red) & in the aggregated state (green). Error bars indicate SDs.

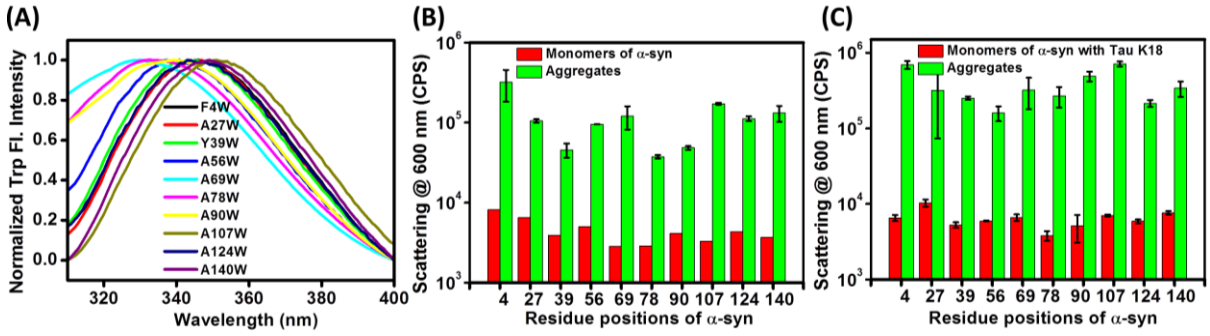

Figure 3.9 (a) Trp fluorescence spectra of all α-synuclein mutants in the aggregated state. (b) α-synuclein scattering in the monomeric (red) & aggregated state (green). (c) α-synuclein and tau K18 scattering at the early oligomeric (red) & aggregated state (green). Error bars indicate SDs.

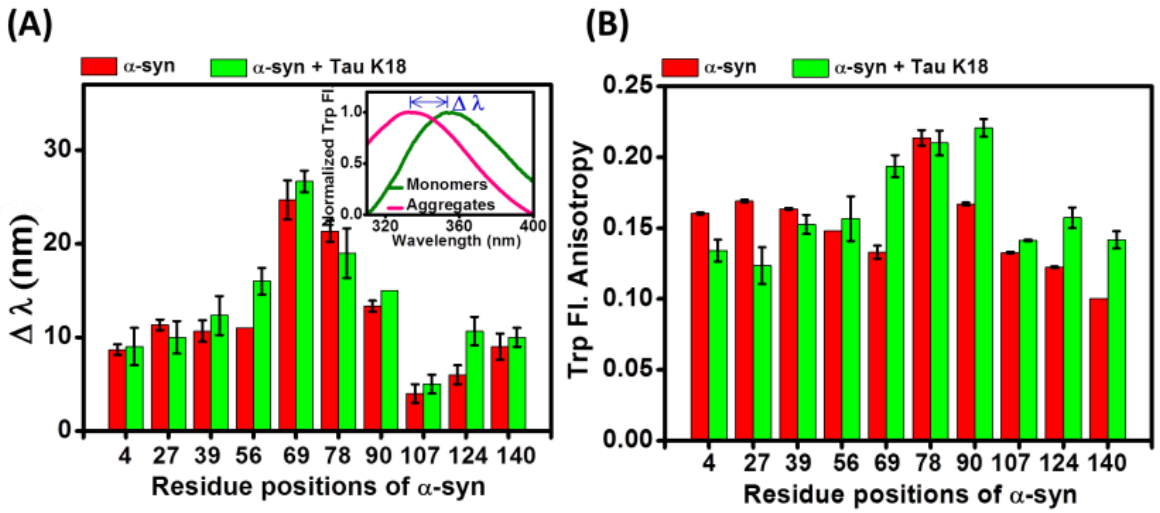

Figure 3.10 Characterization of α-synuclein and tau K18 fibrils. (a) The spectral shift Δλ (Inset shows Δλ, the difference in the Trp emission maxima between monomeric and aggregated state of α-syn) in the presence (green) and absence of tau K18 (red). (b) Trp fluorescence anisotropy of α-synuclein mutants in the aggregated state of α-synuclein in the presence (green) and absence of tau K18 (red).

We then utilized the site-specific Trp fluorescence readouts to elucidate the overall conformational attributes of α-syn. We utilized a simple fluorescence peak shift method that reveals the extent of burial of different Trp residues upon amyloid formation. In the monomeric state, all of the Trp positions are exposed to bulk water and showed emission maxima at ~ 348 nm (Figure 3.6).[21] Upon amyloid formation, depending on the participation of different residues located at various segments of the protein, Trp fluorescence emission maxima showed a varied extent of blue-shift (Figure 3.9). We monitored the site-specific changes in fluorescence maxima since the difference in the Trp emission maxima between monomeric and aggregated state (Δλ) is a measure of the extent of burial (or the gain of structure) within the amyloid architecture (Figure 3.10A). The NAC domain residues (residue position 69, 78 and 90) that are known to constitute the amyloid core[3, 9, 62] exhibited the largest Δλ (~ 15-25 nm) and the N-terminal segment showed moderate Δλ of ~10 nm (Figure 3.10A). The C-terminal residues that do not form the core showed much lower value of Δλ. The overall pattern of Δλ of α-syn aggregates in the presence and absence of tau K18 is similar suggesting the overall amyloid packing of α-syn remains nearly similar. However, the C-terminal residues, particularly residue 124, exhibited larger Δλ in the presence of tau K18 indicating this region of α-syn might be in contact with tau within the fibrils. Next, in order to monitor the residue-specific conformational mobility of α-syn within amyloids, we measured Trp fluorescence anisotropy of α-syn in the absence and presence of tau K18. The anisotropy

map is similar in the absence and presence of tau K18 suggesting again the overall architecture of amyloids are likely to be similar (Figure 3.10B). The C-terminal residues of α-syn showed higher anisotropy in the presence of tau K18 corroborating our Δλ data. These results established that tau K18 interacts with the C-terminal residues of α-syn in the hetero-amyloid state similar to what we found in the early oligomeric state.[44] Therefore, we believe that the early heterotypic interaction between α-syn and tau K18 is retained in the matured amyloid state. It is possible that the co-amyloids are constituted by independent amyloid spines of α-syn and tau K 18 that are connected via electrostatic crosslinks between the two proteins.

3.3.5 Direct observation of heterotypic amyloid fibrils

In order to further verify the formation of heterotypic amyloid fibrils, we used two-color fluorescence imaging to visualize the aggregates. For this set of studies, we created a single Cys mutant (S9C) of α-syn. This single Cys mutant does not alter the properties of wild-type

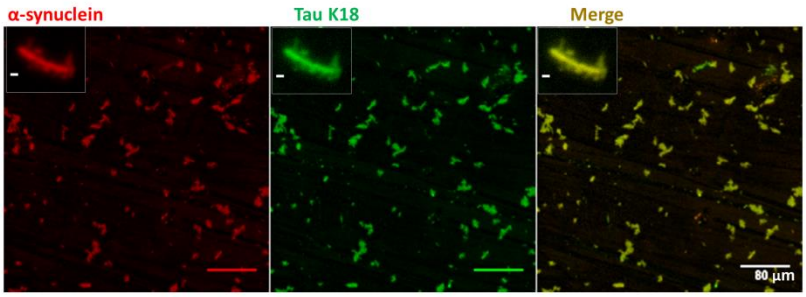

Figure 3.11 Colocalization of α-synuclein (AlexaFluor 488 maleimide labeled S9C of α-syn) and tau K18 (AlexaFluor 594 maleimide labeled native Cys) of heterotypic amyloids of α-syn-tau K18 shown in the confocal image (Inset shows fluorescence microscope image of scale bar 2 µm). Error bars are obtained from at least three independent measurements.

α-syn[63] and was fluorescently labeled with AlexaFluor 594 maleimide. The two native Cys of tau K18 were randomly labeled with AlexaFluor 488 maleimide. We then performed two-color imaging on the hetero-amyloids using confocal fluorescence microscopy and observed ~ 97 % colocalization of red and green fluorescence (Figure 3.11). Our imaging studies indicates that tau K18 and α-syn co-aggregate to form heterotypic amyloid fibrils, which is in accordance with the colocalization results of α-syn and tau using immunofluorescence images of different brain tissues collected from the patients.[64]

3.3.6 Effect of the Parkinson's disease mutant of α-synuclein

Next, we asked the question: what is the effect of tau K18 on a PD mutant of α-syn? In order to answer this question, we created A30P α-syn, a well-known familial PD mutant [33]. A few previous reports suggested that at the monomeric level, wild-type α-syn and the A30P mutant interact with tau in a similar fashion.[33] Whereas, some other reports indicated that the interaction between A30P α-syn and tau is weaker compared to that of wild-type α-syn and tau.[44, 47] However, the effect of A30P α-syn and tau interaction in the oligomerization and amyloid formation remains poorly understood. A30P α-syn is known to aggregate slowly with a longer lag phase that allows accumulation of long-lived oligomeric intermediates that are known to be highly cytotoxic.[47, 65-66] However, the effect of A30P α-synuclein and tau interaction in the oligomerization and amyloid formation remains poorly understood. A30P α-synuclein is known to aggregate slowly with a longer lag phase that allows accumulation of

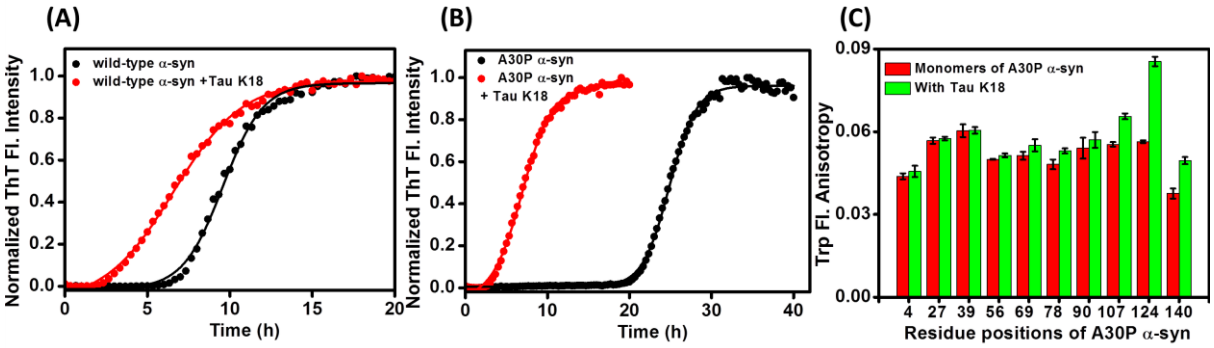

Figure 3.12 Comparison of aggregation of wild-type and A30P α-synucleinin the absence and presence of tau K18. (a) Aggregation kinetics of wild-type α-synucleinin the presence (red) and absence (black) of tau K18 (already shown in Fig. 1c and shown here for comparison with Fig. 6b). (b) Aggregation kinetics of A30P α-synucleinin the presence (red) and absence (black) of tau K18. (c) Trp fluorescence anisotropy map of A30P α-synucleinin the monomeric (red) and upon mixing with tau K18 (green). Error bars are obtained from at least three independent measurements.

long-lived oligomeric intermediates that are known to be highly cytotoxic.[67-69] We also observed that under our aggregation condition, A30P α-syn aggregation kinetics possessed a much longer lag phase (~ 20 h) compared to wild-type α-syn (Figure 3.12A and 3.12B). However, upon addition of tau K 18, there was a profound shortening of the lag time of A30P α-syn aggregation (~ 3 h) (Figure 3.12A). Our results show that the aggregation kinetics of the PD mutant, A30P, is significantly accelerated by the addition of tau K18. In order to characterize the early interaction, we utilized anisotropy of Trp variants harboring A30P

mutation. The conformational mobility map using residue-specific fluorescence anisotropy revealed that, similar to wild-type α-syn, the C-terminal segment of A30P α-syn is responsible for the early interaction with tau K18 (Figure 3.12C). It is possible that the early α-syn-tau interaction might promote facile amyloid maturation that could potentially avoid the accumulation of disease-causing precursors by shortening the lag phase.

3.4 Conclusion

α-Synuclein and tau are amyloidogenic IDPs present in the presynaptic nerve terminals. Under pathological conditions, they are known to form co-amyloids in several neurological ailments such as PD, AD, Down syndrome, multiple system atrophy and so forth.[45-46, 64] In this work, we show that the formation of early heterotypic oligomeric complex of α-syn and tau K18 can promote maturation into fibrils through binding-induced misfolding and aggregation. Our studies suggest that the α-syn:tau ratio critically governs the rate of the amyloid formation. α-syn and tau K18 together aggregate at a much faster rate with a much shorter lag phase compared to the individual proteins. Using an array of biophysical and biochemical tools, we established that the hetero-oligomerization is largely electrostatically driven and the negatively charged C-terminal segment of α-syn interacts with the positively charged tau K18 fragment. The binding assay map of the truncated fragments of α-syn and tau results is consistent with our findings.[44] Previous studies have provided evidence of α-synuclein and tau crosstalk in the presynaptic terminal of the neurons.[48] This interaction could potentially be relevant for pathological consequences. Our work showed that the overall amyloid packing of α-syn remains nearly similar in the absence and presence of tau K18. The C-terminal residues of α-syn fibrils exhibited lower flexibility in the presence of tau K18 indicating that tau K18 interacts with the C-terminal segment of α-syn in the hetero-amyloid state similar to the early oligomeric state. Our findings allowed us to depict a model that shows the proposed binding-misfolding-aggregation events (Figure 3.13). Initial electrostatic neutralization promotes rapid oligomerization and maturation into hetero-fibrils possibly comprising two independent amyloid spines connected by salt bridges. Previous studies have demonstrated the colocalization of α-syn and tau K18 in the immunofluorescence images of different brain tissues from the patients.[64] Many IDPs such as Aβ, tau, α-syn are known to interact with each other in several neurological ailments.[47, 64, 70]

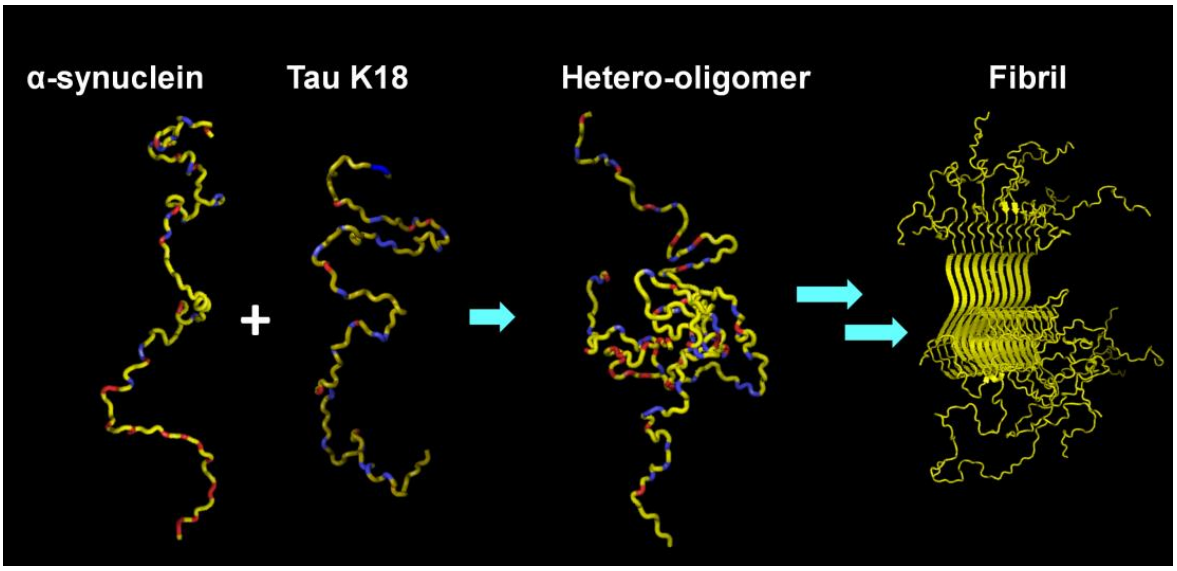

Figure 3.13 A proposed model of α-synucleinand tau K18 co-aggregation mediated by electrostatic interaction. The polypeptide chains are shown in yellow and negative and positive amino acids are indicated in red and blue, respectively. The structures of α-synucleinand tau K18 were taken from the protein ensemble database (PeDB: 9AAC for α-syn; 6AAC for tau K18) and α-synucleinamyloid structure was taken from the protein data bank (PDB: 2n0a). These structures are generated using PyMOL (Version 1.8, Schrödinger, LLC, New York) and are shown for illustration purpose.

A familial PD mutant, A30P α-syn is known to aggregate with a long lag phase.[52-53] Previous studies have shown that oligomeric intermediate species of α-syn are more toxic than the highly ordered amyloid fibrils.[49-52]]. Interestingly, the interaction of A30P α-syn and tau K18 result in a profound shortening of the lag phase. Hence, we propose that tau helps in recruiting the harmful species by forming amyloid-competent heterotypic oligomers that rapidly convert into less fatal amyloid fibrils. Interestingly, many functional amyloids that are involved in biofilm formation in bacteria, melanin biosynthesis in mammals are also known to utilize this strategy to fibrilize without or with a short lag phase to avoid the accumulation of toxic oligomeric intermediates.[71-74] Therefore, this intermolecular interaction might potentially have a protective role in recruiting key pernicious species into amyloids and in delaying the onset of the disease, even for a familial PD mutant. Our results outline a general strategy of protein-protein heterotypic association and binding-induced misfolding/aggregation by which highly amyloidogenic IDPs, when converted into potentially lethal species, are efficiently sequestered into more benign amyloid fibrils.

3.5 References:

1. Knowles, T. P.; Vendruscolo, M.; Dobson, C. M., The amyloid state and its association with protein misfolding diseases. *Nat Rev Mol Cell Biol* **2014,** *15* (6), 384-96.

2. Goedert, M., NEURODEGENERATION. Alzheimer's and Parkinson's diseases: The prion concept in relation to assembled Abeta, tau, and alpha-synuclein. *Science* **2015,** *349* (6248), 1255555.

3. Eisenberg, D.; Jucker, M., The Amyloid State of Proteins in Human Diseases. *Cell 148* (6), 1188-1203.

4. Gershenson, A.; Gierasch, L. M.; Pastore, A.; Radford, S. E., Energy landscapes of functional proteins are inherently risky. *Nat Chem Biol* **2014,** *10* (11), 884-91.

5. Chiti, F.; Dobson, C. M., Protein Misfolding, Amyloid Formation, and Human Disease: A Summary of Progress Over the Last Decade. *Annu Rev Biochem* **2017,** *86*, 27-68.

6. Goedert, M., Alpha-synuclein and neurodegenerative diseases. *Nat Rev Neurosci* **2001,** *2* (7), 492-501.

7. Breydo, L.; Wu, J. W.; Uversky, V. N., Alpha-synuclein misfolding and Parkinson's disease. *Biochim Biophys Acta* **2012,** *2*, 261-85.

8. Uversky, V. N.; Eliezer, D., Biophysics of Parkinson's disease: structure and aggregation of alpha-synuclein. *Curr Protein Pept Sci* **2009,** *10* (5), 483-99.

9. Plotegher, N.; Greggio, E.; Bisaglia, M.; Bubacco, L., Biophysical groundwork as a hinge to unravel the biology of alpha-synuclein aggregation and toxicity. *Q Rev Biophys* **2014,** *47* (1), 1-48.

10. Maroteaux, L.; Campanelli, J. T.; Scheller, R. H., Synuclein: a neuron-specific protein localized to the nucleus and presynaptic nerve terminal. *J Neurosci* **1988,** *8* (8), 2804-15.

11. Watson, J. B.; Hatami, A.; David, H.; Masliah, E.; Roberts, K.; Evans, C. E.; Levine, M. S., Alterations in corticostriatal synaptic plasticity in mice overexpressing human alpha-synuclein. *Neuroscience* **2009,** *159* (2), 501-13.

12. Cooper, A. A.; Gitler, A. D.; Cashikar, A.; Haynes, C. M.; Hill, K. J.; Bhullar, B.; Liu, K.; Xu, K.; Strathearn, K. E.; Liu, F.; Cao, S.; Caldwell, K. A.; Caldwell, G. A.; Marsischky, G.; Kolodner, R. D.; Labaer, J.; Rochet, J. C.; Bonini, N. M.; Lindquist, S., Alpha-synuclein blocks ER-Golgi traffic and Rab1 rescues neuron loss in Parkinson's models. *Science* **2006,** *313* (5785), 324-8.

13. Abeliovich, A.; Schmitz, Y.; Farinas, I.; Choi-Lundberg, D.; Ho, W. H.; Castillo, P. E.; Shinsky, N.; Verdugo, J. M.; Armanini, M.; Ryan, A.; Hynes, M.; Phillips, H.; Sulzer, D.;

Rosenthal, A., Mice lacking alpha-synuclein display functional deficits in the nigrostriatal dopamine system. *Neuron* **2000,** *25* (1), 239-52.

14. Nath, A.; Rhoades, E., A flash in the pan: dissecting dynamic amyloid intermediates using fluorescence. *FEBS Lett* **2013,** *587* (8), 1096-105.

15. Pfefferkorn, C. M.; Jiang, Z.; Lee, J. C., Biophysics of α-synuclein membrane interactions. *Biochimica et Biophysica Acta (BBA) - Biomembranes* **2012,** *1818* (2), 162-171.

16. Yap, T. L.; Pfefferkorn, C. M.; Lee, J. C., Residue-specific fluorescent probes of alpha-synuclein: detection of early events at the N- and C-termini during fibril assembly. *Biochemistry* **2011,** *50* (12), 1963-5.

17. Deleersnijder, A.; Gerard, M.; Debyser, Z.; Baekelandt, V., The remarkable conformational plasticity of alpha-synuclein: blessing or curse? *Trends Mol Med* **2013,** *19* (6), 368-77.

18. Souza, J. M.; Giasson, B. I.; Lee, V. M.; Ischiropoulos, H., Chaperone-like activity of synucleins. *FEBS Lett* **2000,** *474* (1), 116-9.

19. Kim, T. D.; Paik, S. R.; Yang, C. H., Structural and functional implications of C-terminal regions of alpha-synuclein. *Biochemistry* **2002,** *41* (46), 13782-90.

20. Horvath, I.; Wittung-Stafshede, P., Cross-talk between amyloidogenic proteins in type-2 diabetes and Parkinson's disease. *Proc Natl Acad Sci U S A* **2016,** *113* (44), 12473-12477.

21. Jain, N.; Bhasne, K.; Hemaswasthi, M.; Mukhopadhyay, S., Structural and dynamical insights into the membrane-bound alpha-synuclein. *PLoS One* **2013,** *8* (12).

22. Miller, L. M.; Bourassa, M. W.; Smith, R. J., FTIR spectroscopic imaging of protein aggregation in living cells. *Biochim Biophys Acta* **2013,** *10* (46), 25.

23. Giehm, L.; Svergun, D. I.; Otzen, D. E.; Vestergaard, B., Low-resolution structure of a vesicle disrupting α-synuclein oligomer that accumulates during fibrillation. *Proc Natl Acad Sci U S A* **2011,** *108* (8), 3246-51.

24. Serpell, L. C.; Berriman, J.; Jakes, R.; Goedert, M.; Crowther, R. A., Fiber diffraction of synthetic alpha-synuclein filaments shows amyloid-like cross-beta conformation. *Proc Natl Acad Sci U S A* **2000,** *97* (9), 4897-902.

25. Heise, H.; Hoyer, W.; Becker, S.; Andronesi, O. C.; Riedel, D.; Baldus, M., Molecular-level secondary structure, polymorphism, and dynamics of full-length alpha-synuclein fibrils studied by solid-state NMR. *Proc Natl Acad Sci U S A* **2005,** *102* (44), 15871-6.

26. Tuttle, M. D.; Comellas, G.; Nieuwkoop, A. J.; Covell, D. J.; Berthold, D. A.; Kloepper, K. D.; Courtney, J. M.; Kim, J. K.; Barclay, A. M.; Kendall, A.; Wan, W.; Stubbs, G.; Schwieters, C. D.; Lee, V. M.; George, J. M.; Rienstra, C. M., Solid-state NMR structure of a pathogenic fibril of full-length human alpha-synuclein. *Nat Struct Mol Biol* **2016,** *23* (5), 409-15.

27. Der-Sarkissian, A.; Jao, C. C.; Chen, J.; Langen, R., Structural organization of alpha-synuclein fibrils studied by site-directed spin labeling. *J Biol Chem* **2003,** *278* (39), 37530-5.

28. Chen, M.; Margittai, M.; Chen, J.; Langen, R., Investigation of alpha-synuclein fibril structure by site-directed spin labeling. *J Biol Chem* **2007,** *282* (34), 24970-9.

29. de Oliveira, G. A.; Marques, M. A.; Cruzeiro-Silva, C.; Cordeiro, Y.; Schuabb, C.; Moraes, A. H.; Winter, R.; Oschkinat, H.; Foguel, D.; Freitas, M. S.; Silva, J. L., Structural basis for the dissociation of alpha-synuclein fibrils triggered by pressure perturbation of the hydrophobic core. *Sci Rep* **2016,** *6* (37990).

30. Xu, L.; Nussinov, R.; Ma, B., Coupling of the non-amyloid-component (NAC) domain and the KTK(E/Q)GV repeats stabilize the alpha-synuclein fibrils. *Eur J Med Chem* **2016,** *121*, 841-850.

31. Rodriguez, J. A.; Ivanova, M. I.; Sawaya, M. R.; Cascio, D.; Reyes, F. E.; Shi, D.; Sangwan, S.; Guenther, E. L.; Johnson, L. M.; Zhang, M.; Jiang, L.; Arbing, M. A.; Nannenga, B. L.; Hattne, J.; Whitelegge, J.; Brewster, A. S.; Messerschmidt, M.; Boutet, S.; Sauter, N. K.; Gonen, T.; Eisenberg, D. S., Structure of the toxic core of alpha-synuclein from invisible crystals. *Nature* **2015,** *525* (7570), 486-90.

32. Xu, L.; Ma, B.; Nussinov, R.; Thompson, D., Familial Mutations May Switch Conformational Preferences in α-Synuclein Fibrils. *ACS Chemical Neuroscience* **2017,** *8* (4), 837-849.

33. Ono, K.; Ikeda, T.; Takasaki, J.; Yamada, M., Familial Parkinson disease mutations influence alpha-synuclein assembly. *Neurobiol Dis* **2011,** *43* (3), 715-24.

34. Binder, L. I.; Frankfurter, A.; Rebhun, L. I., The distribution of tau in the mammalian central nervous system. *J Cell Biol* **1985,** *101* (4), 1371-8.

35. Couchie, D.; Mavilia, C.; Georgieff, I. S.; Liem, R. K.; Shelanski, M. L.; Nunez, J., Primary structure of high molecular weight tau present in the peripheral nervous system. *Proc Natl Acad Sci U S A* **1992,** *89* (10), 4378-81.

36. Oikawa, T.; Nonaka, T.; Terada, M.; Tamaoka, A.; Hisanaga, S.; Hasegawa, M., alpha-Synuclein Fibrils Exhibit Gain of Toxic Function, Promoting Tau Aggregation and Inhibiting Microtubule Assembly. *J Biol Chem* **2016,** *291* (29), 15046-56.

37. Elbaum-Garfinkle, S.; Ramlall, T.; Rhoades, E., The role of the lipid bilayer in tau aggregation. *Biophys J* **2010,** *98* (11), 2722-30.

38. Goedert, M.; Spillantini, M. G.; Jakes, R.; Rutherford, D.; Crowther, R. A., Multiple isoforms of human microtubule-associated protein tau: sequences and localization in neurofibrillary tangles of Alzheimer's disease. *Neuron* **1989,** *3* (4), 519-26.

39. Ramachandran, G.; Udgaonkar, J. B., Understanding the kinetic roles of the inducer heparin and of rod-like protofibrils during amyloid fibril formation by Tau protein. *J Biol Chem* **2011,** *286* (45), 38948-59.

40. Barghorn, S.; Mandelkow, E., Toward a unified scheme for the aggregation of tau into Alzheimer paired helical filaments. *Biochemistry* **2002,** *41* (50), 14885-96.

41. Akoury, E.; Mukrasch, M. D.; Biernat, J.; Tepper, K.; Ozenne, V.; Mandelkow, E.; Blackledge, M.; Zweckstetter, M., Remodeling of the conformational ensemble of the repeat domain of tau by an aggregation enhancer. *Protein Sci* **2016,** *25* (5), 1010-20.

42. Friedhoff, P.; von Bergen, M.; Mandelkow, E. M.; Davies, P.; Mandelkow, E., A nucleated assembly mechanism of Alzheimer paired helical filaments. *Proc Natl Acad Sci U S A* **1998,** *95* (26), 15712-7.

43. Ambadipudi, S.; Biernat, J.; Riedel, D.; Mandelkow, E.; Zweckstetter, M., Liquid-liquid phase separation of the microtubule-binding repeats of the Alzheimer-related protein Tau. *Nat Commun* **2017,** *8* (1), 017-00480.

44. Jensen, P. H.; Hager, H.; Nielsen, M. S.; Hojrup, P.; Gliemann, J.; Jakes, R., alpha-synuclein binds to Tau and stimulates the protein kinase A-catalyzed tau phosphorylation of serine residues 262 and 356. *J Biol Chem* **1999,** *274* (36), 25481-9.

45. Giasson, B. I.; Forman, M. S.; Higuchi, M.; Golbe, L. I.; Graves, C. L.; Kotzbauer, P. T.; Trojanowski, J. Q.; Lee, V. M., Initiation and synergistic fibrillization of tau and alpha-synuclein. *Science* **2003,** *300* (5619), 636-40.

46. Waxman, E. A.; Giasson, B. I., Induction of intracellular tau aggregation is promoted by alpha-synuclein seeds and provides novel insights into the hyperphosphorylation of tau. *J Neurosci* **2011,** *31* (21), 7604-18.

47. Moussaud, S.; Jones, D. R.; Moussaud-Lamodiere, E. L.; Delenclos, M.; Ross, O. A.; McLean, P. J., Alpha-synuclein and tau: teammates in neurodegeneration? *Mol Neurodegener* **2014,** *9* (43), 1750-1326.

48. Badiola, N.; de Oliveira, R. M.; Herrera, F.; Guardia-Laguarta, C.; Gonçalves, S. A.; Pera, M.; Suárez-Calvet, M.; Clarimon, J.; Outeiro, T. F.; Lleó, A., Tau Enhances α-

Synuclein Aggregation and Toxicity in Cellular Models of Synucleinopathy. *PLoS One* **2011,** *6* (10), e26609.

49. Frieden, C., Protein aggregation processes: In search of the mechanism. *Protein Sci* **2007,** *16* (11), 2334-44.

50. Winner, B.; Jappelli, R.; Maji, S. K.; Desplats, P. A.; Boyer, L.; Aigner, S.; Hetzer, C.; Loher, T.; Vilar, M.; Campioni, S.; Tzitzilonis, C.; Soragni, A.; Jessberger, S.; Mira, H.; Consiglio, A.; Pham, E.; Masliah, E.; Gage, F. H.; Riek, R., In vivo demonstration that alpha-synuclein oligomers are toxic. *Proc Natl Acad Sci U S A* **2011,** *108* (10), 4194-9.

51. Fusco, G.; Chen, S. W.; Williamson, P. T. F.; Cascella, R.; Perni, M.; Jarvis, J. A.; Cecchi, C.; Vendruscolo, M.; Chiti, F.; Cremades, N.; Ying, L.; Dobson, C. M.; De Simone, A., Structural basis of membrane disruption and cellular toxicity by alpha-synuclein oligomers. *Science* **2017,** *358* (6369), 1440-1443.

52. Bengoa-Vergniory, N.; Roberts, R. F.; Wade-Martins, R.; Alegre-Abarrategui, J., Alpha-synuclein oligomers: a new hope. *Acta Neuropathol* **2017,** *134* (6), 819-838.

53. Lemkau, L. R.; Comellas, G.; Kloepper, K. D.; Woods, W. S.; George, J. M.; Rienstra, C. M., Mutant protein A30P alpha-synuclein adopts wild-type fibril structure, despite slower fibrillation kinetics. *J Biol Chem* **2012,** *287* (14), 11526-32.

54. Arora, A.; Ha, C.; Park, C. B., Inhibition of insulin amyloid formation by small stress molecules. *FEBS Lett* **2004,** *564* (1-2), 121-5.

55. Lakowicz, J., *Principles of Fluorescence Spectroscopy*. 2006.

56. Nichols, M. R.; Moss, M. A.; Reed, D. K.; Lin, W. L.; Mukhopadhyay, R.; Hoh, J. H.; Rosenberry, T. L., Growth of beta-amyloid(1-40) protofibrils by monomer elongation and lateral association. Characterization of distinct products by light scattering and atomic force microscopy. *Biochemistry* **2002,** *41* (19), 6115-27.

57. Lindgren, M.; Sorgjerd, K.; Hammarstrom, P., Detection and characterization of aggregates, prefibrillar amyloidogenic oligomers, and protofibrils using fluorescence spectroscopy. *Biophys J* **2005,** *88* (6), 4200-12.

58. Horcas, I.; Fernandez, R.; Gomez-Rodriguez, J. M.; Colchero, J.; Gomez-Herrero, J.; Baro, A. M., WSXM: a software for scanning probe microscopy and a tool for nanotechnology. *Rev Sci Instrum* **2007,** *78* (1), 013705.

59. Bhattacharya, M.; Mukhopadhyay, S., Structural and Dynamical Insights into the Molten-Globule Form of Ovalbumin. *The Journal of Physical Chemistry B* **2012,** *116* (1), 520-531.

60. Schindelin, J.; Arganda-Carreras, I.; Frise, E.; Kaynig, V.; Longair, M.; Pietzsch, T.; Preibisch, S.; Rueden, C.; Saalfeld, S.; Schmid, B.; Tinevez, J. Y.; White, D. J.; Hartenstein, V.; Eliceiri, K.; Tomancak, P.; Cardona, A., Fiji: an open-source platform for biological-image analysis. *Nat Methods* **2012,** *9* (7), 676-82.

61. Jain, N.; Narang, D.; Bhasne, K.; Dalal, V.; Arya, S.; Bhattacharya, M.; Mukhopadhyay, S., Direct Observation of the Intrinsic Backbone Torsional Mobility of Disordered Proteins. *Biophys J* **2016,** *111* (4), 768-774.

62. Vilar, M.; Chou, H. T.; Luhrs, T.; Maji, S. K.; Riek-Loher, D.; Verel, R.; Manning, G.; Stahlberg, H.; Riek, R., The fold of alpha-synuclein fibrils. *Proc Natl Acad Sci U S A* **2008,** *105* (25), 8637-42.

63. Trexler, A. J.; Rhoades, E., α-Synuclein binds large unilamellar vesicles as an extended helix. *Biochemistry* **2009,** *48* (11), 2304-2306.

64. Lee, V. M.; Giasson, B. I.; Trojanowski, J. Q., More than just two peas in a pod: common amyloidogenic properties of tau and alpha-synuclein in neurodegenerative diseases. *Trends Neurosci* **2004,** *27* (3), 129-34.

65. Esposito, A.; Dohm, C. P.; Kermer, P.; Bahr, M.; Wouters, F. S., alpha-Synuclein and its disease-related mutants interact differentially with the microtubule protein tau and associate with the actin cytoskeleton. *Neurobiol Dis* **2007,** *26* (3), 521-31.

66. Qureshi, H. Y.; Paudel, H. K., Parkinsonian neurotoxin 1-methyl-4-phenyl-1,2,3,6-tetrahydropyridine (MPTP) and alpha-synuclein mutations promote Tau protein phosphorylation at Ser262 and destabilize microtubule cytoskeleton in vitro. *J Biol Chem* **2011,** *286* (7), 5055-68.

67. Xu, J.; Kao, S. Y.; Lee, F. J.; Song, W.; Jin, L. W.; Yankner, B. A., Dopamine-dependent neurotoxicity of alpha-synuclein: a mechanism for selective neurodegeneration in Parkinson disease. *Nat Med* **2002,** *8* (6), 600-6.

68. Gosavi, N.; Lee, H. J.; Lee, J. S.; Patel, S.; Lee, S. J., Golgi fragmentation occurs in the cells with prefibrillar alpha-synuclein aggregates and precedes the formation of fibrillar inclusion. *J Biol Chem* **2002,** *277* (50), 48984-92.

69. Conway, K. A.; Lee, S. J.; Rochet, J. C.; Ding, T. T.; Williamson, R. E.; Lansbury, P. T., Jr., Acceleration of oligomerization, not fibrillization, is a shared property of both alpha-synuclein mutations linked to early-onset Parkinson's disease: implications for pathogenesis and therapy. *Proc Natl Acad Sci U S A* **2000,** *97* (2), 571-6.

70. Clinton, L. K.; Blurton-Jones, M.; Myczek, K.; Trojanowski, J. Q.; LaFerla, F. M., *Synergistic Interactions between Aβ, Tau, and α-Synuclein: Acceleration of Neuropathology*

and Cognitive Decline. J Neurosci. 2010 May 26;30(21):7281-9. doi:10.1523/JNEUROSCI.0490-10.2010.

71. Swasthi, H. M.; Mukhopadhyay, S., Electrostatic lipid-protein interactions sequester the curli amyloid fold on the lipopolysaccharide membrane surface. *J Biol Chem* **2017,** *292* (48), 19861-19872.

72. Dogra, P.; Bhattacharya, M.; Mukhopadhyay, S., pH-Responsive Mechanistic Switch Regulates the Formation of Dendritic and Fibrillar Nanostructures of a Functional Amyloid. *J Phys Chem B* **2017,** *121* (2), 412-419.

73. Smith, D. R.; Price, J. E.; Burby, P. E.; Blanco, L. P.; Chamberlain, J.; Chapman, M. R., The Production of Curli Amyloid Fibers Is Deeply Integrated into the Biology of Escherichia coli. *Biomolecules* **2017,** *7* (4).

74. Zeng, G.; Vad, B. S.; Dueholm, M. S.; Christiansen, G.; Nilsson, M.; Tolker-Nielsen, T.; Nielsen, P. H.; Meyer, R. L.; Otzen, D. E., Functional bacterial amyloid increases Pseudomonas biofilm hydrophobicity and stiffness. *Front Microbiol* **2015,** *6* (1099).

Interaction of α-Synuclein with Mitochondrial Heat-shock Proteins: Implication in Parkinson's disease

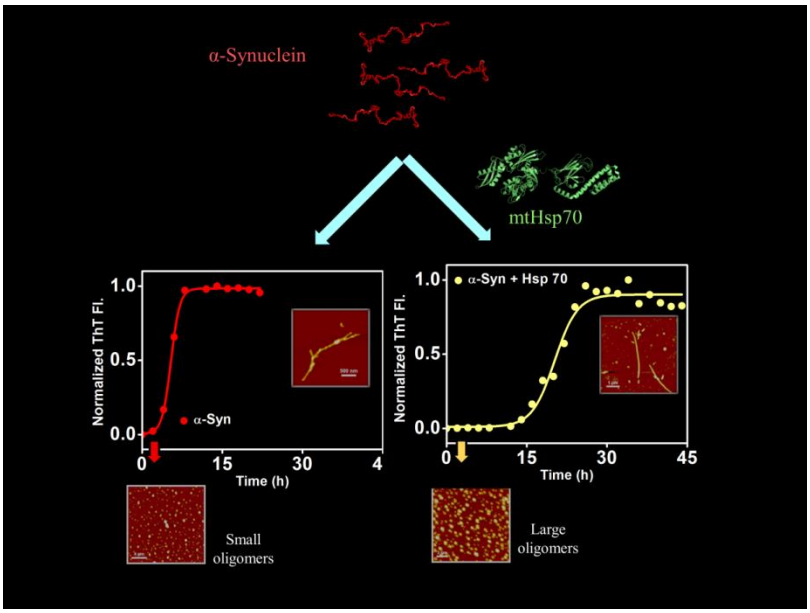

4.1 Introduction

Parkinson's disease (PD) is a long-term neurodegenerative disorder, second in prevalence only to Alzheimer's disease.[1] A variety of non-motor symptoms, including dementia, depression, speech and bladder dysfunction are associated with the progression of PD.[1] In PD condition, the primary symptoms involve impaired motor functions due to selective death of dopaminergic neurons.[2] The pathological feature of PD involves neuronal death within the substantia nigra pars compacta.[3] The PD affected neurons are abundant in protein-rich inclusions known as Lewy bodies.[4-5] These Lewy bodies are rich in aggregates of proteins, namely ubiquitin and α-synuclein.[6] α-Synuclein is a small (14.5 kDa) intrinsically disordered protein (IDP) which is encoded by the *SNCA* gene. The familial form of PD is linked with single point mutations, including A30P, E46K, and A53T. These single point mutations alter the normal fibrillization of the protein. Being an IDP, α-synuclein possesses huge conformational plasticity which is implicated in a variety of functions, including signal transduction, vesicular recycling, synaptic vesicle localization and many others.[7-8] However, it remains controversial whether the monomeric or intermediates or aggregated form of the protein is a causative factor for PD. Previous report has also demonstrated an undefined neuro-protective role of α-synuclein in the amyloid state.[9] Interestingly, recent studies established that the oligomeric intermediate species are the most cytotoxic forms, rather than high molecular weight protein aggregates.[10-11]

α-Synuclein aggregates are abundantly present in the Lewy bodies along with a large number of molecular chaperones, including Hsp70, Hsp40, Hsp60, Hsp90 and Hsp27.[12] Previous studies have shown that overexpression of Hsp70 leads to a significant decrease in the insoluble α-synuclein aggregates in the cells, by promoting refolding.[13-14] Additionally, a drosophila model of PD has revealed that overexpression of Hsp70 suppresses α-synuclein toxicity and as a result, it prevents the dopaminergic neuronal loss.[15] An anti-tumor drug, geldanamycin induces the over expression of Hsp70 and this has been shown to cause reduction in the levels of high molecular weight aggregates of α-synuclein. *In vitro* studies have also demonstrated the inhibition of α-synuclein fibril formation in the presence of Hsp70.[16] Most interestingly, genetic screens of PD patients have revealed a definitive link of α-synuclein to chaperones.[17-18]

Interestingly, under certain stress conditions including PD, α-synuclein is known to import into the mitochondria in spite of possessing only a cryptic mitochondrial-targeting sequence.[19] The mechanism of targeting is believed to be attributed by phosphorylation, high

affinity for cardiolipin, and interaction with mitochondrial import receptors.[20-21] The translocation of α-synuclein is implicated in promoting mitochondrial dysfunction and oxidative stress that result in impairment of mitochondrial dynamics.[20, 22] However, the precise function of α-synuclein in mitochondria remains elusive. It is interesting to note that the mitochondrial chaperone, tumor necrosis factor receptor associated protein-1(TRAP1) is shown to be phosphorylated by the serine/threonine kinase (PINK1), which is also implicated in PD. Therefore, it provides a potential link of PINK1 via TRAP1 to α-synuclein.[23]

In vitro studies demonstrated that the presence of Hsp70 alters the distribution of insoluble to soluble species of α-synuclein by preventing the formation of oligomers, that act as nucleating species during the aggregation process.[24-25] Additionally, studies illustrated that α-synuclein aggregation is inhibited by Hsp70 in a concentration-dependent manner and Hsp 70 significantly reduces the formation of fibrillar α-synuclein as a result its toxicity.[24, 26] The experiments using deletion mutation indicated that the substrate binding domain of Hsp70 interacts with the hydrophobic NAC-domain of α-synuclein and results in assembly inhibition.[26] The budding yeast (*Saccharomyces cerevisiae*) has been successfully used to gain various insights into α-synuclein cytotoxicity and pathobiology.[27-29] Human and yeast mitochondrial Hsp70 (Ssc1) share 66 % of sequence identity and 80 % of sequence homology. Using a yeast mtHsp70 (Ssc1 protein) PD-model, it has been previously shown that a PD-associated mtHsp70 mutation P486S in Ssc1 (corresponding P509S mutation in human mitochondrial Hsp70) results in enhanced interaction with J-protein co-chaperones.[30] It is noteworthy that the ADP-bound Hsp70 demonstrated a very high propensity to co-aggregate with α-synuclein than ATP-bound Hsp70 which suggests that the ATP-bound conformational state of the protein is important for its efficiency.[31]

In this work we investigated the effect of α-synuclein translocation to yeast mitochondria and its interaction with Ssc1 and its PD mutant P486S. We find that targeting of A30P α-synuclein into yeast mitochondria leads to a severe mitochondrial dysfunction phenotype in the wild-type Ssc1 background but not in PD-mutant backgrounds, which are impaired in J-protein interactions. Significantly, increasing the J-protein co-chaperone availability also reverses the protective effects of Ssc1 overexpression. Our *in vitro* studies of heterotypic interaction of multiple chaperones (Hsp70/Hsp40/Hsp78) and α-synuclein corroborates with yeast results. Both wild-type and P486S Ssc1 proteins are equally capable of delaying α-synuclein aggregation by elongating the lag time. However, only the wild-type chaperone was better able to prevent aggregation in the presence of its J-protein co-chaperone. The PD mutant A30P of α-synuclein has an intrinsically lower tendency of

aggregation and shows a pronounced delay in aggregation in the presence of the wild-type chaperone, thereby, strongly favouring the toxic heterogeneous population of oligomers, annular ring like structure and fibrils, which also correlates to the observed lethality in yeast cells. Furthermore, an additional mitochondrial chaperone, Hsp78, which acts in coordination with Hsp70, is found to modulate the effects of wild-type and P486S Ssc1 on α-synuclein aggregation. Only wild-type chaperone was able to prevent α-synuclein aggregation in the presence of Hsp78, whereas PS chaperone did not show significant elongation in the lag time. Taken together, our findings indicate an intriguing possibility that the PD mutation (P486S) in mtHsp70, which affects J-protein interaction and Hsp78, could be a compensatory mutation, which has arisen as a protective mechanism against another PD mutation in α-synuclein (A30P).

4.2 Background

Background contains the experiments carried out by Madhuja Samaddar in the laboratory of Prof. Patrick D'Silva at the Indian Institute of Science, Bangalore, India.

4.2.1 Mitochondrial localization of A30P α-synuclein leads to toxicity and loss of respiratory activity in presence of the wild-type mtHsp70 chaperone machinery

Association of α-synuclein with cellular toxicity has been shown in numerous studies, spanning several model systems. It is also reported to localise in the mitochondria under specific conditions including Parkinson's disease (PD), by undefined trafficking mechanisms. In order to investigate the specific consequences of α-synuclein association with mitochondria, and its interaction with the mitochondrial Hsp70 chaperone network, we have utilized yeast mtHsp70 PD-model.[30] In order to achieve heterologous expression in yeast cells, the human mtHsp70 was cloned into a yeast auxotrophic vector, pRS416 TEF, along with a C-terminal FLAG tag for immuno-detection. The transformed yeast cells were subjected to nutritional selection on Ura^- selective media. By this method, we generated strains expressing regular α-synuclein (non-targeted control) or N-terminal Su9-α-synuclein fusion (mitochondria targeted),[32] and this fusion product was confirmed to localize to the mitochondrial fraction in the transformants. The disease associated variants of α-synuclein, A30P and A53T, were also similarly expressed in yeast, in both their non-targeted and mitochondria-targeted forms. Growth phenotype analysis on selective media revealed that in wild-type Ssc1 expressing yeast cells, the mitochondrial localization of A30P α-synuclein led to a small but distinct decrease in growth (Figure 4.1A, left panel), specifically in the initial

growth phases (Figure 4.1B, left panel). On the other hand, a similar lag time in growth was not observed for mitochondria-targeted wild-type or A53T α-synuclein; or in case of any

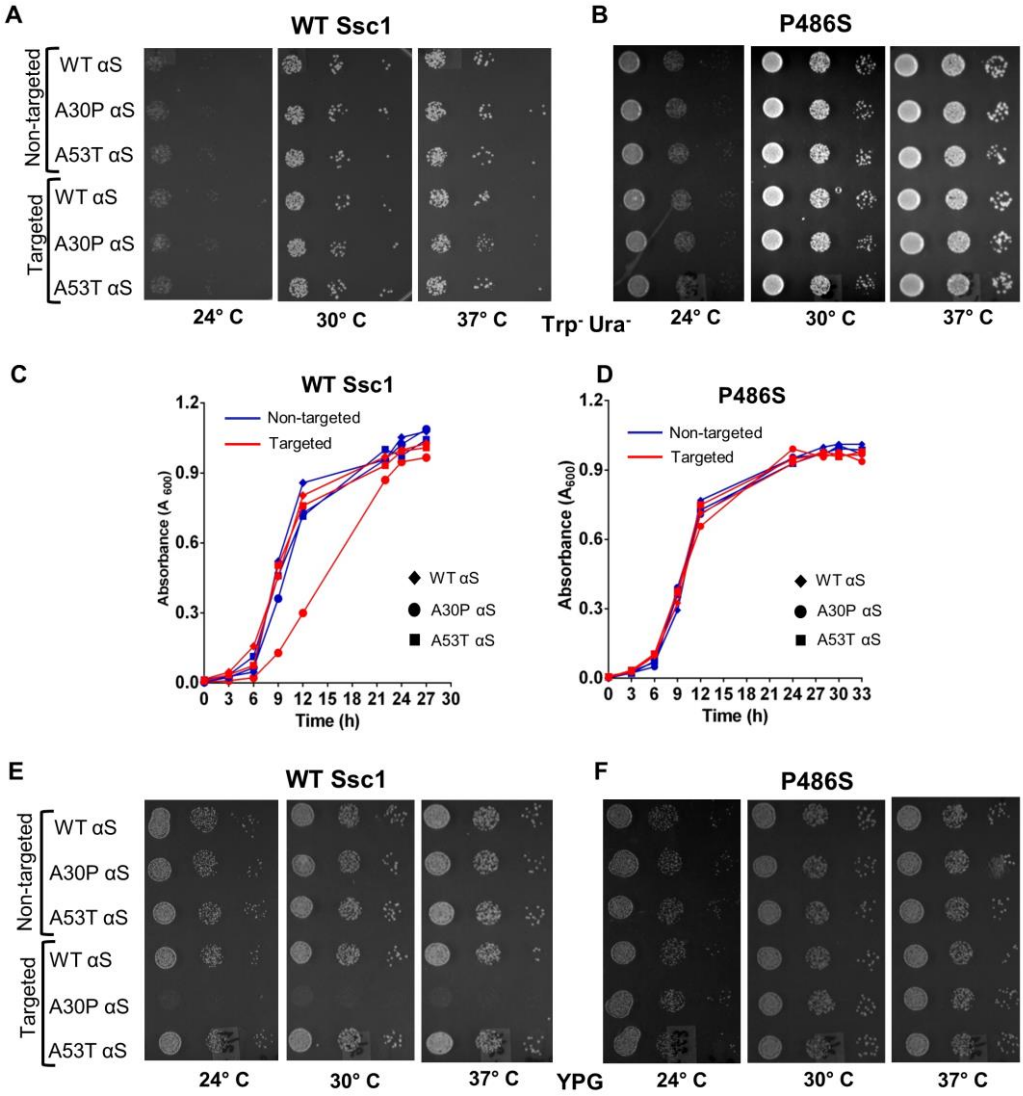

of

Figure 4.1 A growth phenotype analysis of yeast cells expressing either (A) wild-type or (B) P486S Ssc1 were transformed with both forms of wild-type α-synuclein and the respective disease-associated variants. Cells from individual strains were serially diluted, spotted on Trp-Ura- double selection medium, and incubated at the indicated temperatures. The cells were subjected to growth analysis in the liquid selective medium, using equivalent OD of cells in each case (C) wild-type or (D) P486S Ssc1. A mitochondrial respiratory ability of mid-log phase cells of (E) wild-type and (F) P486S Ssc1 chaperone backgrounds, expressing α-synuclein and its variants were serially diluted spotted on non-fermentable YPG medium containing glycerol as the sole carbon source. Plates were incubated at the indicated temperatures for 90 h to check for cell growth and survival. These experiments were performed by Madhuja Samaddar in the laboratory of Prof. Patrick D'Silva at the Indian Institute of Science, Bangalore, India.

the untargeted forms (Figure 4.1A and 1B, left panels). Strikingly, when the various α-synuclein proteins were expressed in the P486S Ssc1 PD-mutant strain, there was no observable growth phenotype (Figure 4.1A and 1B, right panels).

Further, to detect alterations in overall mitochondrial respiration ability due to α-synuclein expression, we performed a similar growth phenotype analysis using a media containing glycerol as the primary carbon source (YPG). Very interestingly, we found that expression of mitochondria-targeted A30P α-synuclein in the wild-type Ssc1 strain background led to complete impairment in respiration by the oxidative phosphorylation pathway. Although the cells were viable on selective medium; they demonstrated a lethal phenotype on non-fermentable YPG medium (Figure 4.1C, left panel). Strikingly, once again this altered growth phenotype was observed only in case of wild-type Ssc1 but not in the P486S Ssc1 strain background (Figure 4.1C, right panel). Furthermore, both wild-type and A53T α-synuclein failed to disrupt respiration ability even in their mitochondria targeted forms, indicating a specific effect due to the A30P mutation.

4.2.2 Modification of mitochondrial chaperone networks alters the toxic effects of A30P α-synuclein localization in wild-type mtHsp70 mitochondria.

Overexpression of chaperones, particularly Hsp70, or its induction, is known to hinder the aggregation of α-synuclein and is associated with cellular toxicity. Furthermore, Hsp70-α-synuclein interactions are known to inhibit fibril assembly, highlighting a key role of the chaperone in modulating α-synuclein cytotoxicity. To test the ability of increased levels of mtHsp70 protein in reversing the deleterious effects of α-synuclein association, wild-type and A30P α- synuclein were targeted to the mitochondria in cells overexpressing the wild-type or P486S Ssc1 chaperones, under the control of a GPD promoter. Growth curve analysis revealed that the slow-growing phenotype of wild-type Ssc1 cells expressing mitochondrial A30P α-synuclein was reversed by overexpression of the same chaperone, leading to elimination of the delay in growth at initial stages (Figure 4.2A, left panel). The overexpressed wild-type Ssc1 chaperone also showed a striking ability to restore mitochondrial respiration thereby, allowing the cells containing A30P α-synuclein to grow on YPG medium at various temperatures (Figure 4.2B). This remarkable reversion of growth defects upon chaperone overexpression was accompanied by the restoration of altered mitochondrial physiology. Consequently, we observed a modification in ROS levels (Figure 4.2C), indicating that the increased cell viability is associated with restoration of

mitochondrial function. Interestingly, overexpression of the P486S PD-mutant chaperone, on the other hand, did not lead to very significant changes in ROS levels (Figure 4.2C).

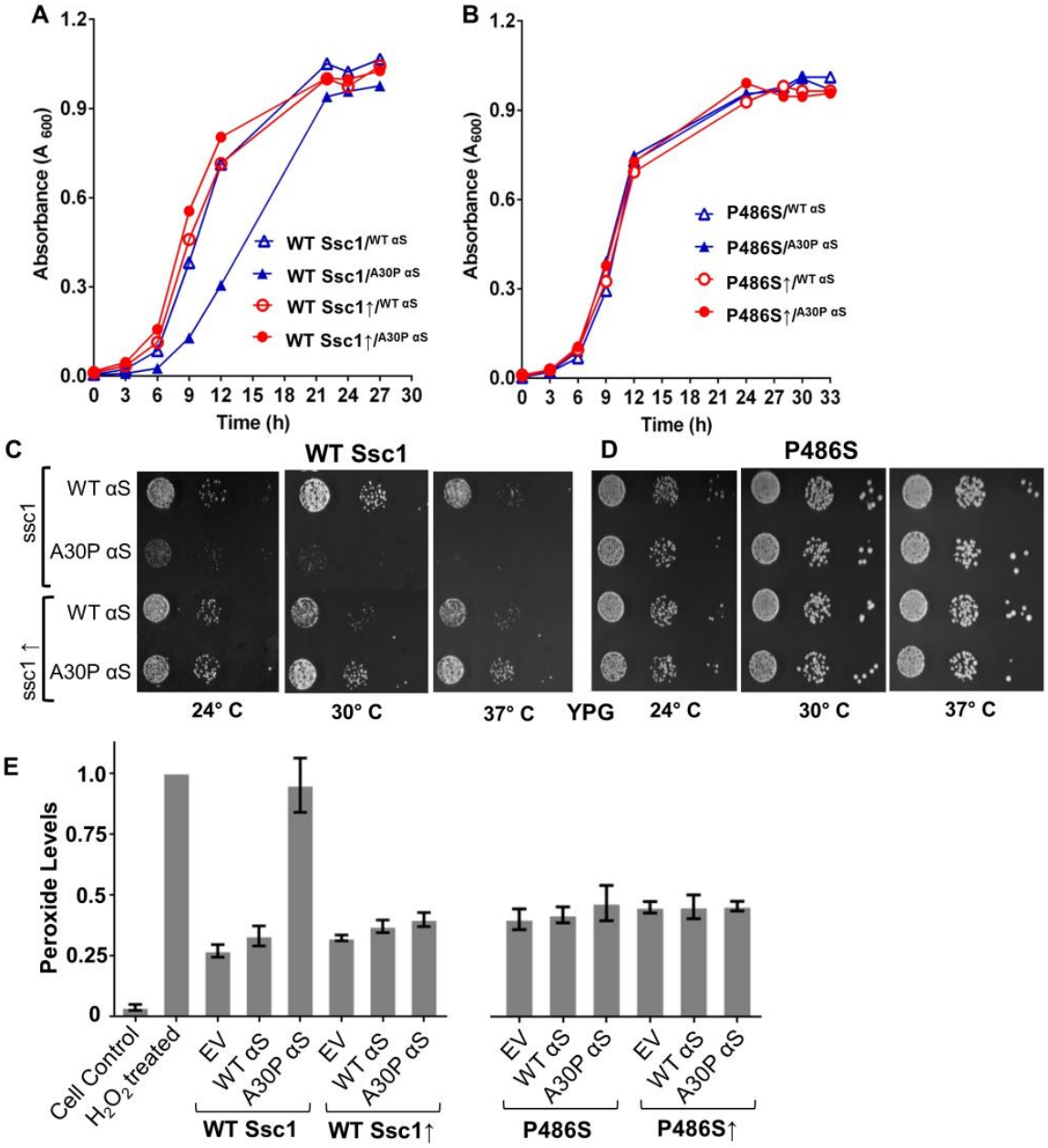

Figure 4.2 Restoration of growth by wild-type and PS chaperone overexpression. The cells were subjected to growth analysis in the liquid selective medium, using equivalent OD of cells in each case of (A) wild-type or (B) P486S Ssc1. Additionally, the cells were subjected to serial dilutions and spotted on YPG media, at various temperatures to determine their respiratory ability of (C) wild-type or (D) P486S Ssc1. (E) Comparison of normalized cellular ROS levels by flow cytometry. Cells of 0.1 OD were stained with H_2DCFDA and the cell numbers were plotted as a function of the fluorescence intensity. The numbers of H_2O_2 treated cells served as the positive control. These experiments were performed by Madhuja Samaddar in the laboratory of Prof. Patrick D'Silva at the Indian Institute of Science, Bangalore, India.

the chaperoning activity of Hsp70-Hsp40 complexes by interacting with the co-chaperone partner.[18] Thus, to examine the effect of altered levels of Mdj1 co-chaperone, we supplemented the endogenous protein levels with additional expression from a plasmid containing TEF promoter. Strikingly, we observed that overexpression of Mdj1 alone was sufficient to restore the growth of wild-type Ssc1 cells expressing mitochondrial A30P α-synuclein, on glycerol containing medium (Figure 4.3). However, when both Ssc1 and Mdj1 were simultaneously overexpressed we did not see any additive effect in their cytoprotective activity. A similar overexpression of Mdj1 in the P486S Ssc1 background strains did not result in any observable changes in the growth phenotype (Figure 4.3).

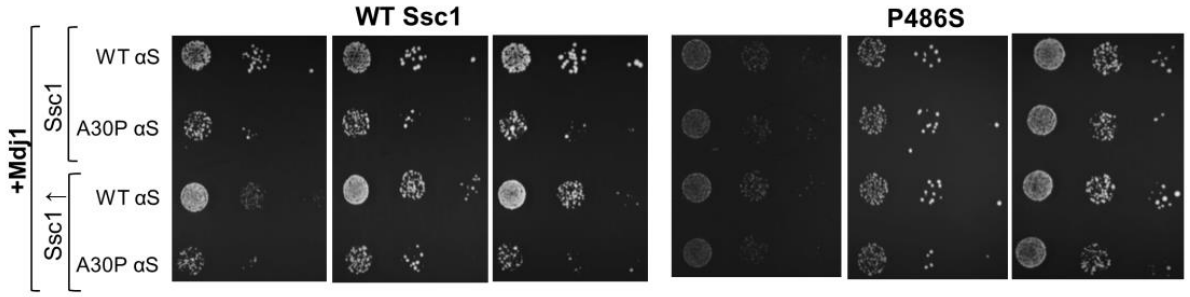

Figure 4.3 Modification of growth phenotype by J-protein overexpression. α-Synuclein and enhanced Mdj1 expressing strains of (A) wild-type and (B) P486S Ssc1 chaperone backgrounds, were serially diluted and subjected to drop test on YPG medium to evaluate the effects of excess Mdj1 on cell growth. These experiments were performed by Madhuja Samaddar in the laboratory of Prof. Patrick D'Silva at the Indian Institute of Science, Bangalore, India.

4.2.3 Summary

The yeast data suggest that the mitochondrial targeting of A30P α-synuclein led to distinctive defects in wild-type Ssc1 expressing cells, including growth retardation and increased generation of ROS. Surprisingly, there was negligible effect on the phenotype of P486S Ssc1 cells due to targeted A30P α-synuclein expression. This clearly indicates that the observed defects are specific consequences arising from intrinsic differences in the chaperoning efficiency of wild-type and P486S Ssc1. A remarkable rescue of the physiological defects was observed by overexpression of wild-type Ssc1 chaperone. The excess wild-type chaperone efficiently corrected increased ROS levels and restored mitochondrial respiration, thereby, promoting overall cell growth. However, once again the P486S Ssc1 chaperone failed to show any significant alterations in the growth phenotypes, upon its overexpression. Thus intriguingly, the cells remained insensitive to α-synuclein stress, in the presence of

enhanced levels of the P486S Ssc1. To further investigate the importance of this interaction, we also independently overexpressed the mitochondrial matrix J-protein co-chaperone, Mdj1. The overexpression of Mdj1 leads to a recovery in the growth of wild-type Ssc1 cells expressing mitochondrial A30P α-synuclein. Thus, both the chaperone and the co-chaperone play distinct, key roles in mitigating α-synuclein toxicity. However, very interestingly, the simultaneous overexpression of both Hsp70 and Hsp40 proteins did not restore growth in an additive manner, suggesting that their relative cellular levels are a pivotal factor for determining the efficiency of chaperoning functions.

4.3 Experimental section

4.3.1 Expression and purification of α-synuclein

Wild-type and mutant α-synuclein were purified using a reported protocol.[33] The pT7-7 plasmid with α-synuclein gene was transformed in BL21 (DE3) strain of *Escherichia coli*. Briefly, 1 % of the overnight grown culture (containing 100 μg/mL ampicillin and 35 μg/mL chloramphenicol) of BL21 (DE3) was transferred into fresh media. Cells were induced at optical density 0.6- 0.8 with 800 μM IPTG for 8 h. To obtain the cell pellet, culture was centrifuged at 4,000 rpm for 30 min at 4 °C. Pellet was resuspended in lysis buffer (50 mM Tris, 150 mM NaCl, 10 mM EDTA, pH 8). The lysed cells were boiled at 95°C for 30 min followed by centrifugation at 12,000 rpm for 30 min at 4 °C. The supernatant was collected and thoroughly mixed with 136 μL/mL of 10 % streptomycin sulphate and 228 μL/mL of glacial acetic acid followed by centrifugation at 12,000 rpm for 30 min at 4 °C. To the clear supernatant, equal volume of saturated ammonium sulphate was added and kept at 4 °C with an intermittent mixing for 1 hour. The precipitated protein, separated by centrifugation at 12,000 rpm for 30 min at 4 ºC was suspended in equal volume of 100 mM ammonium acetate and ethanol followed by centrifugation at 4,000 rpm for 10 min at 4 °C. Finally, the pellet was washed twice with absolute ethanol and dried at room temperature, until ethanol evaporated. The pellet was suspended in equilibrating buffer (10 mM Tris, pH 7.4) and further purified by FPLC (fast performance liquid chromatography) on a Q Sepharose column and the protein was eluted at ~ 300 mM NaCl. The purity of the collected fractions was assessed by SDS-PAGE. The pure fractions were dialyzed in a dialysis buffer (20 mM Tris, 50 mM NaCl, pH 7.4) and stored at -80 ºC. All the molecular chaperones were expressed and purified by Madhuja Samaddar in the laboratory of Prof. Patrick D'Silva.

4.3.2 Kinetics of *in vitro* aggregation

The aggregation reactions were carried out using α-synuclein alone, or in combination with the human or yeast mtHsp70 chaperone systems (wild-type or Proline to Serine PD-mutant of mtHsp70 and the respective Hsp40 co-chaperone). The α-synuclein concentration used was 200 μM while chaperone and co-chaperone concentrations were 2 μM and 0.4 μM respectively. Reactions were set up in Tris buffer containing 20 mM Tris, 100 mM NaCl, 2 mM $MgCl_2$ and 4 mM ATP (pH 7.4) with 800 rpm stirring speed, at 30 ºC (for the yeast proteins) and 37 ºC (for human proteins). Thioflavin T (ThT) (Sigma-Aldrich) 20 μM was included in all the reactions for following α-synuclein aggregation kinetics. The reactions were replenished with 4 mM ATP, every 6 h. Fluorescence was recorded using the parameters λ_{ex} = 450 nm, λ_{em} = 480 nm with excitation and emission bandpass of 0.5 nm and 1 nm respectively, and integration time was fixed at 5 sec. The measurements were carried out on Fluoromax-4 (Horiba Jobin Yvon, NJ) using 10 mm x 10 mm quartz cuvette at 25 ºC. ThT fluorescence intensity data was collected at 2 h intervals for yeast proteins and 1 h for human proteins and the aggregation kinetics data were fitted using the standard equation to calculate the lag time.[34]

4.3.3 AFM imaging

Freshly cleaved mica (muscovite grade V-4 mica from SPI, PA) was washed with MQ water. The undiluted 10 μL of aggregation samples were withdrawn at different time points from the aggregation reaction, were deposited on mica, kept for 10 mins drying followed by washing with 500 μL of MQ water. After washing, the mica was dried under mild stream of nitrogen gas for 30 min. Tapping mode AFM images were recorded on a Bruker innova AFM in the air. The collected images were processed and analyzed using SPIP (from Image Metrology).

4.4 Results

4.4.1 Aggregation kinetics of α-synuclein, in the presence of yeast wild-type / PD mutant (P486S) of Hsp70 with its co-chaperones (Mdj1)

α-Synuclein is an amyloidogenic intrinsically disordered protein which deposits as intracellular aggregates in PD. The aggregation kinetics of amyloid formation is commonly studied *in vitro* by the Thioflavin T (ThT) fluorescence assay.[35] ThT contains a benzothiazole moiety which intercalates into the solvent-exposed side chains of a cross β-sheet structure,

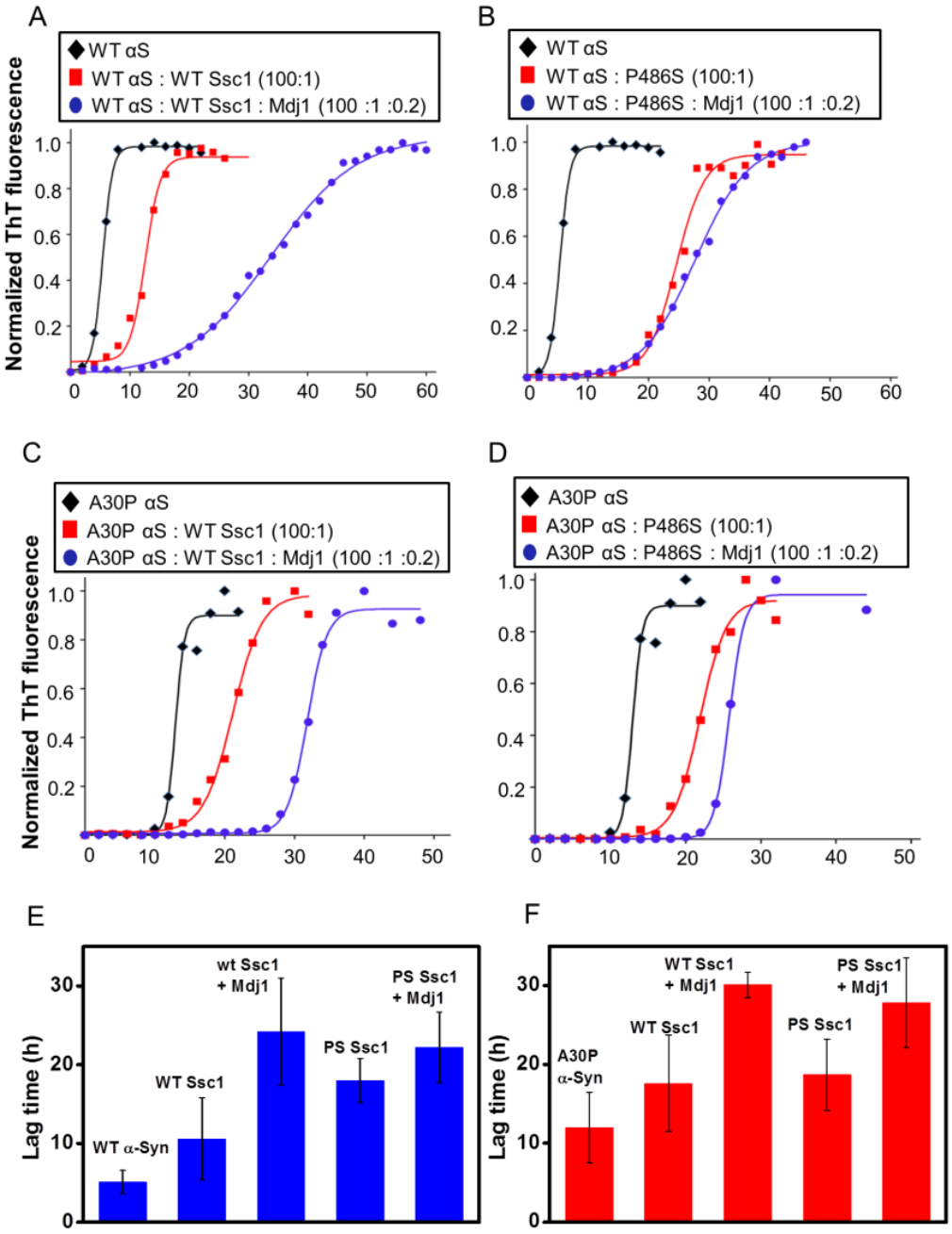

Figure 4.4 Normalized ThT fluorescence of α-synuclein aggregation kinetics and effect of yeast mitochondrial Ssc1. (A and B) Wild-type α-synuclein aggregation (black) in the presence of wild-type Ssc1 (A)/ P486S Ssc1 (B) (red) and Mdj1 (blue). (C and D) A30P α-synuclein aggregation (black) in the presence of wild-type Ssc1 (A)/ P486S Ssc1 (red) (B) and Mdj1 (blue). A30P α-synuclein aggregation (black) in the presence of wild-type Ssc1 (red) and Mdj1 (blue). Bar plots of lag time recovered from the fits of the aggregation kinetics of (E) wild-type α-synuclein and (F) A30P α-synuclein in the presence of wild-type and P486S Ssc1. Error bars are obtained from at least three independent measurements. The concentration of α-synuclein, Ssc1 and Mdj1 were 200 μM, 2 μM and 0.4 μM, respectively.

typical of amyloid fibrils, and this stoichiometric association leads to a strong fluorescence emission. Owing to the stoichiometry of the dye-fibril association, the formation of the fibrils is quantifiable, and can be monitored as a function of time. α-Synuclein aggregation follows a nucleation-dependent polymerization pathway with an initial lag phase, an exponential phase, and a final saturation phase.[36-37] The elongation in the lag time of α-synuclein aggregation indicates better inhibition.

In order to discern the effect of wild-type Ssc1 and PS mutant of Ssc1 on α-synuclein aggregation, we initiated our studies by monitoring the kinetics of α-synuclein aggregation in the presence of yeast mitochondrial Hsp70 chaperone (Ssc1) and its co-chaperone partner (Mdj1), using ThT fluorescence. The lag time of aggregation of purified wild-type α-synuclein was significantly enhanced from an average of 5 h, to 10 h and 18 h, respectively in the presence of wild-type and P486S PD-mutant Ssc1 (Figure 4.4A and 4B). Interestingly, in the presence of the Mdj1 co-chaperone partner, the two chaperones showed very different abilities to further inhibit aggregation. While wild-type Ssc1 was significantly assisted by Mdj1in increasing the lag time (from 10 h to 24 h), P486S Ssc1 showed only a modest improvement in its chaperoning ability in the presence of Mdj1 (from 18 h to 22 h) (Figure 4.4A and 4B). This difference in chaperoning abilities in the presence of the co-chaperone partner was further pronounced in case of A30P α-synuclein aggregation. The A30P mutant is known to have a slower rate of oligomer to fibril transition and correspondingly, an intrinsically longer lag time, during which oligomeric species accumulate.[38] We found a similar enhancement in the average lag time for A30P α-synuclein (12 h), which was further increased in the presence of wild-type and P486S Ssc1 to 18 h and 19 h respectively (Figure 4.4C and 4D). In the presence of Mdj1, the lag times were further extended to 30 h and 28 h, respectively. This highlights the differential ability of Mdj1 in assisting the wild-type and P486S chaperones in their action (Figure 4.4C and 4D).

4.4.2 Aggregation kinetics of α-synuclein, in the presence of human wild-type / PD mutant (P509S) of Hsp70 with its co-chaperones (Tid1s)

To verify the relevance of the above results for the human system, we also performed similar experiments using the human mitochondrial chaperone and their counterparts. In this case, we observed an increment in the lag time of wild-type α-synuclein from 3 h to 10 h and 9 h in the presence of purified wild-type and P509S mtHsp70 proteins, respectively (Figure 4.5A and 5B). The lag times were further extended to 14 h and 11 h upon addition of the co-chaperone

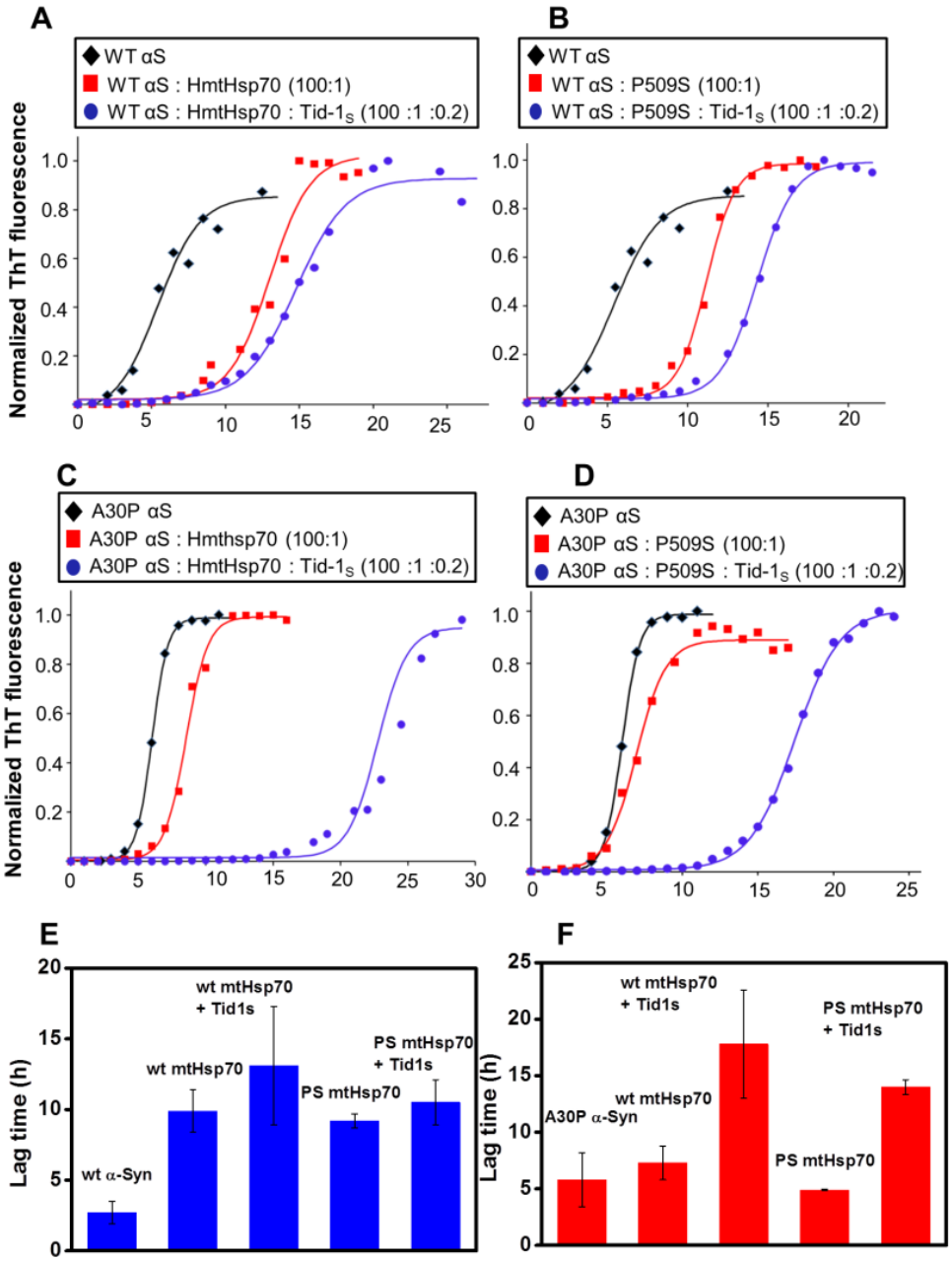

Figure 4.5 Normalized ThT fluorescence of α-synuclein aggregation kinetics and effect of human mitochondrial Ssc1. (A and B) Wild-type α-synuclein aggregation (black) in the presence of wild-type Ssc1 (A)/ P486S Ssc1 (B) (red) and Mdj1 (blue). (C and D) A30P α-synuclein aggregation (black) in the presence of wild-type Ssc1 (A)/ P486S Ssc1 (red) (B) and Mdj1 (blue). A30P α-synuclein aggregation (black) in the presence of wild-type Ssc1 (red) and Mdj1 (blue). Bar plots of lag time recovered from the fits of the aggregation kinetics of (E) wild-type α-synuclein and (F) A30P α-synuclein in the presence of wild-type and P486S Ssc1. Error bars are obtained from at least three independent measurements. The concentration of α-synuclein, Ssc1 and Mdj1 were 200 μM, 2 μM and 0.4 μM, respectively.

Tid1S (Figure 4.5A and 4.5B). In case of A30P α-synuclein, the intrinsic lag time of 5.3 h was changed to 7 h and 5 h by wild-type and P509S mtHsp70; and further to 18 h and 14 h in presence of the co-chaperone (Figure 4.5C and 5D). Thus, overall both wild-type and the Proline to Serine mtHsp70 PD-variant, are individually capable of delaying α-synuclein aggregation to comparable extents. However, only the wild-type chaperone is assisted significantly further by the presence of a J-protein co-chaperone partner, in case of both

human and yeast proteins (Figure 4.5C and 5D). This cooperation of the wild-type chaperones and the corresponding co-chaperones in delaying aggregation is especially marked in case of A30P α-synuclein, which has an intrinsically longer lag time.

4.4.3 Time-dependent Atomic force Microscopy images of wild-type α-synuclein aggregation, in the presence of wild-type / PD mutant (P509S) of Hsp70 with its co-chaperones (Tid1s)

In order to visualize the morphological transformations as a function of time, we utilized atomic force microscopy(AFM) (Figure 4.6 and Table 4.1), which provides insights into the

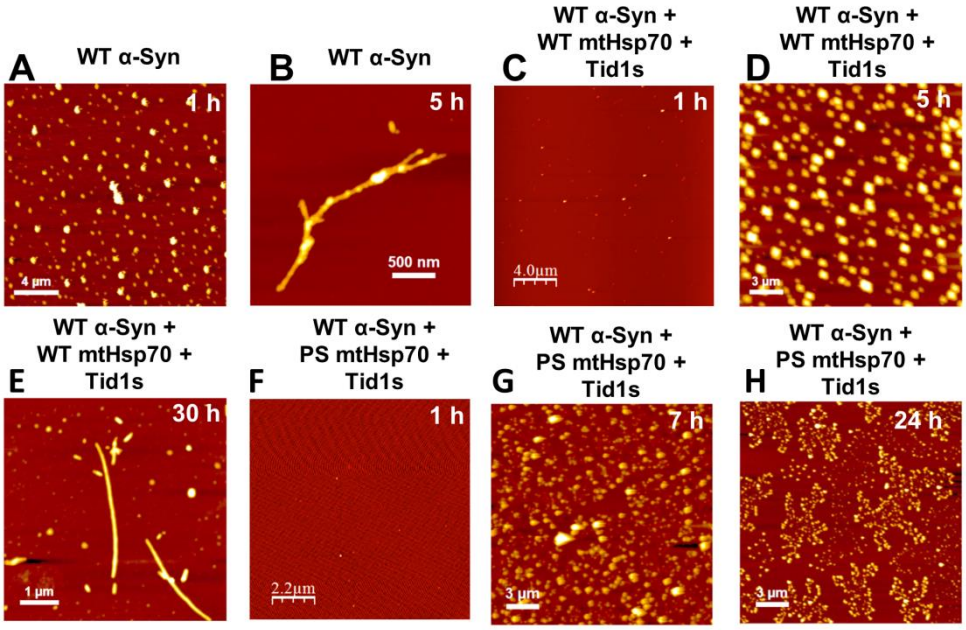

Figure 4.6. Time-dependent AFM images of wild-type α-synuclein aggregation and in the presence of wild-type or P509S Hsp70 in the presence of Tid1s.

time-dependent evolution of the topography of the supramolecular nanoscale assemblies. The height distribution as well as statistical analyses (Figure 4.6 A and B) revealed that the wild-

type α-synuclein formed large oligomers (of average height ~ 48 nm) which transformed into branched fibrils (of average height ~ 6 nm) in the saturation phase. It is known for wild-type α-synuclein to forms fibrils of height 5-6 nm.[39] Interestingly, in the presence of wild-type Hsp70 and Tid1s, the size of the oligomers (of average height ~ 75 nm) is larger than that of only α-synuclein oligomers (Figure 4.6 D). This increase in the size of the oligomers could be the result of α-synuclein and Hsp interaction during oligomer formation. Previous studies have also shown that Hsp70 inhibits the fibril formation of α-synuclein via interacting with the prefibrillar oligomers.[25] Upon prolonged incubation, these large oligomers were transformed into straight fibrils of average height ~ 9 nm in the saturation phase (Figure 4.6 E). The topographical distribution of α-synuclein in the presence of PS Hsp70 and Tid1s reflected large oligomers of an average height of ~71 nm, but these oligomers were not capable of forming fibrils. The large oligomers showed a decrease in size from ~ 71 nm to two different pollutions of oligomers of average height of ~ 7 nm and 50 nm (Figure 4.6 F-H). This intriguing observation suggested that the mechanism of inhibition of α-synuclein aggregation in the presence of wild-type Hsp70 and PD mutant of Hsp70 (P509S) is different.

4.4.4 Time-dependent Atomic force Microscopy images of A30P α-synuclein aggregation, in the presence of wild-type / PD mutant (P509S) of Hsp70 with its co-chaperones (Tid1s)

Next, in order to investigate the nanoscopic changes in the morphologies of A30P α-synuclein during aggregation in the presence of wild-type Hsp70 or PS Hsp70, we utilized AFM. We observed that A30P α-synuclein formed large spherical oligomers of average height ~ 60 nm; which converted into annular protofibrils (of average height ~ 9 nm) in the saturation phase (Figure 4.7 A and B). Previous studies have also shown that A30P α-synuclein forms pore like annular protofibrils at the saturation phase of aggregation.[40] *In vitro* a variety of proteins and peptides have been shown to form annular pores and protofibrils.[41-44] Interestingly, in the presence of wild-type Hsp70 and Tid1s, oligomers of average height ~ 20 nm were obtained which transformed into a heterogeneous population distribution dominated by oligomers, annular protofibrils and fibrils in the log phase(Figure 4.7 C-H). An extensive height profile analysis of this heterogeneous population revealed that the pore-like annular protofibrils and fibrils were of ~ 7 nm. However, these structures also have small oligomers or Hsp molecules attached to it, which result in an increase in the height to 15-20 nm. These structures resemble the "beads-on-a-string" morphologies of α-antitrypsin aggregates shown by electron micrograph.[45-47] This heterogeneous population was then utilized as a scaffold

which triggered the higher-order supramolecular fibril formation (of average height ~ 12 nm). Additionally, in the presence of PS Hsp70 with its co-chaperone, A30P α-synuclein showed a population of small oligomers of ~ 9 nm in the lag phase of aggregation. These oligomers were consistent during the course of aggregation from lag phase to saturation phase.

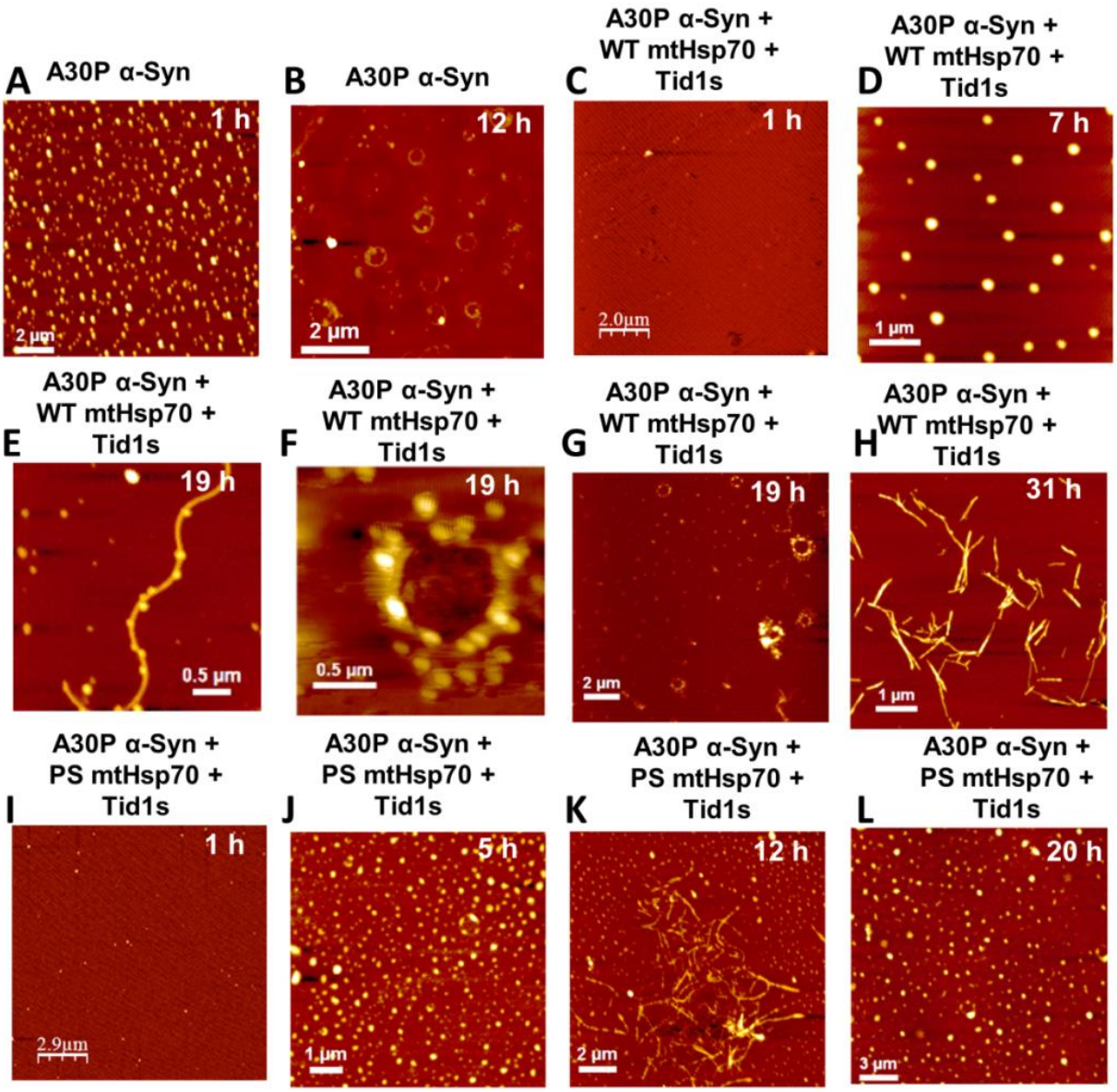

Figure 4.7 Time-dependent AFM images of A30P α-synuclein aggregation and in the presence of wild-type or P509S Hsp70 in the presence of Tid1s.

Table 4.1

Height profile analysis of AFM images shown in figures 6 and 7 using SPIP software.

Aggregation conditions	Lag/Log/ Saturation phase of aggregation	Oligomers (Height in nm)	Annular ring (Height in nm)	Fibrils (Height in nm)
WT α-Synuclein	Lag	48 ± 18		
	Saturation			6 ± 2
WT α-Synuclein + WT mtHsp70 + Tid1s	Lag	75 ± 24		
	Saturation			9 ± 3
WT α-Synuclein + PS mtHsp70 + Tid1s	Lag	71 ± 10		
	Saturation	7 ± 2 & 50 ± 12		
A30P α-Synuclein	Lag	60 ± 18		
	Saturation		9 ± 3	
A30P α-Synuclein + WT mtHsp70 + Tid1s	Lag	20 ± 5		
	Log		25 ± 5	10 ± 2
	Saturation			12 ± 2
A30P α-Synuclein + PS mtHsp70 + Tid1s	Lag	9 ± 4		
	Log	9 ± 4		9 ± 2
	Saturation	7 ± 2		

However, in the log phase of aggregation, we encountered a small population of fibrils as well. Interestingly, in the saturation phase those fibrils were broken into small oligomers of similar height ~ 9 nm (Figure 4.7 I-L). Therefore, it supports our observation on wild-type α-synuclein, the mechanism of inhibition of α-synuclein aggregation in the presence of wild-type Hsp70 and PD mutant of Hsp70 (P509S) is different.

4.4.5 Effect of Hsp78 on α-synuclein aggregation, in the presence of wild-type / PD mutant (P486S) of Hsp70 with co-chaperone (Mdj1)

Next, we steered toward delineating the role of Hsp78 on α-synuclein aggregation. In addition to the Hsp70-Hsp40 system, Hsp78 chaperone of the yeast mitochondrial matrix represents an additional system for the resolution of protein aggregates.[48-50] Hsp78 is a close homologue of Hsp104 in yeast cells and is known for protein disaggregation.[51] Our *in vitro* wild-type α-synuclein aggregation studies revealed that yeast mitochondrial Hsp78 elongates the lag time of aggregation in a concentration-dependent manner (Figures 8A and 8B). At a high concentration (1 μM) of Hsp78, the extent of inhibition was more as compared to at a low concentration (0.2 μM) of Hsp78 (Figure 4.8B). The lag time of aggregation of wild-type α-synuclein was significantly enhanced from an average of 5 h to 9 h in the presence of Hsp78 (Figure 4.8A), suggesting that Hsp78 is individually capable of inhibiting wild-type α-synuclein aggregation. As shown above, wild-type Ssc1 in the presence of its co-chaperone decelerated the aggregation and resulted in lag time of 24 h. Interestingly, a profound increase in the lag time (~ 40 h) of α-synuclein aggregation was observed in the presence of multiple chaperones (wild-type Ssc1 with Mdj1 and Hsp78), as shown in Figure 4.9A. This

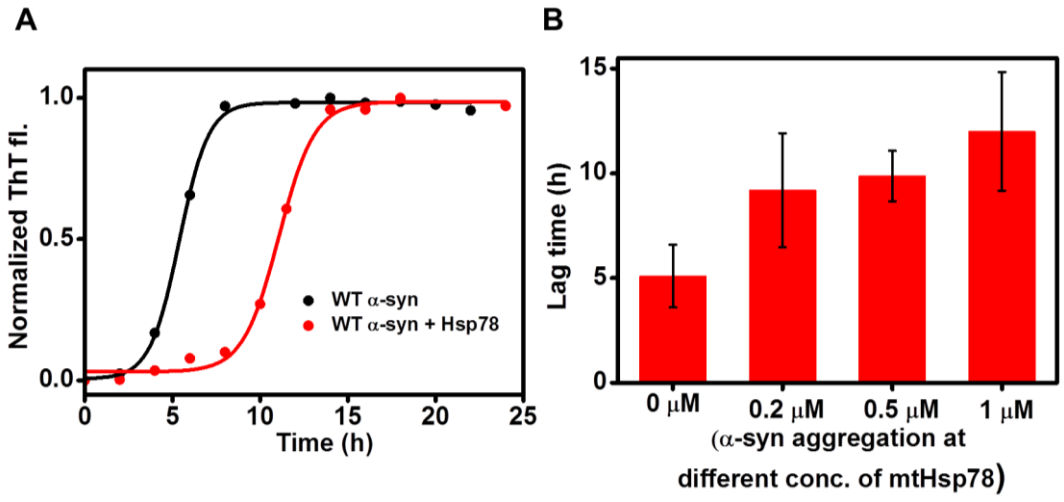

Figure 4.8 (A) Normalized ThT fluorescence of wild-type α-synuclein (200 μM) aggregation kinetics (black) and modulation in kinetics in the presence of Hsp78 (0.2 μM) (red). (B) Bar plots of lag time recovered from the fits of the aggregation kinetics of wild-type α-synuclein at concentration titration of Hsp78 (0.2 - 1 μM). Error bars are obtained from at least three independent measurements.

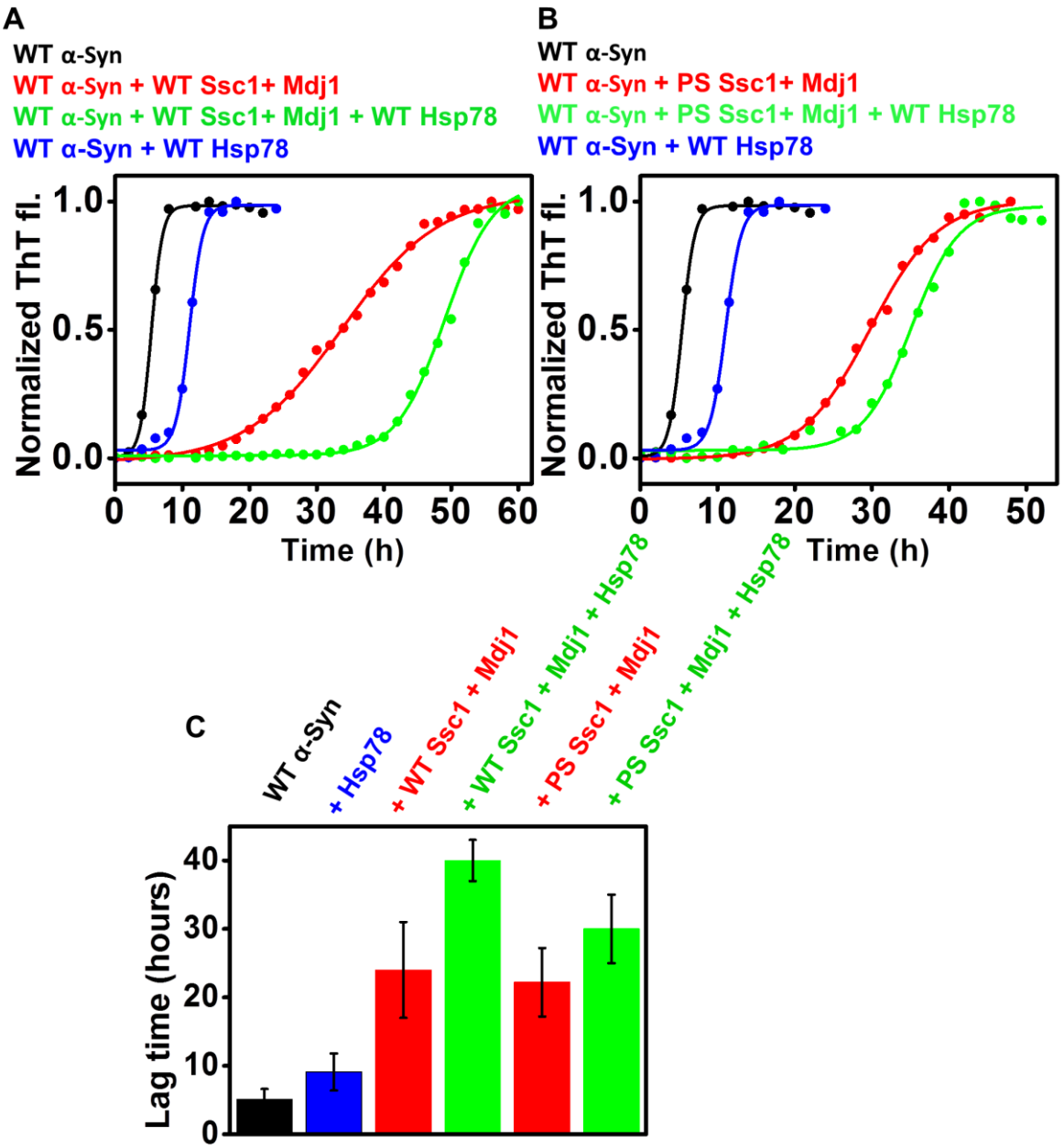

Figure 4.9 Normalized ThT fluorescence of wild-type α-synuclein aggregation kinetics and effect of mitochondrial Hsp70 and Hsp78. (A) α-synuclein aggregation (black) in the presence of (A) wild-type Hsp70-Mdj1 (red), Hsp78 (blue) and all the chaperones together (green). (B) α-synuclein aggregation (black) in the presence of P486 Ssc1-Mdj1 (red), Hsp78 (blue) and all the chaperones together (green). (C) Bar plots of lag time recovered from the fits of the aggregation kinetics of wild-type α-synuclein in the presence of different Hsp. Error bars are obtained from at least three independent measurements.

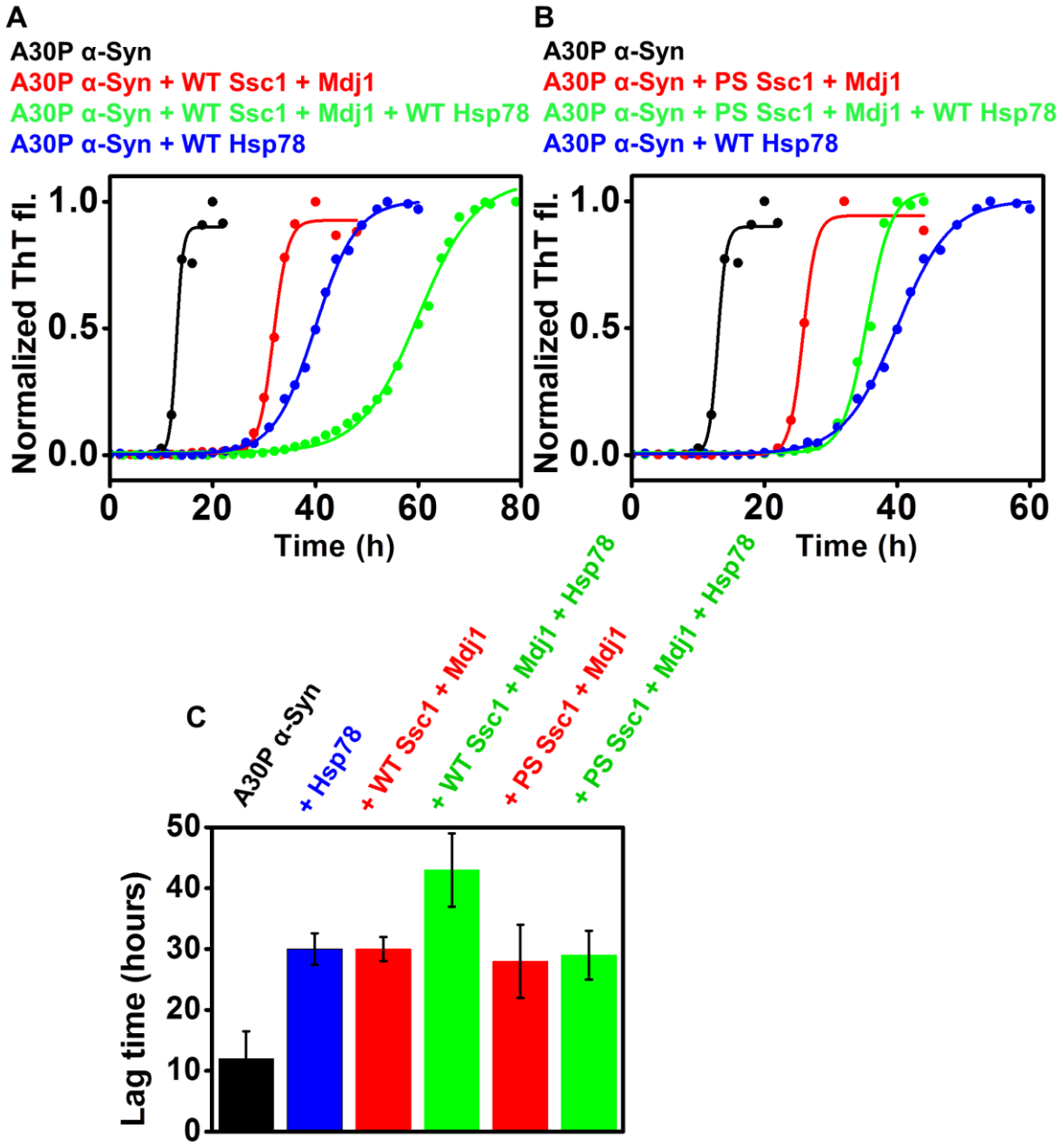

Figure 4.10 Normalized ThT fluorescence of A30P α-synuclein aggregation kinetics and effect of mitochondrial Hsp70 and Hsp78. (A) α-synuclein aggregation (black) in the presence of (A) wild-type Hsp70-Mdj1 (red), Hsp78 (blue) and all the chaperones together (green). (B) α-synuclein aggregation (black) in the presence of P486 Ssc1-Mdj1 (red), Hsp78 (blue) and all the chaperones together (green). (C) Bar plots of lag time recovered from the fits of the aggregation kinetics of wild-type α-synuclein in the presence of different Hsp. Error bars are obtained from at least three independent measurements.

dramatic increase in lag time could be the outcome of concord work of multiple chaperones and it also establishes that Hsp78 might be a key player in inhibiting the α-synuclein aggregation. We next examined the effect of PS mutant of Ssc1 in the presence of its co-chaperones and Hsp78, on α-synuclein aggregation. Apparently, in presence of the multiple chaperones (PS mutant of Ssc1 with Mdj1 and Hsp78) an increase in the lag time (~ 30 h) of wild-type α-synuclein aggregation was observed (Figure 4.9B), whereas, PS mutant with Mdj1 showed a lag time of ~ 22 h. While wild-type Ssc1 with Mdj1 was significantly assisted by Hsp78 in increasing the lag time (from 25 h to 40 h), P486S Ssc1with Mdj1 showed only a modest improvement in its chaperoning ability in the presence of Hsp78 (from 22 h to 30 h) (Figure 4.9A and 9B). These results shed light into the distinguishing ability of wild-type and PS mutant of Ssc1 in the presence of Hsp78. The bar graph in Figure 4.9C shows the lag times obtained from wild-type α-synuclein aggregation in the presence of different chaperones.

In order to gain further insights into the chaperoning abilities of wild-type and PS mutant of Hsp70, in the presence of Hsp78 partner, we used A30P mutant of α-synuclein. This familial PD mutant is known to show a slower rate of fibril formation with an elongated lag time.[38] The aggregation lag time of A30P α-synuclein was prominently increased from an average of 12 h to 30 h in the presence of Hsp78 (Figure 4.10A).We found a similar enhancement in the average lag time of A30P α-synuclein aggregation in the presence of wild-type Ssc1 with Mdj1 (30 h) (Figure 4.10A). These results indicated that Hsp78 is individually capable of inhibiting the A30P α-synuclein aggregation to a similar extent as shown by wild-type Ssc1 in the presence of Mdj1. However, a striking elongation in the lag time to ~ 43 h was obtained in the presence of wild-type Ssc1 with Mdj1 and Hsp78 (Figure 4.10A) which suggests that plausibly multiple chaperones work together more efficiently in elongating the lag time of A30P α-synuclein aggregation. On the other hand, the presence of PS mutant of Ssc1 with Mdj1 and Hsp78 resulted in no significant increase in the lag time (~ 29 h) as compared to only PS mutant of Ssc1 with Mdj1 (~ 28 h) (Figure 4.10B). The bar graph shown in Figure 4.10C represents the lag times obtained from A30P α-synuclein aggregation in the presence of different chaperones.

4.4.6 Time-dependent Atomic force Microscopy images of α-synuclein aggregation, in the presence of wild-type / PD mutant (P486S) of Hsp70 with Mdj1 and Hsp78

In order to watch the morphological transitions during α-synuclein aggregation in the presence of Hsp78 and other chaperones, we used AFM imaging (Figure 4.11 and 4.12 and Table 4.2). Wild-type α-synuclein in the presence of Hsp78 formed large oligomers (of average height ~ 40 nm) which transformed into branched like fibrils (of average height ~ 6 nm) (Figure 4.11 A-C). Interestingly, in the presence of wild-type Ssc1-Mdj1 and Hsp78, we visualized the formation of oligomers (of average height ~ 18 nm) that matured into annular protofibrils and finally transformed into small oligomers (of average height ~ 7 nm) (Figure 4.11 D-G) On the other hand, in the presence of PS Ssc1-Mdj1 and Hsp78, the size of the oligomers was reduced to an average height of ~ 27 nm and these oligomers were converted into smaller oligomers (of average height ~ 7 nm) and fibrils(Figure 4.11 H-K). Additionally, our AFM images of A30P α-synuclein aggregation in the presence of Hsp78 showed larger

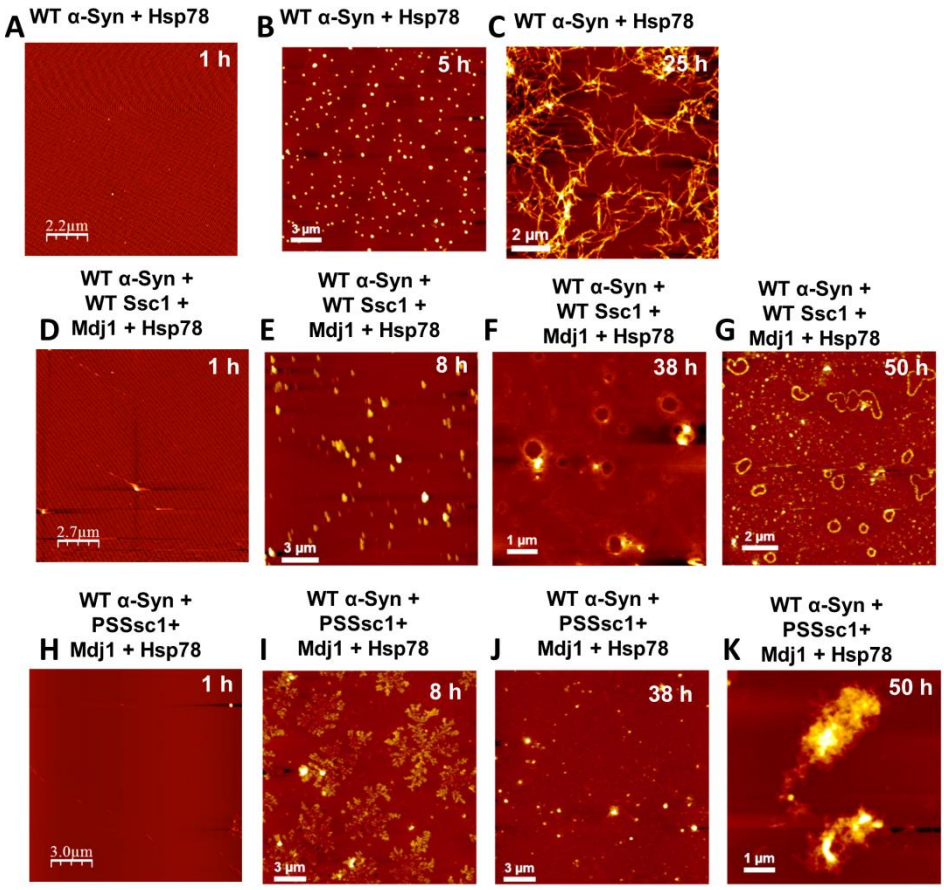

Figure 4.11 Time-dependent AFM images of wild-type α-synuclein aggregation and in the presence of different chaperones (Hsp78, wild-type or P486S Ssc1 in the presence of Mdj1) α-synuclein aggregation.

.oligomer formation (of average height ~ 100 nm) which converted into oligomers of average height ~ 60 nm (Figure 4.12 A-D). The large size of the oligomers could be the result of A30P α-synuclein and Hsp78 molecules present together during the oligomer formation. Interestingly, during the lag phase of aggregation of A30P α-synuclein in the presence of wild-type Ssc1-Mdj1 and Hsp78, we encountered the oligomers of ~ 40 nm height that converted into smaller oligomers of average height of ~ 6 nm (Figure 4.12 E and F). Similar effect was also observed in the presence of PS Ssc1-Mdj1 and Hsp78 and resulted in no fibril formation during the course of aggregation. However, the early oligomers which were formed of average height ~ 9 nm, were sequentially converted into smaller oligomers of average height ~ 5 nm (Figure 4.12 G-I). Hence, the extensive analysis of AFM images and aggregation kinetics established the different mechanism of inhibition of both the Ssc1 (wild-type and PS mutant). The common route of protein aggregation or higher-order nanostructure formation passes through oligomer formation. The exposed hydrophobic patches of the proteins result in the sequestration of monomeric proteins into oligomers. In the presence

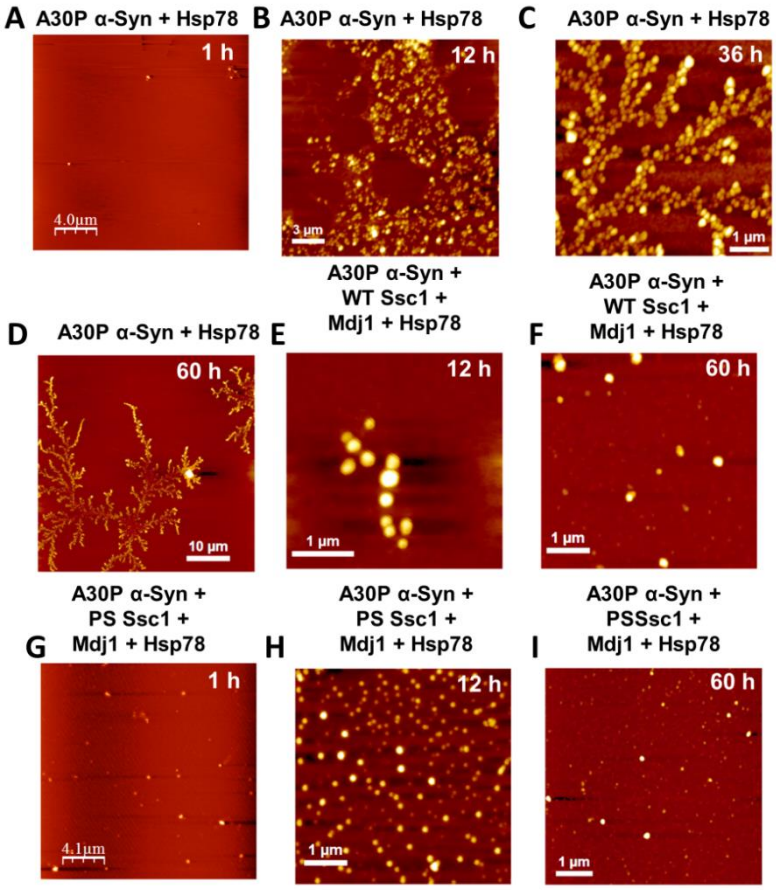

of **Figure 4.12** Time-dependent AFM images of A30P α-synuclein, in the presence of different chaperones (Hsp78, wild-type or P486S Ssc1 in the presence of Mdj1).

wild-type Ssc1-Mdj1 and Hsp78, small oligomers were the end product of the wild-type as well as A30P α-synuclein aggregation. However, in the presence of PS mutant of Ssc1-Mdj1 and Hsp78, wild-type α-synuclein showed fibrils as the end product, whereas, A30P α-synuclein resulted in the formation of small oligomers. Our results established the different chaperoning ability of wild-type and PS mutant of Hsp70 in the presence and absence of its co-chaperone and Hsp78. The single point mutation in the substrate binding site might be resulting in the structural change of the Hsp70, thereby, resulting in the different chaperoning ability. These results also indicated that the extents of aggregation lag time as well as the nanoscopic morphologies formed during aggregation are important for toxicity.

Table 4.2

Height profile analysis of AFM images shown in figures 11 and 12 using SPIP software.

Aggregation conditions	Lag/Log/ Saturation	Oligomers (Height in nm)	Annular ring like structure (Height in nm)	Fibrils (Height in nm)
WT α-Synuclein + Hsp78	Lag	40 ± 10		
	Saturation			10 ± 5
WT α-Synuclein + WT Ssc1+ Mdj1+ Hsp78	Lag	18 ± 8		
	Saturation	7 ± 3	8 ± 3	
WT α-Synuclein + PS Ssc1+ Mdj1+ Hsp78	Lag	27 ± 7		
	Saturation	7 ± 2		fibrils
A30P α-Synuclein + Hsp78	Lag	100 ± 20		
	Saturation	60 ± 20		
A30P α-Synuclein + WT Ssc1+ Mdj1+ Hsp78	Lag	40 ± 5		
	Saturation	6 ± 2		
A30P α-Syn uclein+	Lag	9 ± 3		

PS Ssc1+ Mdj1+ Hsp78	Saturation	5 ± 2		

4.5 Discussion

α-Synuclein is a presynaptic protein which has been linked to PD progression based on genetic and pathological data.[2] Several point mutations, including A30P, E46K, and A53T have been identified in the SNCA locus in familial, early-onset cases, providing a definite link between the protein and PD.[52-54] In a previous study of Parkinson's disease-associated mutations of the mtHsp70 protein, it has been demonstrated that a Proline to Serine mutation at a conserved residue of the substrate binding domain, leads to reduced chaperoning ability resulting in mitochondrial dysfunction and compromised protein quality control.[30] This mutation (P509S in human mtHsp70; and correspondingly P486S in yeast Ssc1) leads to a specific defect in modulation of the chaperone cycle, due to enhanced interaction with J-protein co-chaperones.[30] Additionally, α-synuclein also associates with mitochondria and is trafficked to the organelle by poorly-defined mechanisms under conditions of neuronal stress including diseases like PD.[20-21] However, the relevance of this translocation event is still elusive. In order to gain insight into the mitochondrial involvement in PD progression, it is thus imperative to understand the interplay of α-synuclein and mtHsp70 chaperone system.

The results from growth phenotype analysis, toxicity assay, *in vitro* aggregation kinetics and AFM imaging analysis of wild-type and A30P α-synuclein, in the presence of Hsp70 (both wild-type and PS mutant) and their co-chaperones, corroborate with each other. Wild-type and the Proline to Serine mtHsp70 PD-variant, are individually capable of delaying α-synuclein aggregation to comparable extents. However, only the wild-type chaperone is assisted significantly further by the presence of a J-protein co-chaperone partner, in case of both human and yeast proteins. The investigation of *in vitro* aggregation kinetics and AFM imaging analysis revealed that wild-type and PD mutant of Hsp70 have distinguished mechanisms of inhibition of α-synuclein aggregation. Both wild-type and A30P α-synuclein formed oligomers, that transformed into fibrils and annular protofibrils, respectively in the saturation phase, which is in agreement with the previous studies.[39, 40] A variety of other proteins and peptides have been shown to form annular pores and protofibrils *in vitro*.[41-44] The formation of oligomers (of variable height) plausibly served as templates for the genesis of other protein nanoscale assemblies. In the presence of wild-type Hsp70 and Tid1s, fibrils were the end product of the both wild-type and A30P α-synuclein aggregation

via morphologically different intermediates having different toxicity. Wild-type Hsp70 in the presence of A30P α-synuclein showed a long-lived toxic heterogeneous population of oligomers, pore like annular protofibrils and fibrils that might also be the consequence of growth phenotype defect in yeast cells. However, in the presence of PS mutant of Hsp70 and Tid1s, wild-type α-synuclein or A30P α-synuclein transform into benign small oligomers. Interestingly, the PS mutant of Hsp70 does not show any growth defect in yeast growth phenotype, which could be the result of small oligomers formed in the elongated lag time of aggregation. Previous studies suggest that the conformation of intermediates formed during the course of aggregation are important for its toxicity and the transient oligomers formed in the lag phase of α-synuclein aggregation are known to be highly cytotoxic.[55-56] In contradiction, recent studies have shown two different oligomeric forms of α-synuclein having similar sizes and morphologies with different abilities to disrupt lipid bilayers, human neuroblastoma SH-SY5Y cells and rat primary cortical neurons.[57-58] Hence, it is difficult to state whether the oligomers or the fibrils are the toxic species, suggesting that the conformations of the oligomers or fibrils are of prime importance for its toxicity.

A similar pattern of inhibition was observed by wild-type and PS Ssc1 in the presence of Hsp78. The wild-type Ssc1 with Mdj1 was significantly assisted by Hsp78 in increasing the lag time (from 30 h to 43 h), which indicates better efficiency of inhibition. These results raise the possibility that the binding of Hsp78 might be increasing the efficient binding of α-synuclein to Ssc1, which then elongates the lag time. Apparently, the PD mutant P486S of Ssc1 with Mdj1 in the presence of Hsp78 showed negligible improvement in its chaperoning ability (from 28 h to 29 h). This suggests that the P486S mutation in the substrate binding domain of Ssc1 might result in conformational changes in the protein and as a consequence dampening the binding efficiency of α-synuclein to PS mutant of Ssc1. These results again shed light into the different chaperoning ability of wild-type and PS mutant of Ssc1 in the presence of Hsp78 and Mdj1. The single point mutation in the substrate binding site might be resulting in the structural change of the protein and hence resulting in the better association with wild-type Ssc1 as compared to PS mutant of Ssc1. AFM analysis showed intriguing results in the presence of wild-type Ssc1-Mdj1 and Hsp78, small oligomers were the end product of the wild-type as well as A30P α-synuclein. However, in the presence of PS mutant of Ssc1-Mdj1 and Hsp78, wild-type α-synuclein and A30P α-synuclein showed fibrils and small oligomers, respectively as the end product. Our results established the different chaperoning ability of wild-type and PS mutant of Hsp70 in the presence and absence of its co-chaperone and Hsp78, in inhibiting the α-synuclein aggregation. The single point mutation

in the substrate binding site might be resulting in the structural change of the Hsp70, hence, exhibiting different chaperoning ability. These results also indicated that the extents of aggregation lag time as well as the nanoscopic morphologies formed during aggregation are important for its toxicity.

Our results raise an intriguing possibility that disease-associated mutations of human mtHsp70, such as P509S, provide an advantage in a scenario where the normal cellular homeostatic mechanism can be deleterious. This naturally arising variant in PD patients could thus be a compensatory mechanism to counter the damaging effects of α-synuclein, and more specifically the PD-variant A30P α-synuclein. Therefore, instead of contributing to PD progression, the unique gain of function of increased interaction could be assisting in slowing down the disease progression. Taken together, our results revealed that the mitochondrial dysfunction due to α-synuclein aggregation might be modulated by the effect of multiple chaperones of the mitochondria and the final cellular outcomes are determined by their levels within the organelle matrix.

4.6 Reference:

1. Shulman, J. M.; De Jager, P. L.; Feany, M. B., Parkinson's disease: genetics and pathogenesis. *Annu Rev Pathol* **2011,** *6*, 193-222.

2. Davie, C. A., A review of Parkinson's disease. *Br Med Bull* **2008,** *86*, 109-27.

3. Bernheimer, H.; Birkmayer, W.; Hornykiewicz, O.; Jellinger, K.; Seitelberger, F., Brain dopamine and the syndromes of Parkinson and Huntington. Clinical, morphological and neurochemical correlations. *J Neurol Sci* **1973,** *20* (4), 415-55.

4. Dauer, W.; Przedborski, S., Parkinson's disease: mechanisms and models. *Neuron* **2003,** *39* (6), 889-909.

5. Forno, L. S., Neuropathology of Parkinson's disease. *J Neuropathol Exp Neurol* **1996,** *55* (3), 259-72.

6. Spillantini, M. G.; Crowther, R. A.; Jakes, R.; Hasegawa, M.; Goedert, M., alpha-Synuclein in filamentous inclusions of Lewy bodies from Parkinson's disease and dementia with lewy bodies. *Proc Natl Acad Sci U S A* **1998,** *95* (11), 6469-73.

7. Ono, K.; Ikeda, T.; Takasaki, J.; Yamada, M., Familial Parkinson disease mutations influence alpha-synuclein assembly. *Neurobiol Dis* **2011,** *43* (3), 715-24.

8. Burre, J.; Sharma, M.; Sudhof, T. C., Systematic mutagenesis of alpha-synuclein reveals distinct sequence requirements for physiological and pathological activities. *J Neurosci* **2012,** *32* (43), 15227-42.

9. Lashuel, H. A.; Overk, C. R.; Oueslati, A.; Masliah, E., The many faces of alpha-synuclein: from structure and toxicity to therapeutic target. *Nat Rev Neurosci* **2013,** *14* (1), 38-48.

10. Goldberg, M. S.; Lansbury, P. T., Jr., Is there a cause-and-effect relationship between alpha-synuclein fibrillization and Parkinson's disease? *Nat Cell Biol* **2000,** *2* (7), E115-9.

11. Winner, B.; Jappelli, R.; Maji, S. K.; Desplats, P. A.; Boyer, L.; Aigner, S.; Hetzer, C.; Loher, T.; Vilar, M.; Campioni, S.; Tzitzilonis, C.; Soragni, A.; Jessberger, S.; Mira, H.; Consiglio, A.; Pham, E.; Masliah, E.; Gage, F. H.; Riek, R., In vivo demonstration that alpha-synuclein oligomers are toxic. *Proc Natl Acad Sci U S A* **2011,** *108* (10), 4194-9.

12. Ebrahimi-Fakhari, D.; Wahlster, L.; McLean, P. J., Molecular chaperones in Parkinson's disease--present and future. *J Parkinsons Dis* **2012,** *1* (4), 299-320.

13. Klucken, J.; Shin, Y.; Masliah, E.; Hyman, B. T.; McLean, P. J., Hsp70 Reduces alpha-Synuclein Aggregation and Toxicity. *J Biol Chem* **2004,** *279* (24), 25497-502.

14. Yokoyama, K.; Fukumoto, K.; Murakami, T.; Harada, S.; Hosono, R.; Wadhwa, R.; Mitsui, Y.; Ohkuma, S., Extended longevity of Caenorhabditis elegans by knocking in extra copies of hsp70F, a homolog of mot-2 (mortalin)/mthsp70/Grp75. *FEBS Lett* **2002,** *516* (1-3), 53-7.

15. Auluck, P. K.; Chan, H. Y.; Trojanowski, J. Q.; Lee, V. M.; Bonini, N. M., Chaperone suppression of alpha-synuclein toxicity in a Drosophila model for Parkinson's disease. *Science* **2002,** *295* (5556), 865-8.

16. McLean, P. J.; Klucken, J.; Shin, Y.; Hyman, B. T., Geldanamycin induces Hsp70 and prevents alpha-synuclein aggregation and toxicity in vitro. *Biochem Biophys Res Commun* **2004,** *321* (3), 665-9.

17. Burbulla, L. F.; Schelling, C.; Kato, H.; Rapaport, D.; Woitalla, D.; Schiesling, C.; Schulte, C.; Sharma, M.; Illig, T.; Bauer, P.; Jung, S.; Nordheim, A.; Schols, L.; Riess, O.; Kruger, R., Dissecting the role of the mitochondrial chaperone mortalin in Parkinson's disease: functional impact of disease-related variants on mitochondrial homeostasis. *Hum Mol Genet* **2010,** *19* (22), 4437-52.

18. De Mena, L.; Coto, E.; Sanchez-Ferrero, E.; Ribacoba, R.; Guisasola, L. M.; Salvador, C.; Blazquez, M.; Alvarez, V., Mutational screening of the mortalin gene (HSPA9) in Parkinson's disease. *J Neural Transm* **2009,** *116* (10), 1289-93.

19. Nakamura, K.; Nemani, V. M.; Azarbal, F.; Skibinski, G.; Levy, J. M.; Egami, K.; Munishkina, L.; Zhang, J.; Gardner, B.; Wakabayashi, J.; Sesaki, H.; Cheng, Y.; Finkbeiner, S.; Nussbaum, R. L.; Masliah, E.; Edwards, R. H., Direct membrane association drives

mitochondrial fission by the Parkinson disease-associated protein alpha-synuclein. *J Biol Chem* **2011,** *286* (23), 20710-26.

20. Devi, L.; Raghavendran, V.; Prabhu, B. M.; Avadhani, N. G.; Anandatheerthavarada, H. K., Mitochondrial import and accumulation of alpha-synuclein impair complex I in human dopaminergic neuronal cultures and Parkinson disease brain. *J Biol Chem* **2008,** *283* (14), 9089-100.

21. Devi, L.; Anandatheerthavarada, H. K., Mitochondrial trafficking of APP and alpha synuclein: Relevance to mitochondrial dysfunction in Alzheimer's and Parkinson's diseases. *Biochim Biophys Acta* **2010,** *1802* (1), 11-9.

22. Bueler, H., Impaired mitochondrial dynamics and function in the pathogenesis of Parkinson's disease. *Exp Neurol* **2009,** *218* (2), 235-46.

23. Pridgeon, J. W.; Olzmann, J. A.; Chin, L. S.; Li, L., PINK1 protects against oxidative stress by phosphorylating mitochondrial chaperone TRAP1. *PLoS Biol* **2007,** *5* (7), e172.

24. Dedmon, M. M.; Christodoulou, J.; Wilson, M. R.; Dobson, C. M., Heat shock protein 70 inhibits alpha-synuclein fibril formation via preferential binding to prefibrillar species. *J Biol Chem* **2005,** *280* (15), 14733-40.

25. Huang, C.; Cheng, H.; Hao, S.; Zhou, H.; Zhang, X.; Gao, J.; Sun, Q. H.; Hu, H.; Wang, C. C., Heat shock protein 70 inhibits alpha-synuclein fibril formation via interactions with diverse intermediates. *J Mol Biol* **2006,** *364* (3), 323-36.

26. Luk, K. C.; Mills, I. P.; Trojanowski, J. Q.; Lee, V. M. Y., INTERACTIONS BETWEEN HSP70 AND THE HYDROPHOBIC CORE OF ALPHA–SYNUCLEIN INHIBIT FIBRIL ASSEMBLY. *Biochemistry* **2008,** *47* (47), 12614-12625.

27. Franssens, V.; Boelen, E.; Anandhakumar, J.; Vanhelmont, T.; Buttner, S.; Winderickx, J., Yeast unfolds the road map toward alpha-synuclein-induced cell death. *Cell Death Differ* **2010,** *17* (5), 746-53.

28. Ocampo, A.; Barrientos, A., Developing yeast models of human neurodegenerative disorders. *Methods Mol Biol* **2011,** *793*, 113-27.

29. Outeiro, T. F.; Lindquist, S., Yeast cells provide insight into alpha-synuclein biology and pathobiology. *Science* **2003,** *302* (5651), 1772-5.

30. Goswami, A. V.; Samaddar, M.; Sinha, D.; Purushotham, J.; D'Silva, P., Enhanced J-protein interaction and compromised protein stability of mtHsp70 variants lead to mitochondrial dysfunction in Parkinson's disease. *Hum Mol Genet* **2012,** *21* (15), 3317-32.

31. Roodveldt, C.; Bertoncini, C. W.; Andersson, A.; van der Goot, A. T.; Hsu, S. T.; Fernandez-Montesinos, R.; de Jong, J.; van Ham, T. J.; Nollen, E. A.; Pozo, D.;

Christodoulou, J.; Dobson, C. M., Chaperone proteostasis in Parkinson's disease: stabilization of the Hsp70/alpha-synuclein complex by Hip. *Embo J* **2009,** *28* (23), 3758-70.

32. Westermann, B.; Neupert, W., Mitochondria-targeted green fluorescent proteins: convenient tools for the study of organelle biogenesis in Saccharomyces cerevisiae. *Yeast* **2000,** *16* (15), 1421-7.

33. Jain, N.; Bhasne, K.; Hemaswasthi, M.; Mukhopadhyay, S., Structural and Dynamical Insights into the Membrane-Bound α-Synuclein. *PLOS ONE* **2013,** *8* (12), e83752.

34. Arora, A.; Ha, C.; Park, C. B., Inhibition of insulin amyloid formation by small stress molecules. *FEBS Lett* **2004,** *564* (1-2), 121-5.

35. Polymeropoulos, M. H.; Lavedan, C.; Leroy, E.; Ide, S. E.; Dehejia, A.; Dutra, A.; Pike, B.; Root, H.; Rubenstein, J.; Boyer, R.; Stenroos, E. S.; Chandrasekharappa, S.; Athanassiadou, A.; Papapetropoulos, T.; Johnson, W. G.; Lazzarini, A. M.; Duvoisin, R. C.; Di Iorio, G.; Golbe, L. I.; Nussbaum, R. L., Mutation in the alpha-synuclein gene identified in families with Parkinson's disease. *Science* **1997,** *276* (5321), 2045-7.

36. Uversky, V. N.; Eliezer, D., Biophysics of Parkinson's disease: structure and aggregation of alpha-synuclein. *Curr Protein Pept Sci* **2009,** *10* (5), 483-99.

37. Nath, A.; Rhoades, E., A flash in the pan: dissecting dynamic amyloid intermediates using fluorescence. *FEBS Lett* **2013,** *587* (8), 1096-105.

38. Kruger, R.; Kuhn, W.; Muller, T.; Woitalla, D.; Graeber, M.; Kosel, S.; Przuntek, H.; Epplen, J. T.; Schols, L.; Riess, O., Ala30Pro mutation in the gene encoding alpha-synuclein in Parkinson's disease. *Nat Genet* **1998,** *18* (2), 106-8.

39. Apetri, M. M.; Maiti, N. C.; Zagorski, M. G.; Carey, P. R.; Anderson, V. E., Secondary structure of alpha-synuclein oligomers: characterization by raman and atomic force microscopy. *J Mol Biol* **2006,** *355* (1), 63-71.

40. Lashuel, H. A.; Petre, B. M.; Wall, J.; Simon, M.; Nowak, R. J.; Walz, T.; Lansbury, P. T., Jr., Alpha-synuclein, especially the Parkinson's disease-associated mutants, forms pore-like annular and tubular protofibrils. *J Mol Biol* **2002,** *322* (5), 1089-102.

41. Mukhopadhyay, S.; Nayak, P. K.; Udgaonkar, J. B.; Krishnamoorthy, G., Characterization of the formation of amyloid protofibrils from barstar by mapping residue-specific fluorescence dynamics. *J Mol Biol* **2006,** *358* (4), 935-42.

42. Kagan, B. L.; Jang, H.; Capone, R.; Teran Arce, F.; Ramachandran, S.; Lal, R.; Nussinov, R., Antimicrobial properties of amyloid peptides. *Mol Pharm* **2012,** *9* (4), 708-17.

43. Capone, R.; Jang, H.; Kotler, S. A.; Kagan, B. L.; Nussinov, R.; Lal, R., Probing structural features of Alzheimer's amyloid-beta pores in bilayers using site-specific amino acid substitutions. *Biochemistry* **2012,** *51* (3), 776-85.

44. Zhu, M.; Han, S.; Zhou, F.; Carter, S. A.; Fink, A. L., Annular oligomeric amyloid intermediates observed by in situ atomic force microscopy. *J Biol Chem* **2004,** *279* (23), 24452-9.

45. Lomas, D. A.; Evans, D. L.; Finch, J. T.; Carrell, R. W., The mechanism of Z alpha 1-antitrypsin accumulation in the liver. *Nature* **1992,** *357* (6379), 605-7.

46. Dafforn, T. R.; Mahadeva, R.; Elliott, P. R.; Sivasothy, P.; Lomas, D. A., A Kinetic Mechanism for the Polymerization of α1-Antitrypsin. *Journal of Biological Chemistry* **1999,** *274* (14), 9548-9555.

47. Lomas, D. A.; Finch, J. T.; Seyama, K.; Nukiwa, T.; Carrell, R. W., Alpha 1-antitrypsin Siiyama (Ser53-->Phe). Further evidence for intracellular loop-sheet polymerization. *J Biol Chem* **1993,** *268* (21), 15333-5.

48. Krzewska, J.; Langer, T.; Liberek, K., Mitochondrial Hsp78, a member of the Clp/Hsp100 family in Saccharomyces cerevisiae, cooperates with Hsp70 in protein refolding. *FEBS Lett* **2001,** *489* (1), 92-6.

49. Moczko, M.; Schonfisch, B.; Voos, W.; Pfanner, N.; Rassow, J., The mitochondrial ClpB homolog Hsp78 cooperates with matrix Hsp70 in maintenance of mitochondrial function. *J Mol Biol* **1995,** *254* (4), 538-43.

50. Rottgers, K.; Zufall, N.; Guiard, B.; Voos, W., The ClpB homolog Hsp78 is required for the efficient degradation of proteins in the mitochondrial matrix. *J Biol Chem* **2002,** *277* (48), 45829-37.

51. Glover, J. R.; Lindquist, S., Hsp104, Hsp70, and Hsp40: a novel chaperone system that rescues previously aggregated proteins. *Cell* **1998,** *94* (1), 73-82.

52. Zarranz, J. J.; Alegre, J.; Gomez-Esteban, J. C.; Lezcano, E.; Ros, R.; Ampuero, I.; Vidal, L.; Hoenicka, J.; Rodriguez, O.; Atares, B.; Llorens, V.; Gomez Tortosa, E.; del Ser, T.; Munoz, D. G.; de Yebenes, J. G., The new mutation, E46K, of alpha-synuclein causes Parkinson and Lewy body dementia. *Ann Neurol* **2004,** *55* (2), 164-73.

53. Brown, D. R., Oligomeric alpha-synuclein and its role in neuronal death. *IUBMB Life* **2010,** *62* (5), 334-9.

54. Kayed, R.; Head, E.; Thompson, J. L.; McIntire, T. M.; Milton, S. C.; Cotman, C. W.; Glabe, C. G., Common structure of soluble amyloid oligomers implies common mechanism of pathogenesis. *Science* **2003,** *300* (5618), 486-9.

55. Conway, K. A.; Lee, S. J.; Rochet, J. C.; Ding, T. T.; Williamson, R. E.; Lansbury, P. T., Jr., Acceleration of oligomerization, not fibrillization, is a shared property of both alpha-synuclein mutations linked to early-onset Parkinson's disease: implications for pathogenesis and therapy. *Proc Natl Acad Sci U S A* **2000,** *97* (2), 571-6.

56. Gosavi, N.; Lee, H. J.; Lee, J. S.; Patel, S.; Lee, S. J., Golgi fragmentation occurs in the cells with prefibrillar alpha-synuclein aggregates and precedes the formation of fibrillar inclusion. *J Biol Chem* **2002,** *277* (50), 48984-92.

57. Fusco, G.; Chen, S. W.; Williamson, P. T. F.; Cascella, R.; Perni, M.; Jarvis, J. A.; Cecchi, C.; Vendruscolo, M.; Chiti, F.; Cremades, N.; Ying, L.; Dobson, C. M.; De Simone, A., Structural basis of membrane disruption and cellular toxicity by alpha-synuclein oligomers. *Science* **2017,** *358* (6369), 1440-1443.

58. Cremades, N.; Cohen, Samuel I. A.; Deas, E.; Abramov, Andrey Y.; Chen, Allen Y.; Orte, A.; Sandal, M.; Clarke, Richard W.; Dunne, P.; Aprile, Francesco A.; Bertoncini, Carlos W.; Wood, Nicholas W.; Knowles, Tuomas P. J.; Dobson, Christopher M.; Klenerman, D., Direct Observation of the Interconversion of Normal and Toxic Forms of α-Synuclein. *Cell 149* (5), 1048-1059.

Parkinson's disease is the second most prevalent neurodegenerative disease after Alzheimer's disease. The brain tissues of Parkinson's disease patient is characterized by the deposition of α-synuclein amyloids along with many other proteins, that results in neuronal death. Being an intrinsically disordered protein, α-synuclein is known to adopt different structures upon interaction with different binding partners (discussed in detail in chapter 1). A wealth of information has been obtained to understand the interplay of α-synuclein and its binding partners in Parkinson's disease. However, the precise function of α-synuclein and mechanism of amyloid formation remains elusive. The work described in this thesis addresses the underlying molecular mechanism of interaction of α-synuclein with lipid membranes, tau and chaperones. Below, I briefly summarize:

(i) The α-synuclein dynamics (chapter 2) on lipid membrane is highly dependent on membrane curvature as well as phospholipid head-group chemistry,

(ii) The mechanism of interaction between α-synuclein and tau (chapter 3) that has both functional as well as pathological relevance,

(iii) How molecular chaperones work together to modulate α-synuclein amyloid formation (chapter 4)

An array of biophysical techniques were used to decipher the different aspect of α-synuclein, which include fluorescence spectroscopy (steady-state & time-resolved) and microscopy, atomic force microscopy (AFM), confocal microscopy, circular dichroism (CD), stopped-flow fluorescence/CD and many others. The conformational changes in proteins upon membrane binding and during amyloid formation were mainly studied using circular dichroism (CD), atomic force microscopy (AFM) and fluorescence spectroscopy, and the dynamics of α-synuclein on the membrane was monitored using picosecond time-resolved fluorescence spectroscopy.

The conformational plasticity of α-synuclein allows it to interact with multiple partners. Upon interaction with negatively charged membranes, it adopts anα-helical structure, which plays a crucial role, both in the regulation of synaptic plasticity and in the etiology of Parkinson's disease progression. We utilized picosecond time-resolved fluorescence depolarization kinetics measurements to capture the site-specific structural and dynamical changes in membrane-bound α-synuclein. Our fluorescence depolarization results reveal the presence of three dynamically distinct types of motions, namely, the wobbling-in-cone motion of the fluorophore, the segmental motion of the protein and translational diffusion of protein on the membrane surface. The translational diffusion coefficient of α-

synuclein on the POPA and POPG membrane were 2.92 ± 0.06 x 10^{-10} m^2/s and 8.71 ± 0.06 x 10^{-10} m^2/s. We speculate that the translational diffusion of α-synuclein on membrane modulate the local/temporal concentration of the protein on the membrane which can potentially trigger pathological amyloid formation. Therefore, we believe that the interplay of membrane properties and α-synuclein diffusion might be of prime importance for its regulatory role in neurotransmitter release as well as in the etiology of PD progression.

The conformational plasticity of α-synuclein also allows it to interact with tau protein (an amyloidogenic IDP, implicated in Alzheimer's disease) and form pathological amyloids in many neurodegenerative diseases. The electrostatic interaction between α-synuclein and tau K18 fragment facilitate the early heterotypic association. This heterotypic association results in rapid formation of oligomers that readily mature into hetero-fibrils with a much shorter lag phase compared to the individual proteins. Our findings suggest the mechanistic underpinning of bypassing toxicity and also suggest a general strategy by which detrimental amyloidogenic precursors are efficiently sequestered into more benign amyloid fibrils. It is interesting to note that many functional amyloids that are involved in biofilm formation in bacteria, melanin biosynthesis in mammals and many others also known to utilize this strategy to fibrilize without or with a short lag phase to avoid the accumulation of toxic oligomeric intermediates.

During the course of evolution, molecular chaperones were evolved to prevent the misfolding and aggregation of proteins. Wild-type and the Proline to Serine mtHsp70 PD-variant, are individually capable of delaying α-synuclein (wild-type or A30P) aggregation to comparable extents. However, only the wild-type chaperone is assisted significantly further by the presence of its co-chaperone partner, in case of both human and yeast mtHsp70. The investigation of *in vitro* aggregation kinetics and AFM imaging analysis revealed that wild-type and PD mutant of Hsp70 have distinguished mechanisms of inhibition of α-synuclein aggregation. Our results established the different chaperoning ability of wild-type and PS mutant of Hsp70 in inhibiting the α-synuclein aggregation. The PS mutation in Hsp70 could be a consequence of compensatory mutations against the A30P mutation of α-synuclein in the diseased condition. We speculate that the single point mutation in the substrate binding site might be resulting in the structural change of the Hsp70 and as a result displaying different chaperoning ability. Our results from growth phenotype analysis, toxicity assay, in vitro aggregation kinetics and AFM imaging analysis of wild-type and A30P α-synuclein, in the presence of Hsp70 (both wild-type and PS mutant) and their co-chaperones, corroborate with

each other. The results also indicated that the extents of aggregation lag time as well as the nanoscopic morphologies formed during aggregation are important for its toxicity.

Figure 5.1 shows a schematic representation of α-synuclein interaction with lipid membranes, tau and chaperones. The structural and dynamical insights into the interplay of α-synuclein and its partner is important for designing small molecule inhibitors for anti-amyloid therapeutics. We believe that our molecular mechanistic studies will open new avenues for the designing of therapeutic agents to combat the deadly neurodegenerative diseases.

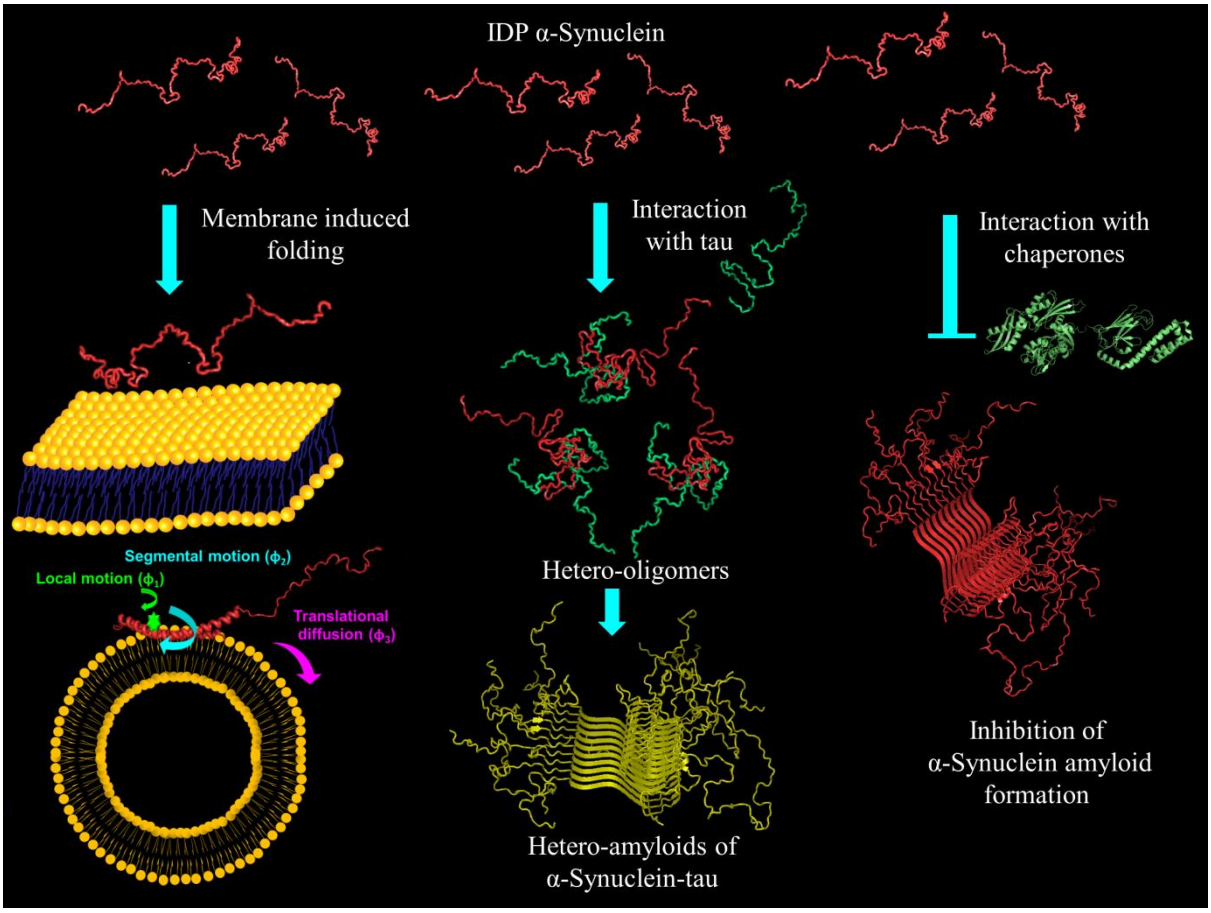

Figure 5.1 A schematic representation of α-synuclein interaction with lipid membranes, tau and chaperones. The structure of membrane-bound α-synuclein and α-synuclein amyloid structures were taken from the protein database (PDB: 1XQ8 for membrane-bound; 2n0a for amyloid), IDP structures of α-syn and tau K18 were taken from the protein ensemble database (PeDB: 9AAC for α-synuclein; 6AAC for tau K18) These structures are generated using PyMOL (Version 1.8, Schrödinger, LLC, New York) and are shown for illustration purpose.

Conclusions and future direction